Fall 2021

Liquid-Vapor Distributions in Evacuated Small Diameter Channels for Improved Accuracy of Initial Conditions in Modeling of Oscillating Heat Pipes

Travis Mayberry
Southern Methodist University, tmayberry@smu.edu

LIQUID-VAPOR DISTRIBUTIONS IN

EVACUATED SMALL DIAMETER CHANNELS FOR

IMPROVED ACCURACY OF INITIAL CONDITIONS IN

MODELING OF OSCILLATING HEAT PIPES

Approved by:

_____

Prof. Paul Krueger
Professor of Mechanical Engineering

_____

Prof. Minjun Kim
Professor of Mechanical Engineering

_____

Prof. David Willis
Professor of Mechanical Engineering

_____

Prof. Ali Beskok
Professor of Mechanical Engineering

_____

Dr. Mary Herndon
Engineering Fellow, Raytheon

LIQUID-VAPOR DISTRIBUTIONS IN EVACUATED SMALL DIAMETER CHANNELS FOR IMPROVED ACCURACY OF INITIAL CONDITIONS IN MODELING OF OSCILLATING HEAT PIPES

A Praxis Presented to the Graduate Faculty of

Bobby B. Lyle School of Engineering

Southern Methodist University

in

Partial Fulfillment of the Requirements

for the degree of

Doctor of Engineering

with a

Major in Mechanical Engineering

by

Travis Lee Mayberry

B.S.E.T., Mechanical Engineering Technology, University of North Texas, Denton, Texas

M.S., Systems Engineering, Southern Methodist University, Dallas, Texas

December 18, 2021

ACKNOWLEDGMENTS

I could not have completed this journey without the unyielding support of my wife, Elisabeth Mayberry. Her regular encouragement, understanding, and persistent attempts to keep me focused over the past years have been instrumental to my completion of this work. I would not have any form of my sanity remaining throughout this endeavor without her by my side.

I would also like to express my sincere gratitude for all the support my advisor, Dr. Paul Krueger, my research assistant, Benjamin Kuo, and the entire Mechanical Engineering Department at the Lyle School of Engineering have provided while I conducted this research. The learning opportunities I have experienced throughout the past several years have substantially accelerated my personal and professional development. I would also like to extend a special thank you to Joe Boswell and Dr. Bruce Drolen for their outstanding support at ThermAvant Technologies, as they have helped guide this work toward industry-relevant needs. My employer, Raytheon, is also to thank for their exceptional dedication to higher education, where I have been supported throughout this program while I have continued to work part-time.

Last, I cannot express enough gratitude to my mentor, Dr. Mary Herndon, who has gone above and beyond in every regard to help me succeed in this program. She helped me get started, helped navigate funding for my project, and has provided a lifetime's worth of advice and support along the way. I simply could not have done this without her help.

Mayberry, Travis Lee

B.S.E.T., Mechanical Engineering Technology, University of North Texas, Denton, 2012
M.S., Systems Engineering, Southern Methodist University, Dallas, 2014

Liquid-Vapor Distributions in
Evacuated Small Diameter Channels for
Improved Accuracy of Initial Conditions in
Modeling of Oscillating Heat Pipes

Advisor: Professor Paul Krueger

Doctor of Engineering conferred December 18, 2021

Praxis completed November 1, 2021

Oscillating heat pipes, also known as pulsating heat pipes, are increasingly becoming a preferred high-performance thermal ground plane in a variety of heat spreading applications due to a number of advantages over traditional copper-water wicked heat pipes, including their lighter weight, thinner profiles, simpler fabrication, and greater variety of material and working fluid options. A major barrier to even wider adoption, however, is the lack of comprehensive analytical models to simulate their performance. A key input to first principles models simulating the fundamental physics of the devices is the initial condition of liquid and vapor segment lengths and their distribution throughout the device. To investigate the initial distribution of liquid and vapor segments in a representative system, water was charged into evacuated glass tubes with an inner diameter of 4 mm and the resulting distribution of liquid and vapor segment lengths recorded. The device was charged to three fill ratios, and the rate at which the working fluid is introduced was also varied. These variables all showed different results in the distribution of liquid segment lengths in the device, specifically noting more consistent and shorter average

liquid lengths at slower fluid introduction rates and lower fill ratios, and conversely greater variation and longer average liquid lengths at faster fluid introduction rates and higher fill ratios. A critical fill ratio was also observed, where new liquid entering the channel began growing in average length once the first-most liquid-vapor segments had reached the far-end of the channels, referred here as the compression effect. These results lead to a better understanding of initial conditions in support of improved analytical models seeking to predict the device's behavior more accurately. The initial conditions presented in this work and the methodology of collecting such initial conditions could lead to improved models for oscillating heat pipes and improved methods for charging these devices, saving time and cost during integration of the device by reducing the amount of experimental validation needed during the development of each new device.

TABLE OF CONTENTS

LIST OF FIGURES

LIST OF TABLES

LIST OF EQUATIONS

LIST OF SYMBOLS

OHP	Oscillating Heat Pipe
PHP	Pulsating Heat Pipe
ID	Inside Diameter
OD	Outside Diameter
α	Volumetric Fill Ratio
η	Non-Dimensional Liquid Segment Length (ratio of segment length to tube inner diameter)
r	Liquid Segment Position as a Percent of the Total Channel Length
ν	Dimensionless Injection Rate
k	Liquid Segment Count Factor
Bo	Bond Number
g	Gravity
D_h	Hydraulic Diameter
ρ_L	Density of Liquid Phase
ρ_G	Density of Gas Phase
σ	Surface Tension
$\dot{V}$	Volumetric Injection Rate

FRG	Full Range Gauge
L	Liquid Segment Length
C	Count of Liquid Segments in the OHP
L_{TLIQ}	Total Length of Liquid Segments in the OHP
L_{avg}	Average Length of Liquid Segments in the OHP
L_{TCHAN}	Total Length of Channel in the OHP
$\bar{\eta}$	Average Non-Dimensional Liquid Segment Length
λ_m	Most Unstable Wavelength of the Condensate Film (Instability Theory of Condensate Films
a	Undisturbed Radius of the Condensate Film Inner Surface

I dedicate this work to Jim Pruett, who gave me the courage to embark on this journey.

CHAPTER 1.

INTRODUCTION AND OVERVIEW

1.1 Introduction to the Oscillating Heat Pipe

The Oscillating Heat Pipe (OHP), also known as the Pulsating Heat Pipe (PHP), is a relatively new two-phase, wickless, heat transfer device patented by Akachi in 1990 [1]. Since its introduction to the field, this high-performance thermal management device has shown several advantages over traditional copper-water wicked heat pipes in a number of domains, including land, air, and space operating environments. However, a major barrier to entry of the OHP for wider adoption throughout the industry involves modeling the complex two-phase nature of the device, as well as a lack of characterized initial conditions for the device, which serve a basis of predicting a device's performance from first principles using computational simulations of the physical operation of the device. Currently, the industry relies on correlations and assumptions as inputs for modeling the OHP's behavior, though eventually more accurate initial conditions and models will be needed in order for the many advantages of this device to be realized [2], [3].

Physically, a typical OHP consists of a sealed, open- or closed-loop (channels that are unconnected or connected to itself) microchannel path, typically arranged in a serpentine pattern. The OHP also contains at least one evaporator (heat input) section and at least one condenser (heat output) section, as shown in Figure 1. The channel(s) is evacuated to remove non-condensable gasses and then partially-filled with the desired working fluid [4]. As the working fluid is introduced to partially-fill the total volume of the evacuated channels, the fluid self-

stratifies into a series, or “train”, of liquid slugs and vapor segments, which can be described as Taylor bubbles in small diameter channels [5]–[7].

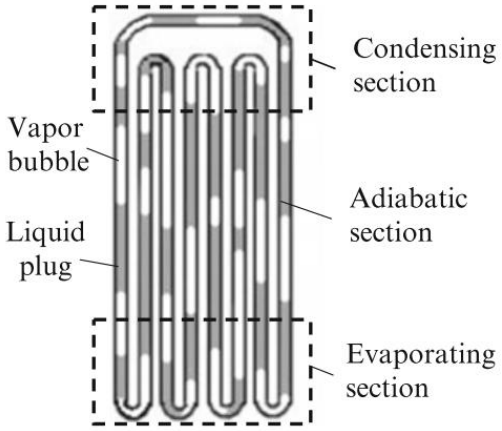

Figure 1 Oscillating Heat Pipe, Closed-Loop [8].

Though the OHP is self-pumping and does not rely on a secondary pump to move the device’s fluid, it is still considered an “active” heat transfer device since it converts heat into kinetic energy that moves the liquid segments throughout its channels. This self-pumping in an OHP occurs when there is a sufficient temperature difference between the evaporating and condensing regions to begin expanding and contracting the vapor segments. As the vapor segments grow and shrink, an unsteady pressure gradient is generated throughout the device due to adjacent tails of liquid segments evaporating into vapor and expanding in the evaporating region, and vapor segments condensing and shrinking in the condensing region. The pressure gradients generated by the unsteady and non-uniform expanding and shrinking of vapor segments result in an oscillating motion of the liquid segments, moving the shrinking and

expanding liquid segments back and forth along the channels in the device as they pass through its evaporating, adiabatic, and condensing regions.

During the startup phase, when liquid segments are stationery and heat and temperatures are still low, nucleate boiling and subsequent vapor generation can occur in the liquid segments in the evaporating region, where small vapor bubbles eventually coalesce to become complete vapor segments. Also during startup, the tail edges of the liquid segments evaporate, known as film boiling, and expand the neighboring vapor segment, as shown in Figure 2(a). As the device continues to operate, film boiling becomes the primary evaporation contribution that expands the neighboring vapor segment. As heat inputs increase in an OHP, higher rates of evaporation result in higher amplitude and frequency of oscillations throughout the device, which subsequently results in greater heat transfer.

As heat is removed in the condenser section, as shown in Figure 2(b), the vapor segment shrinks as it partially returns to a liquid, condensing into a liquid film on the channel wall and thus continuing to move the adjacent liquid-vapor segments. Fluid is pumped from the film on the channel wall into the adjacent liquid plug via capillary forces. The resulting pressure drop due to condensation shrinks the vapor plug, again inducing movement of the liquid phase and therefore additional bulk convection. The condenser section can be considered as two regions, the thin film and meniscus region. Heat is primarily transferred between the vapor plug and the channel wall though the thin film section, as opposed to through the meniscus adjacent to the liquid plug [8], [9].

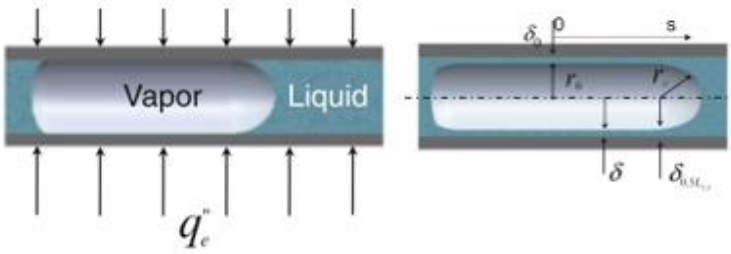

Figure 2 Evaporating Section (a) and Condensing Section (b) [10].

Simultaneous and uneven rates of shrinking and expanding vapor plugs, i.e. fluctuating pressure gradients, throughout the serpentine channels create an imbalanced oscillatory motion, and can be described as a chaotic damped spring-mass system, as illustrated schematically in Figure 3. In this analogy, the mass of the liquid segment is driven by the pressure differences between the evaporator and condenser, and several of these masses are connected by a vapor spring and dampened by frictional resistance. Every OHP's oscillating motion is determined by its vapor spring constant due to expansion and contraction in the evaporator and condenser, respectively [8]. This results in low amplitude oscillations of the liquid segments as these vapor plugs grow due to the evaporation and shrink due to condensation at different rates.

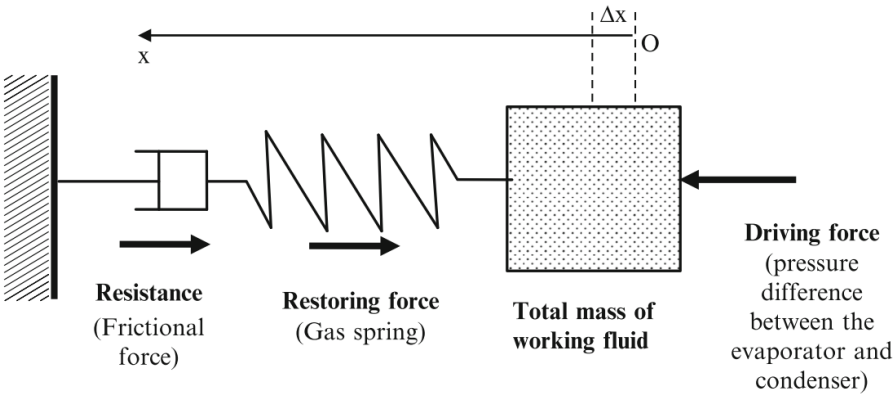

Figure 3 Damped Spring-Mass System Analogy to Describe OHP Motion [8].

Though evaporation and condensation play a key role in the physical motion of the OHP, these phase change processes are believed to have little contribution to the overall heat transfer, estimated to be between just 2-10% [4], [8], [11], [12]. The greater contribution to heat transfer is by forced convection, or sensible heat transfer, of the thermally-excited liquid and vapor train as it oscillates between the evaporating and condensing regions. This assertation has been challenged, however, new numerical and experimental models argue that latent heat can have a considerable and dominant effect during heat transfer [13]–[15]. This remains an active area of research.

1.2 Design Considerations

The overall objective an OHP is to provide lowest thermal resistance between the heat source(s) and sink(s), which involves optimizing a number of parameters in the design space. One fundamental parameter when designing an OHP is the hydraulic diameter of the channel, which must be sized in accordance with the desired working fluid and operating conditions. The

channel diameter and working fluid relationship can be characterized by the Bond Number (Bo), defined as

$$Bo = \frac{g\ {D_h}^2\ (\rho_L - \rho_G)}{\sigma}. \quad [1]$$

where g is the gravitational constant, D_h is the hydraulic diameter of the channel, ρ_L is the density of the liquid phase, ρ_G is the density of the gas phase, and σ is the surface tension of the working fluid. The Bond number relates surface tension forces to gravitational forces, and is used to define the maximum channel diameter required to maintain stratified liquid segments. If the channel diameter is too large for the given working fluid, the liquid will pool in the bottom of the channel instead of forming a liquid segment that spans the cross-section of the channel. The channel diameter of an OHP has traditionally been sized give $Bo < 2.0$ to ensure liquid segment formation, however recent investigations and controlled experiments suggest a Bo of 2.40-2.74 may be allowable, which would allow for a larger maximum channel diameter, faster start-up, and greater heat transport [16]. Typical channel sizes in industry are specific to the given working fluid, and therefore can range from microchannels on the order of 0.25 mm hydraulic diameter to 6.50 mm or greater.

The working fluid selection is also a critical consideration. Common working fluids include water, acetone, methanol, R134a, butane, fluids containing nanoparticles (nanofluids), and, for certain applications, working fluid mixtures [8], [17], [18]. Working fluids should exhibit properties such as high $(dP/dT)_{sat}$ to ensure a small temperature change in the evaporator results in a large pressure change in the expanding vapor bubble to drive oscillating flow, low dynamic viscosity to generate lower shear stress at the wall, and high specific heat given that it is widely understood that sensible heat transport is the primary heat transfer

mechanism [4], [19]. The working fluid should also be compatible with the material composing the device's channels, such as aluminum or titanium, and should not corrode, outgas, generate undesirable surface effects, or produce non-condensable gasses over time.

The fill ratio of the device, α, or percentage of working fluid to total channel volume, typically ranges from 20-80% and is specific to each OHP's unique boundary and operating conditions. An OHP will operate at a number of different fill ratios, but generally has an optimal fill ratio where the device operates with the lowest thermal resistance between the heat source(s) and sink(s). Lower fill ratios generate higher amplitude and frequency of oscillations than higher fill ratios since there is less mass to move, however they transport less heat since there is less liquid for sensible heat transfer. Higher fill ratios have more mass for sensible heat transfer, but result in lower amplitude and frequency of oscillations and a less effective device. The optimal fill ratio for an OHP will balance having enough liquid mass for heat transport with enough vapor space for optimal amplitude and frequency of oscillations, and is often determined experimentally [4], [8].

It should also be noted that the device's volumetric fill ratio, α, is dependent on ambient and fluid temperature, though the fluid mass will be conserved regardless of temperature [20]. This is to say that even though a device has a fill ratio of 50% at 22C, for example, there is a certain vapor quality and mass in the non-liquid regions throughout the device. As the device's fixed volume is heated and the liquid segments evaporate into vapor, the mass of working fluid within the device is conserved though the amount of visible liquid is reduced.

The orientation of the OHP's channels while operating should also be considered, since gravity can affect the device's thermal performance. The effect of gravity is minimized, however, by increasing the number of serpentine turns and by reducing the channel hydraulic

diameter, which in-turn increases the effect of surface tension effects on liquid segment formation in the channel [21], [22]. A number of experiments characterize the performance of OHPs in different orientations, such as the vertical orientation with bottom-heating (evaporator on below the condenser) and top-heating conditions, and angled and horizontal orientations. These experiments broadly report that the bottom-heating orientation results in the lowest thermal resistance, though other factors such as fill ratio may change depending on orientation [2], [21], [23], [24]. As alluded to earlier, typical applications include a number of different environments which may involve various orientations or gravity environments, ranging from simple planes of serpentine channels in the horizontal orientation to remove heat from circuit card assemblies in a non-moving environment, to complex non-linear and parallel routing of channels to remove heat in high-gravity environments [8]. In any operating environment, the routing of the channels and number of serpentine passes is an important consideration.

A critical and often under-reported consideration is the system's vacuum level, and details of the outgassing process [17]. Since the OHP's performance depends on the difference in saturation pressure between the evaporator and condenser, as described in the previous section, it is important to remove as much non-condensable gas from the system as possible to achieve the best performance [25]. Unfortunately, vacuum level for different systems is rarely reported (or not reported in detail), suggesting this parameter may account for variability in experimental results [16], [26].

Contrary to conventional copper-water wicked heat pipes, also known as Constant Conductance Heat Pipes (CCHPs), where liquid is transported through a sintered copper wick and heat is primarily transported through latent heat of vaporization as a vapor through the hollow core, OHPs do not contain a wick and instead transport heat primarily through sensible

heat transport, as described above [27]. Because OHPs do not contain a wick for transporting liquid or a hollow core for vapor, the two major limits for CCHPs, the capillary and entrainment limits, do not apply to OHPs [8], [16], [28]. The capillary limit of a CCHP involves a dry-out condition in the wick structure when a critical heat flux is experienced, and fluid cannot be pumped to the evaporating region of the wick fast enough to support the rate of evaporation. The entrainment limit of a CCHP involves the shearing interface of the high-speed vapor moving through the hollow core counter to the liquid being pumped by capillary action through the wick, where liquid from the wick is entrained in the counter-flowing vapor, thus leading to a dry-out condition in the wick at the evaporator. The absence of these limiting conditions for OHPs enables them to operate over a much wider range of heat fluxes, but also introduces new limits that may not apply to CCHPs. New limits specific to OHPs include the Vapor Inertia Limit, which occurs at high temperatures in the working fluid where surface tension of the liquid segment is reduced and, due to rapid evaporation, the velocity of the adjacent vapor segment is high enough that the rapidly expanding vapor is able to pierce the adjacent liquid segments and create a continuous vapor core surrounded by a liquid film on the channel walls; the Viscous Limit, which affects start up at cold temperatures; and the Swept Length Limit, where the heat input section is relatively long along the evaporator channels, causing dryout at lower powers than expected relative to the same power in devices with a smaller footprint and/or higher heat flux [16].

The fact that OHPs are wick-less makes them significantly simpler to manufacture, which is attractive to a number of industries interested in producing this high-performance passive heat spreader as an alternative to the relatively complex manufacturing of the CCHP [29]. However, simpler manufacturing aside, one of the major barriers to wider adoption of the OHP is the

inherent complexity of modeling and simulation of the motion and heat transfer of this two-phase, non-linear device.

1.3 Modeling the Oscillating Heat Pipe

Modeling an OHP's complete oscillating motion and heat transfer is inherently challenging given a combination of factors, including oscillation frequency and amplitude, liquid segment length, number of turns in the channel, gravity, and boiling and condensation heat transfer [8], [29]. Due to these challenges, a handful of simplified models for certain regimes of OHP performance have been developed, and some models are based on empirical correlations which do not provide much latitude to move between different designs. These models include spring-mass-damped systems [8], [10], [30], dimensionless correlations of device performance [31], [32], and first principles models, including numerical methods involving Volume of Fraction models which tracks the surface of two immiscible fluids [33], and other approaches include using commercial finite element software to model the dynamics and heat transfer to simulate and better understand OHPs [34]–[37].

First principles models that involve the direct modeling of liquid and vapor interaction and evolution in an OHP will naturally make assumptions regarding initial conditions of the device, including a wide variation in reports of initial evacuation procedures, which can affect the removal of non-condensable gasses from the system, impacting the OHP's overall performance [16]. In particular, models that discretely track the behavior of individual liquid and vapor segments tend to make assumptions regarding the initial length, distribution, and location of the segments. Some models simply assume that the fill ratio of liquid begins as a continuous segment in the evaporator region [2], [3], [38], [39]. Though this method is simple, it does not represent the actual nature of the fluid in the device, which can affect startup behavior, and is

better modeled by a distribution of liquid-vapor segments [3], [40]. An alternative method to this end involves determining the initial liquid lengths using instability theory of condensate film and capillary blocking in small diameter tubes [32], [41]. Though this method is an improvement to modeling a continuous slug of liquid, it only considers the diameter of the OHP to generate approximate initial liquid segment lengths, and does not factor in important parameters related to the fluid, such as viscosity, surface tension, or how the device was charged with the working fluid. Other models assume a set of possible different initial distributions and validate the analytical predictions with experimental results [3]. This method provides interesting conclusions in the differing results, however, in practical applications it is likely to prove time-consuming and ultimately does not provide a repeatable prediction method for determining liquid-vapor lengths and distributions for future devices that are to be modeled without building and testing first. No known body of work exists that appropriately defines the initial liquid-vapor distribution in OHPs.

Numerical models, [32], [42], use one of these methods of determining the initial liquid segment length and distribution. The length and distribution of liquid “slugs” and vapor “plugs” within an OHP plays an important role in the device’s startup behavior, though it is very hard to experimentally reproduce or specify the initial distribution of these segments in OHPs [3], [43]. A better understanding of these initial conditions is needed for a given working fluid, diameter, and fill ratio in order to inform more accurate models, perhaps based on first principles. This work aims to improve first principles models that rely on discrete modeling of liquid and vapor segments in their initial conditions, and improved models will in turn provide better design guidance for new systems.

1.4 Economic Factors

Accurate models describing OHP behavior are a fundamental need and a major barrier for wider adoption of OHPs in industry. Currently, industrial designers and users of OHPs rely on incomplete or partial models of the device's behavior, assumed initial conditions, or a body of correlations to predict a device's performance. While this approach is useful as a starting point, it is ad hoc and hinders the long-term adoption of the technology by potential future users. Higher accuracy and well characterized initial conditions, such as the initial liquid and vapor lengths and distributions, will accelerate the generation of these improved models by saving time currently spent on experimentally validating the performance of a device with assumed initial conditions against existing models. This knowledge will also reduce the cycle time involved with developing new OHP designs.

Given that OHPs present an opportunity for lighter, simpler, and more effective heat transfer mechanisms, broader adoption is expected to result in cost reduction across an extensive portfolio of applications as a superior heat transfer technology to alternatives such as copper-water wicked heat pipes and other conventional heat spreaders. One of the major barriers to this broader adoption of OHPs, however, is the lack of a comprehensive theoretical first principles model and known initial conditions. This research advances understanding in this area.

1.5 Objectives

This work explores the initial distribution of liquid segments of water in 4 mm ID × 1220 mm long quartz tubes at three fill ratios and three injection rates, representative of conditions in an OHP device. The specific objectives of the research are to understand the lengths, location, distribution, and count of liquid and vapor segments throughout the length of the channel across different fill ratios and injection rates. The data produced provides practical insight into the fill

ratio and injection rates' effect on liquid and vapor segment lengths in OHP devices, and uncovers broader trends related to key input parameters that affect this critical initial condition. This research provides more accurate, experimentally validated initial conditions for analytical models that aim to discretely model the liquid and vapor interactions in an OHP. This understanding is expected to improve the accuracy of these models in time, thus reducing the amount of burden associated with designing, validating, and integrating new OHPs, and accelerate adoption of this technology throughout the industry as a whole.

CHAPTER 2.

EXPERIMENTAL METHODS

2.1 Overview

This investigation was designed to create easily observable liquid and vapor segments in a representative OHP geometry in a lab environment. In order to accomplish this, straight borosilicate glass tubes were arranged to introduce a known volume of working fluid, ASTM Grade II deionized water, into an evacuated channel, representing an open-loop OHP configuration, at different injection rates, as shown in Figure 4. A range of fill ratios were examined, each of which were introduced to the apparatus at a range of different injection rates. The fill ratios used in these tests were representative of common design points in OHPs, however injection, or charging, rate of the working fluid into an OHP has not been previously investigated. These variables were found to have different effects on the resulting liquid-vapor distributions throughout the channels.

The total volume of the sealed glass tube region was 16 ± 0.10 mL. Nominal fill ratios, α, of 25%, 50%, and 75% that are commonly used in OHP designs were tested, which corresponded to a volume of water introduced to the sealed tube region of 4 mL, 8 mL, and 12 mL, respectively. For each α, the rate of injected water was also varied to determine the impact this variable had on the resulting liquid-vapor lengths and distribution. The results of this work describe the injection rate dimensionlessly as,

$$\nu = \frac{\dot{V}^2 \Delta\rho}{\sigma D_h^2} \quad [2]$$

where $\dot{V}$ was the volumetric injection rate of the working fluid, $\Delta\rho$ was the difference in density of the liquid and gas phase of the working fluid, σ was the surface tension of the working fluid, and D_h was the hydraulic diameter of the tube. The volumetric injection rate, $\dot{V}$, ranged from 0.10 mL/sec to 0.80 mL/sec, or ν = 0.002-0.132, and was grouped in 3 broad sets, called Slow (ν = 0.002-0.012), Nominal (ν = 0.013-0.051), and Fast (ν = 0.052-0.132) in order to more clearly describe trends based on injection rate. This will be discussed in greater detail later in this chapter.

Each set of data (fill ratio at a given injection rate range, giving nine total data sets) contained at least 30 individual tests, and each test contained dozens of liquid length data points. The experimental setup, shown in Figure 4, consisted of five horizontal borosilicate glass tubes that were each 4 mm ID × 1220 mm long and connected to a common manifold. The tubes and manifold were connected to a turbo-vacuum pump and common manifold on one end to evacuate the tubes, and each tube had a micro-metering valve (IDEX P-447) with a syringe (Norm-Ject) on the opposite end to precisely control the introduction of liquid into the tube. A mechanical stopper was placed between the barrel and plunger of each syringe to consistently control the volume of fluid introduced to the channels. These five tubes were evacuated in parallel by the turbo-vacuum pump, and were tested individually, independent of the other tubes. There were five tubes in this setup in order to increase the throughput and quantity of tests, and each tube was used to perform one test at a time.

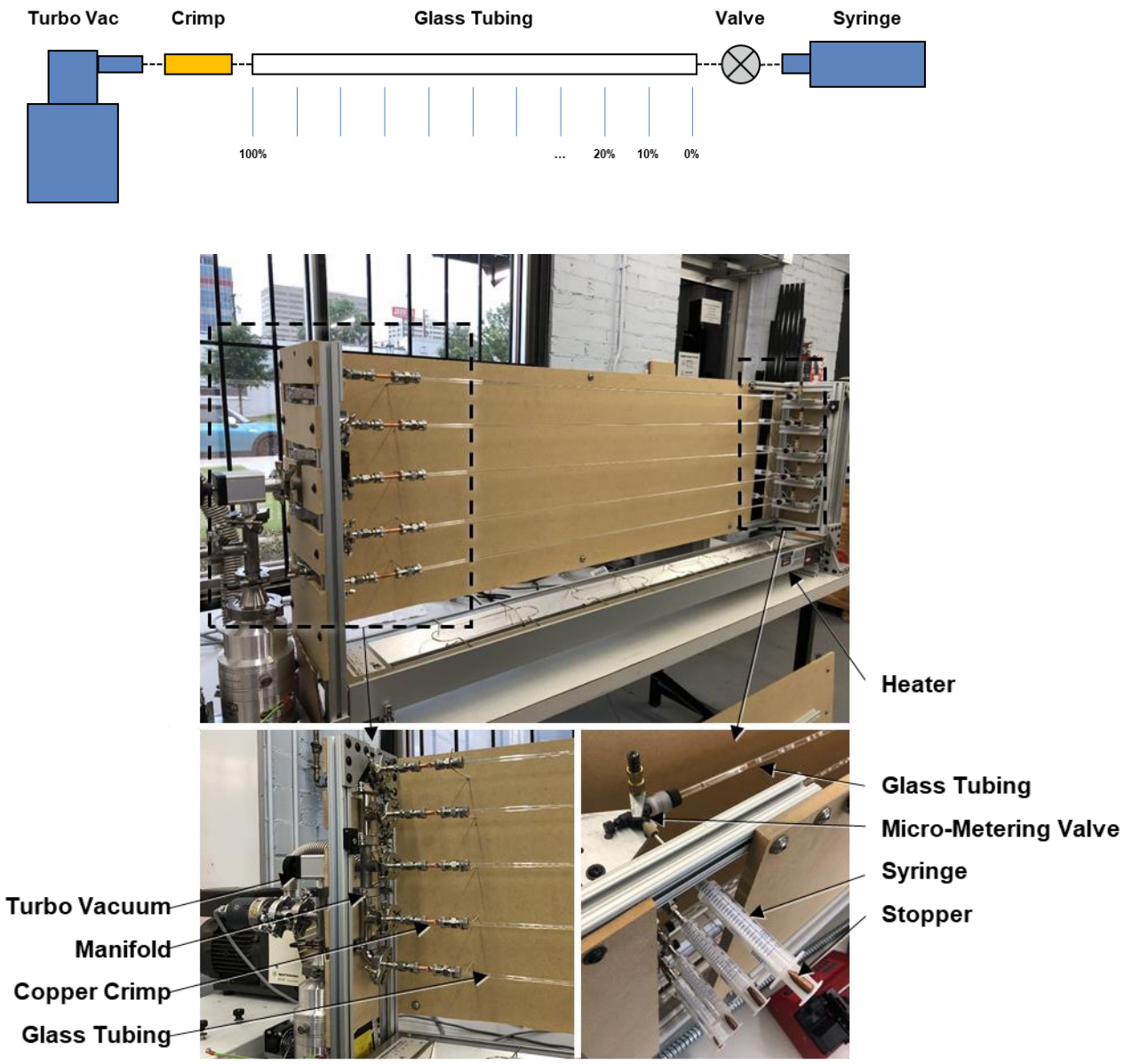

Figure 4 Test Set-Up Assembly.

2.2 Test Preparation

The test procedure involved the evacuating the tubes, sealing one end of the open loop, and then exposing the desired volume of working fluid to the evacuated sealed tube before

sealing the other end of the open loop where the water was introduced. There are several methods of introducing working fluids to an OHP, such as filling 100% and evacuating small volumes of working fluid to a negative pressure environment until the desired fill ratio (or mass) is obtained, and other methods as described by Ma [8]. The method that is used in industry can vary depending on the make-up and intent of the device (engineering or lab use, low-rate production, or high-rate (1000s of units) serial production). The filling method this work used was representative of a high-quantity production charging method used in industry due to the relatively fast nature of the fill process.

To prepare the working fluid for the test, deionized ASTM Type II water was "deaerated" in a flask that was sealed from the atmosphere, as shown in Figure 5. Though water is inherently challenging to completely degas, this deaeration procedure was found to improve the nature of the working fluid for the test by removing small bubbles from the water that were evident during the test and in the syringe prior to injection into the tube, as shown in Figure 6. The deaeration procedure involved exposing the water located in the sealed flask to a mild vacuum (approximately 1×10^{-3} mbar) for 30 minutes at room temperature with a slow spinning bar to agitate and assist air removal from the water. No heat was applied to the water during the deaeration process. During the deaeration, a significant amount of air bubbles was typically observed as being evacuated from the water, and over time the amount of air bubbles observed as being evacuated gradually declined and then stopped, which indicated the water had been deaerated. Though the process and controls do not qualify as a complete "degassing" of the liquid, this step reduced the number of bubbles that would otherwise be injected into the tube and improved the fidelity of the resulting measurements.

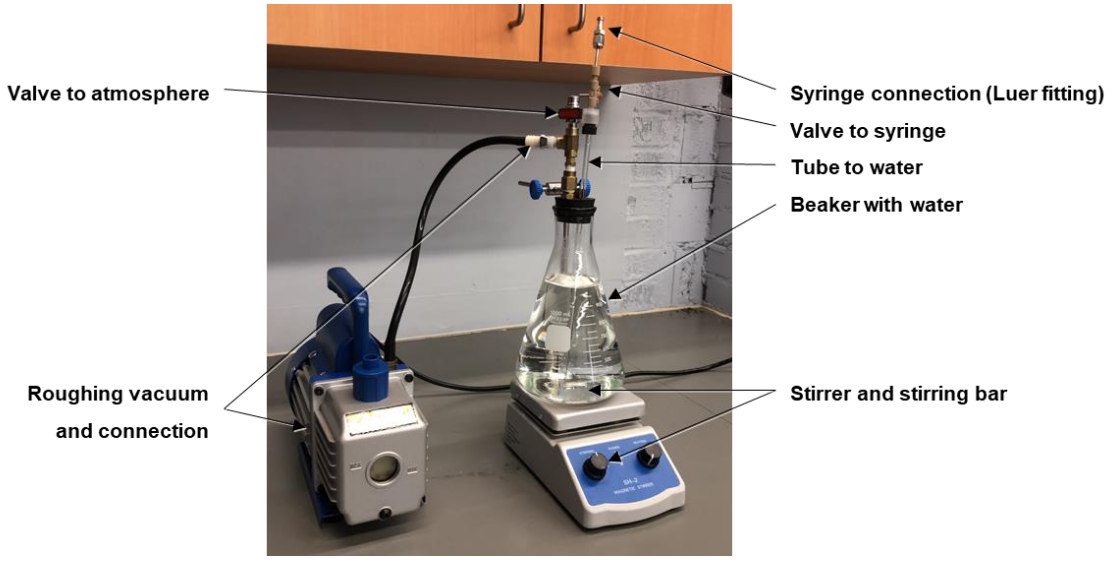

Figure 5 Deaeration Station.

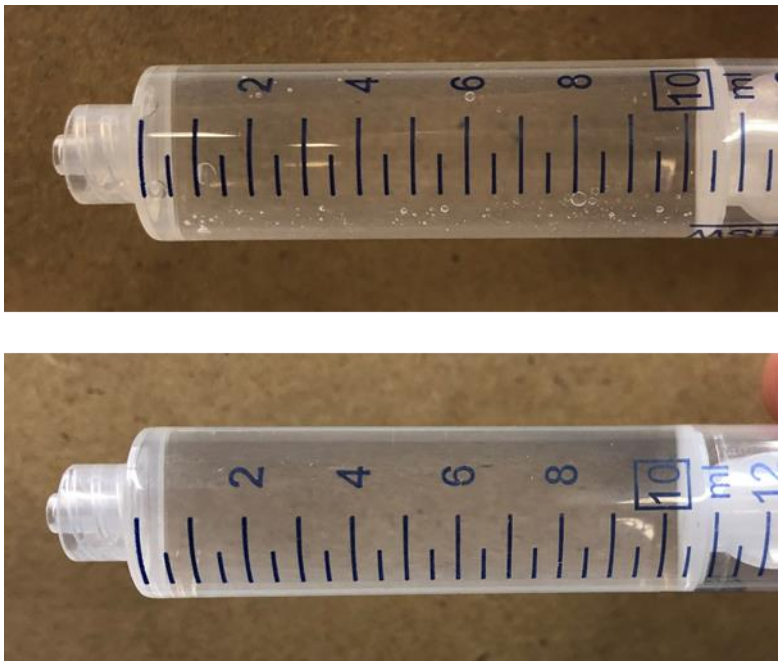

Figure 6 Syringe and liquid with no deaeration (top) and syringe with deaeration (bottom).

After deaeration was completed, the vacuum was disconnected from the deaeration station. The flask was then returned to atmospheric pressure by opening the valve to atmosphere before the desired amount of water was pulled into a new, single-use plastic syringe and attached to the station via a Luer lock fitting, shown in Figure 5. This was repeated until a total of 5 syringes were filled with the desired amount of water for each tube position. These water-filled syringes were then connected to the valve-end of the glass tubes and purged through the valve to ensure no air remained in the injection path between the valve and the syringe, shown in Figure 4. A stopper was then placed on the plunger of the syringe to ensure a precise volume of fluid was injected into the tube during each test, shown in Figure 4.

On the opposite end of the tube that connects to the manifold and turbo-vacuum, a short piece of consumable 4.0 mm ID × 6.2 mm OD soft-copper tube was installed and connected to the glass tube using a Swagelok UltraTorr union fitting comprised of an o-ring gland seal. This copper tube was later crimped prior to performing the test to hermetically seal the tube from the turbo-vacuum and other tubes connected to the common manifold. This consumable copper tube and crimp method was used instead of a valve due to faster evacuation through a wider opening.

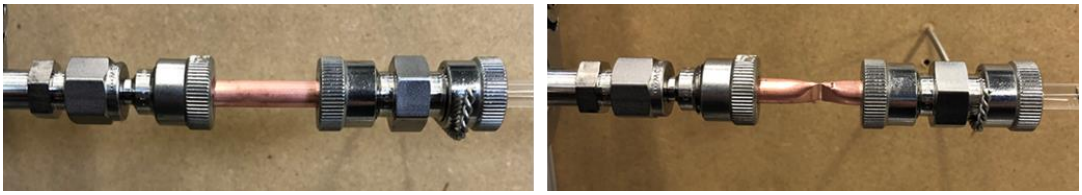

Figure 7 Un-crimped (left) and crimped (right) copper tube.

The assembled tubes with filled syringes and fresh copper installed are shown in Figure 4. All five tubes, connected by the common manifold to the vacuum pump, were evacuated in parallel for a minimum of 18 hours using the turbo-vacuum with rotary vane backing pump. The tubes were also exposed to 4 hours of moderate heating (50-60 ºC) during the evacuation period from a heater located underneath the tubes in order to assist with the desorption of residual water and gas from previous tests remaining on the inside surface of the tubes.

To arrive at this evacuation methodology, a set of experimental studies were performed to determine the duration at which the system achieved its lowest steady-state pressure. These tests were performed with an Agilent Pirani Vacuum Full Range Pressure Gauge (FRG-700KF25) first at the neck of the turbo, and then at the far-end of the glass tube to identify each side's lowest steady-state pressure as a function of time, as shown in Figure 8.

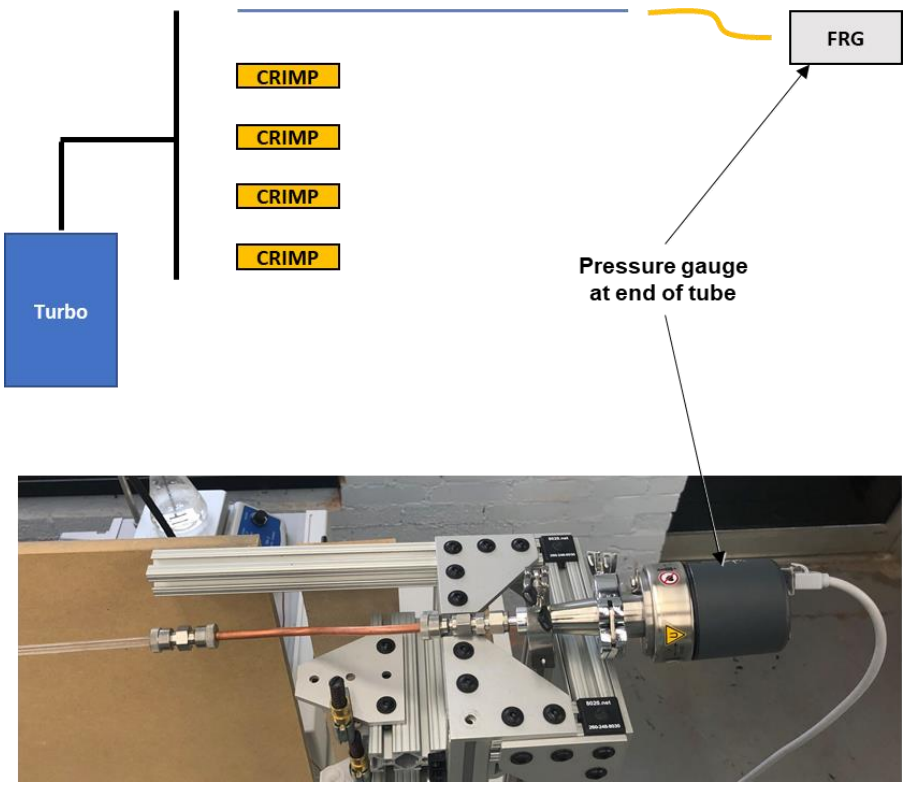

Figure 8 Evacuation Pressure Test Set Up.

The pressure at the neck of the turbo was naturally lower than the pressure at the valve-end of the set up due to conductance through the 4 mm ID glass tube and several differences in performance limits of the different vacuum seals and o-rings throughout the assembly of manifolding and fittings [44]. The steady-state pressure was achieved after 18 hours, indicated by the blue dashed line in Figure 9 Evacuation pressure measurements with gauge at the valve-end of the tubing. below, and was found to be on the order of 1×10^{-6} mbar at the neck of the turbo, and 1×10^{-4} mbar at the valve-end of the apparatus. This knowledge provided a baseline measure of goodness for the pressure of the system before running each test, namely, that if the pressure reading at the neck of the turbo was on the order of 1×10^{-6} mbar then the integrity of the apparatus and evacuation procedure had been successful, permitting for a test to proceed.

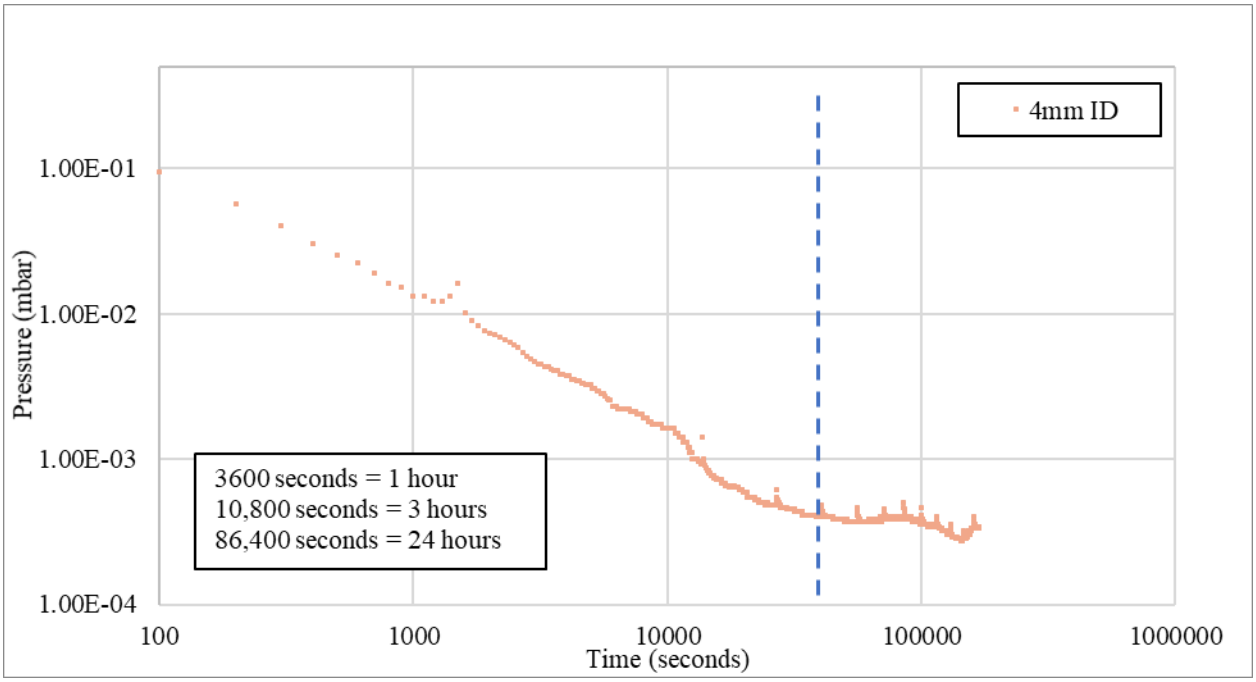

Figure 9 Evacuation pressure measurements with gauge at the valve-end of the tubing.

Details around evacuation procedures are often under-reported for OHPs and are important for controlling the amount of non-condensable gas (i.e., air) in the system during operation [8], [16]. Non-condensable gasses in the system can adversely affect the evaporation and condensation of the working fluid within an OHP, and should be carefully considered during the manufacturing of any OHP design.

2.3 Test Method

To perform each test, the copper tube on the turbo-side of the apparatus was crimped using a cold-weld crimp device (IdealVac P108191) to hermetically segregate the tube from the turbo, creating a sealed test region in the glass tube from between this crimp joint to the closed valve on the opposite end, as shown in Figure 4. On the valve end with the syringe, water was introduced to the desired fill ratio and the injection rate to the sealed glass tube was controlled by opening the micro-metering needle valve. Once the valve was opened, water was pulled freely, as opposed to being pushed or otherwise controlled by a syringe pump metering the injection, into the evacuated tube. The syringe pump method was explored, however there were challenges with its implementation and the resulting liquid-vapor distributions proved to be qualitatively different.

The micro-metering needle valve was opened by hand and the injection rate was controlled manually by opening the needle valve to specific positions. The injection rate was verified and timed by a video recording of a dial indicator measuring the syringe hammer as it moved when the valve was opened. It was observed and verified by measurements from a slow-motion camera that the injection rate was nearly-constant throughout all fill ratios and injection rates, so only average injection rates were measured and reported. Once the hard stopper on the

syringe was engaged, indicating the correct volume of fluid had been introduced into the system, the valve was closed to re-seal the tube.

2.4 Data Collection Method

The resulting liquid-vapor distribution was recorded photographically and the positions and lengths of the liquid slugs were measured from the images using FIJI/ImageJ software [45]. To help correct for parallax in the image, the FIJI measurements were re-calibrated every 250 mm along the tubes, as shown in Figure 10.

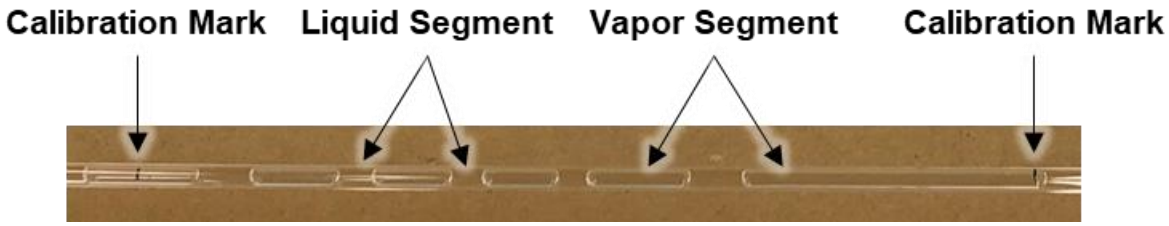

Figure 10 Exemplary Section of Test Image for Measurement.

When selecting the point to measure for the ends of each liquid segment, the mid-point of the segment in the tube cross-section was used. Other criteria for measurements included only measuring fully-formed liquid segments, i.e., liquid that was pooled at the bottom of the tube was not measured, which typically only occurred in the early portion of the tube prior to the location of liquid segment formation during each test. A representative amount of liquid that was typically observed in this region is shown below in Figure 11, and appeared to be an artifact of how the water entered the tube on the bottom of the glass prior to forming a full liquid segment, occurring mostly in the first 100 mm into the glass tube. Additionally, small bubbles in a liquid segment that did not form a full vapor segment were not measured.

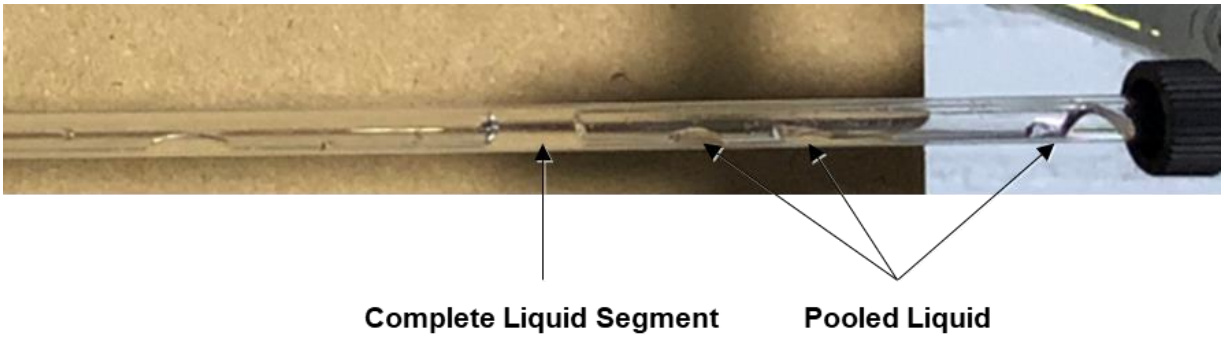

Figure 11 Complete Liquid Segment and Pooled Liquid.

After the results of each test were measured, the liquid segment length was converted to a volume and compared to the intended fill ratio volume as verification of the measurements. Though the length of the glass tube was 1220 mm and the total volume between the crimp and valve was measured to be 1273 mm, there was only 1178 mm of visible glass length once the attaching fittings were subtracted out. When comparing the sum of the liquid segment lengths to the fill ratio, the volume of the visible region (14.8 mL) was used instead of the full volume of the system (16 mL) with the assumption that liquid and vapor were similarly distributed in the non-visible regions covered by fittings. FIJI measurements verified in this way were used as an indicator of cases that needed to be remeasured.

Two types of error related to the measurements were considered: (a) repeatability (precision) of the measurements taken by hand using ImageJ, and (b) error from parallax, or differences in camera position angle to record the image.

Repeatability was determined by measuring liquid-vapor edges in the same tube five times consecutively, resulting in a total of 220 independent liquid segment length measurements.

Each of the five different measurements of the same tube were compared to determine the difference in measured length for corresponding liquid segments. This resulted in an average difference between measurements (the average difference of each liquid segment measured five times, averaged together) of 0.42 mm, or approximately 4.2% of the average liquid segment length. The standard deviation of the differences in liquid segment length was 0.32 mm, or 3.2% of the average liquid segment length.

Error from parallax was determined by varying the position of the camera used to take the images, as shown with approximate angles in Figure 12. The camera angles used for this error measurement were representative of worst-case scenarios, and markings on the floor were used for repeatable camera placement during each test. The measurements of the same tube at the five camera positions were compared to one another to generate average and standard deviations of differences in liquid segment length for each camera position. This resulted in an average difference in measurements of 0.66 mm, or 6.6% of the average liquid segment length. The standard deviation of the differences in liquid segment length was 0.49 mm, or 4.9% of the average liquid segment length. The resulting error from parallax was slightly higher than that of the repeatability error. The difference between the average measurements from each of the five camera positions to each other were consistent with the overall average and standard deviation of the parallax error measurements, i.e., measurement error due to parallax between each of the five positions was not shown to be significantly different for any given position and the difference between 0 and 15 degrees and 0 and 30 degrees was not significantly different.

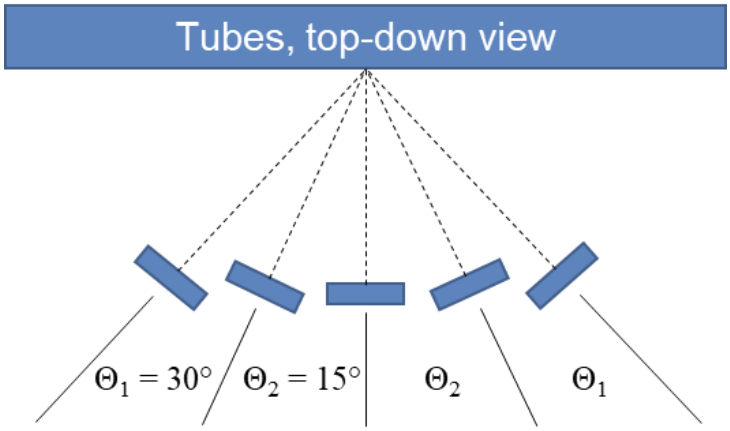

Figure 12 Five camera positions to measure parallax, top-down view.

CHAPTER 3.

RESULTS

3.1 Experimental Data

The primary parameters of interest are the lengths and distribution of the liquid segments formed in the tube. The liquid segment lengths were described dimensionlessly as,

$$\eta = \frac{L}{D_h} \quad [3]$$

where L is the length of the liquid segment and D_h is the hydraulic diameter of the tube.

In addition to measuring η for each liquid slug, the far-position of each liquid slug (side of the slug facing the crimp) as a fraction of the tube length, r, was determined. Both η and r were determined for the given fill ratio, α, and dimensionless injection rate, ν. Additionally, the dimensionless liquid segment count, k, was determined and is described later in section 3.1.4.

All data were collected in an indoor lab environment, with temperature ranging from 20-27°C and at atmospheric pressure.

3.1.1 Length vs Location

The liquid segment lengths across tests from all injection rates were compared with respect to each liquid segment's location in the tube. The graphs below summarize the results of the liquid length and distribution in the 4.00 mm ID tube ($Bo = 2.07$) for the α = 25, 50, and 75% tests. Each injection rate, ν, range is shown in a different color, grouped in three categories called Slow (ν = 0.002-0.012, or 0.10-0.24 mL/sec), Nominal (ν = 0.013-0.051, or 0.25-0.49 mL/sec), and Fast (ν = 0.052-0.132, or 0.50-0.80 mL/sec). The scatter plots below, Figure 13-15, graphs all individual liquid lengths, η, as a function of position relative to the length of the tube,

r, and the yellow line shows the trend in the average η, with error bars indicating the standard deviation for each 10% increment in r.

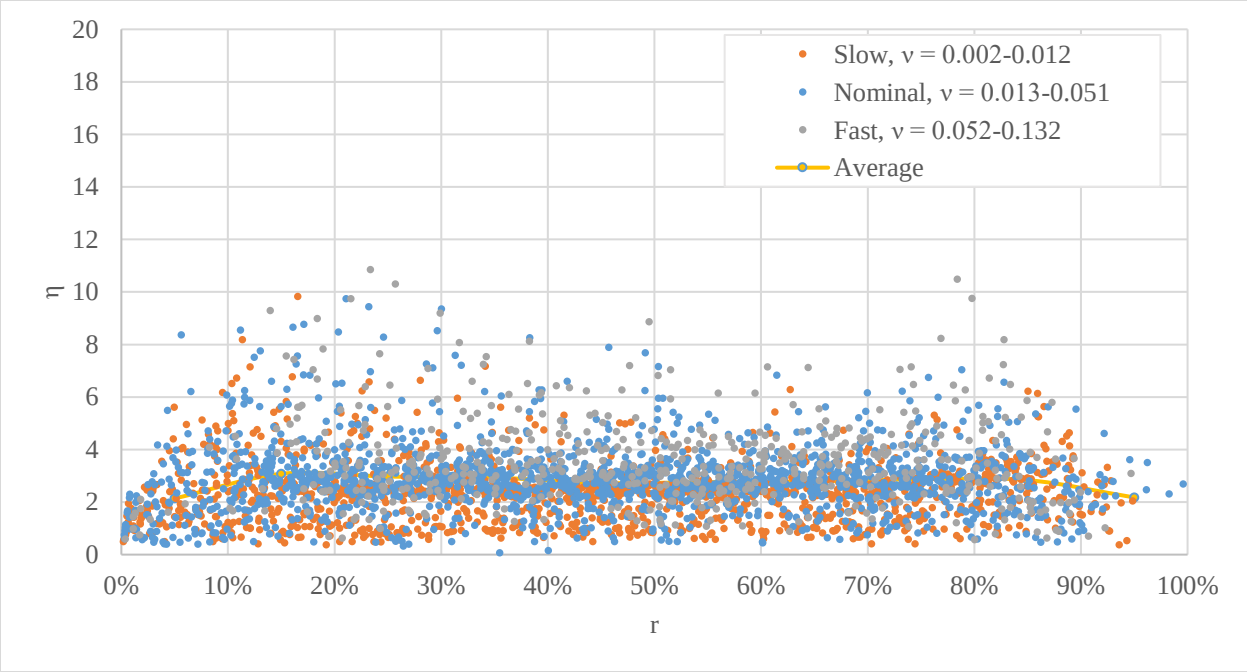

(a)

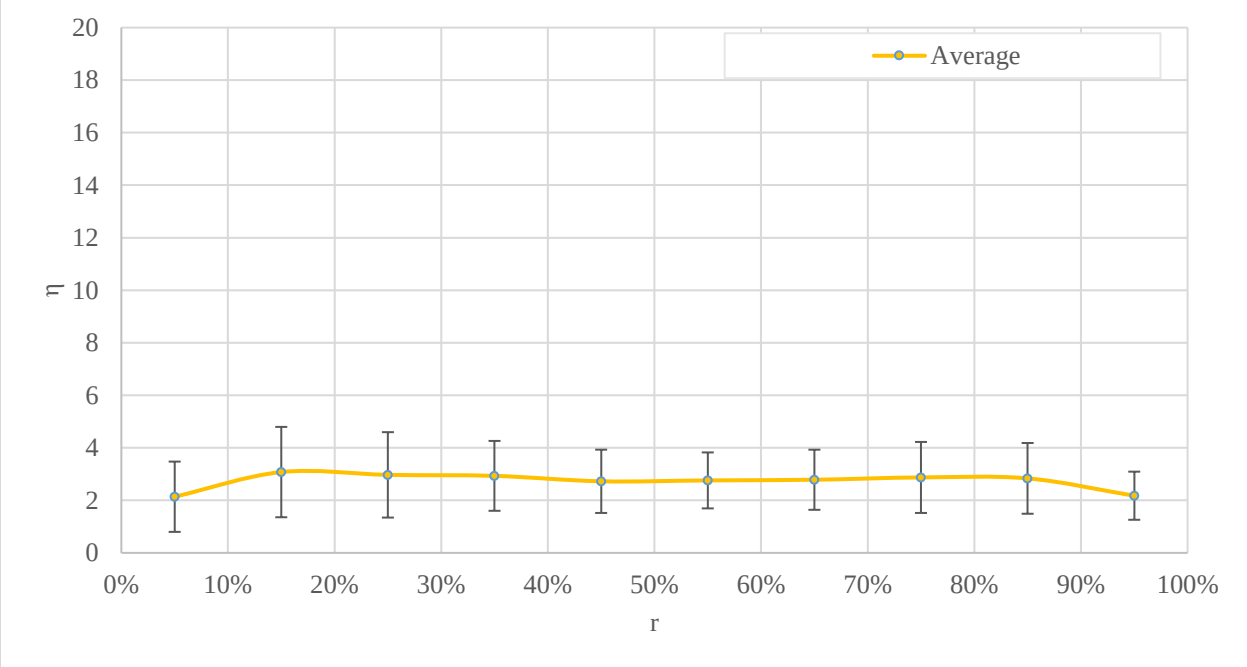

(b)

Figure 13 (a) η distribution for all ν ranges at α = 25%, (b) average η for each 10% increment in r at α = 25% (error bars indicate standard deviation).

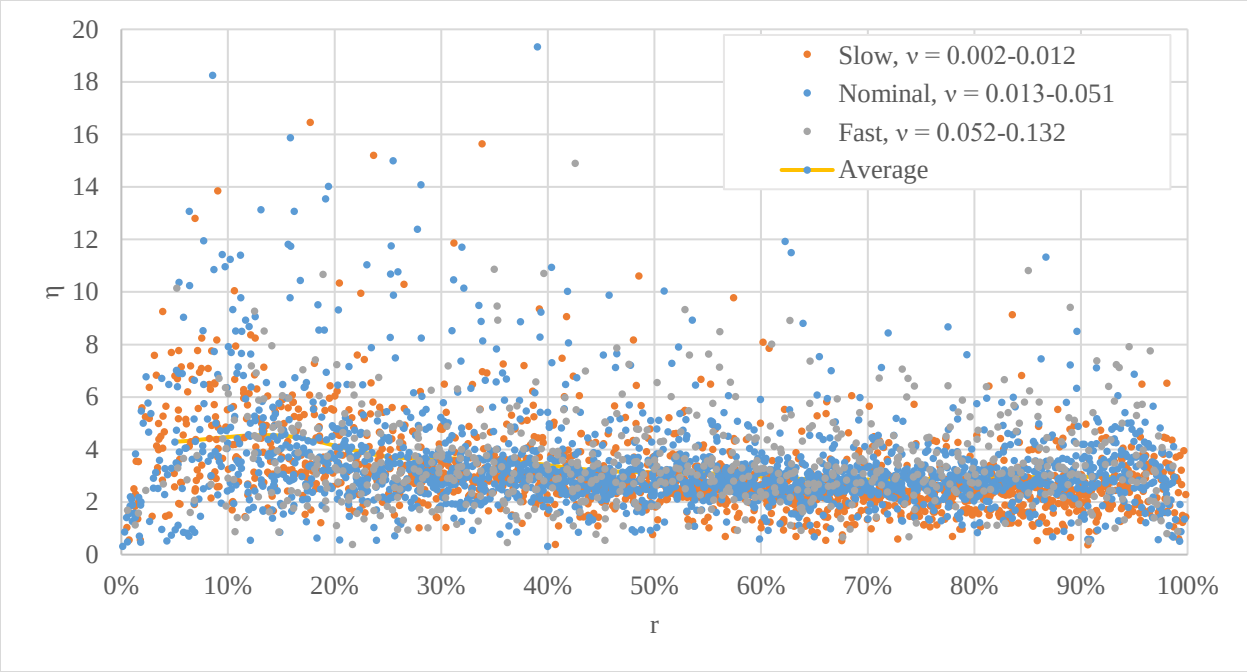

(a)

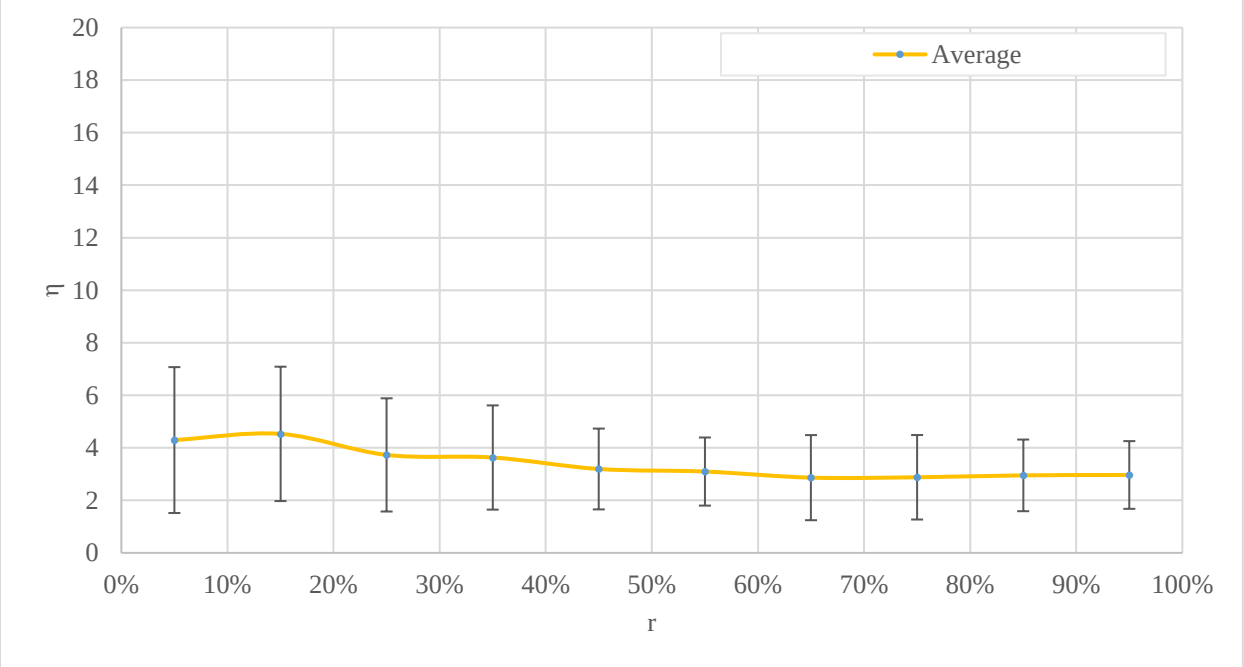

(b)

Figure 14 (a) η distribution for all ν ranges at α = 50%, (b) average η for each 10% increment in r at α = 50% (error bars indicate standard deviation).

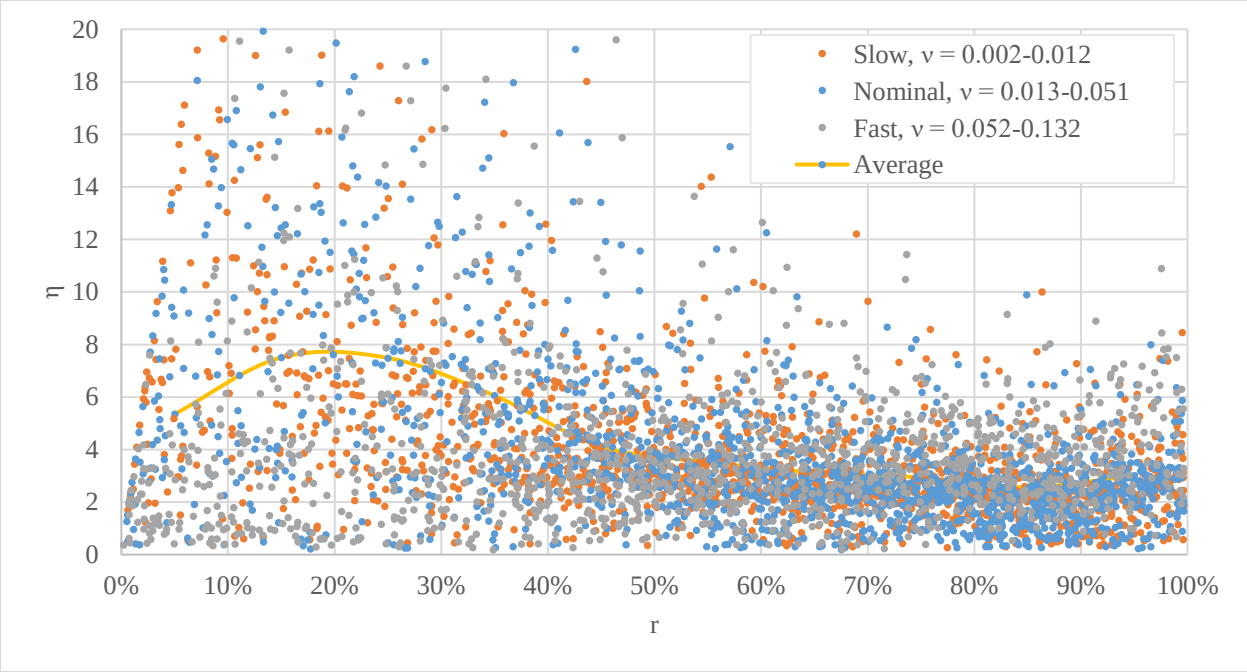

(a)

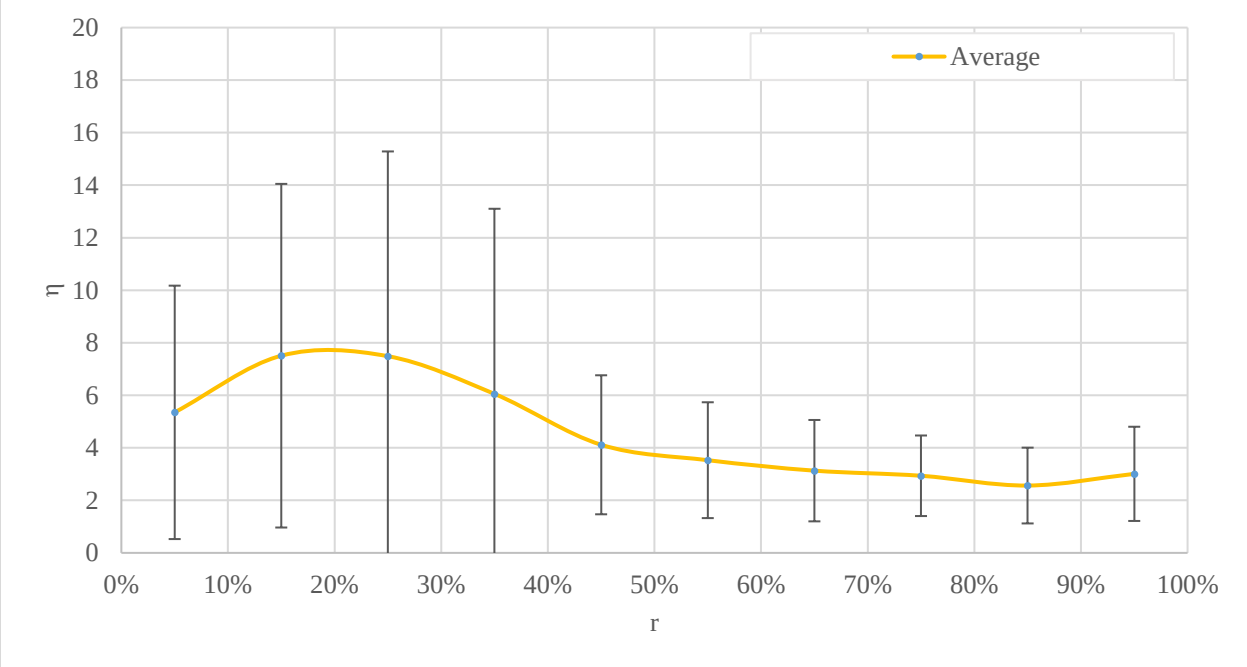

(b)

Figure 15 (a) η distribution for all ν ranges at α = 75%, (b) average η for each 10% increment in r at α = 75% (error bars indicate standard deviation).

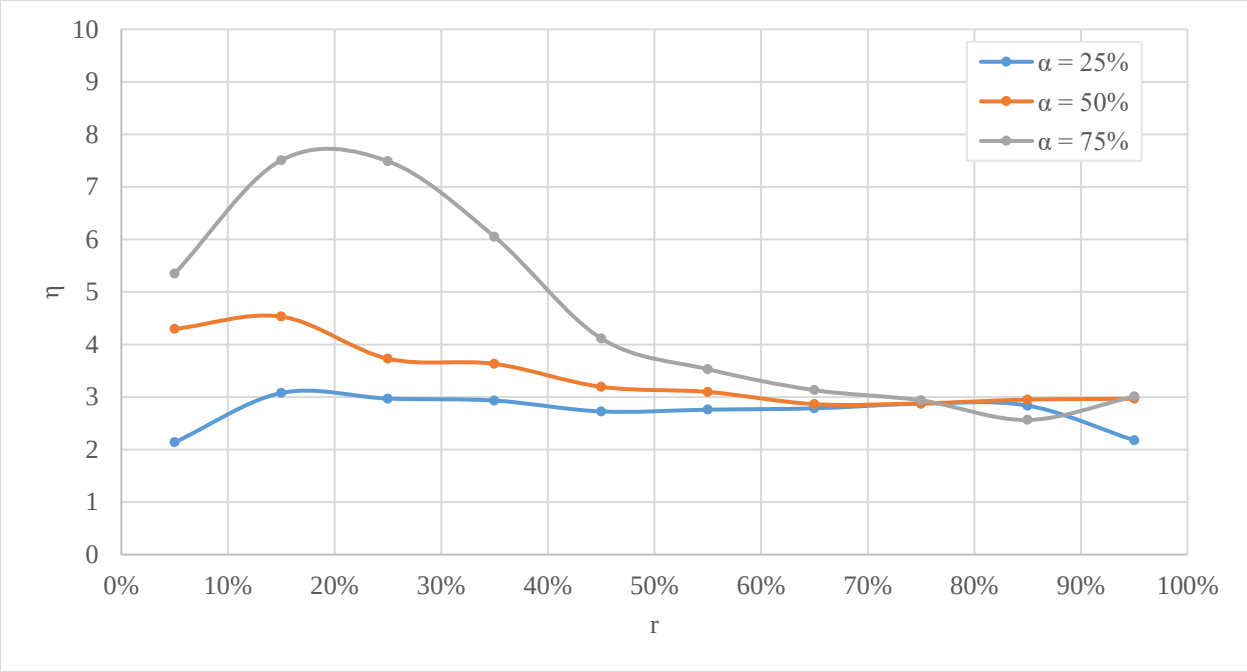

Figure 16 Summary of average η for α = 25%, 50% and 75%.

Table 1 Summary of average η for α = 25%, 50% and 75%.

	α = 25% Avg η / std dev	α = 50% Avg η / std dev	α = 75% Avg η / std dev
Slow (ν = 0.002-0.012)	2.48 / 1.09	3.06 / 2.04	3.60 / 4.04
Nominal (ν = 0.013-0.051)	2.95 / 1.19	3.30 / 1.79	4.02 / 4.87
Fast (ν = 0.052-0.132)	3.54 / 1.68	3.59 / 2.19	4.06 / 3.55
All (ν = 0.002-0.132)	2.86 / 1.31	3.26 / 1.99	4.04 / 4.13

Comparing Figure 13 (a) η distribution for all ν ranges at α = 25%, (b) average η for each 10% increment in r at α = 25%Figure 13-(b)

Figure 15, and

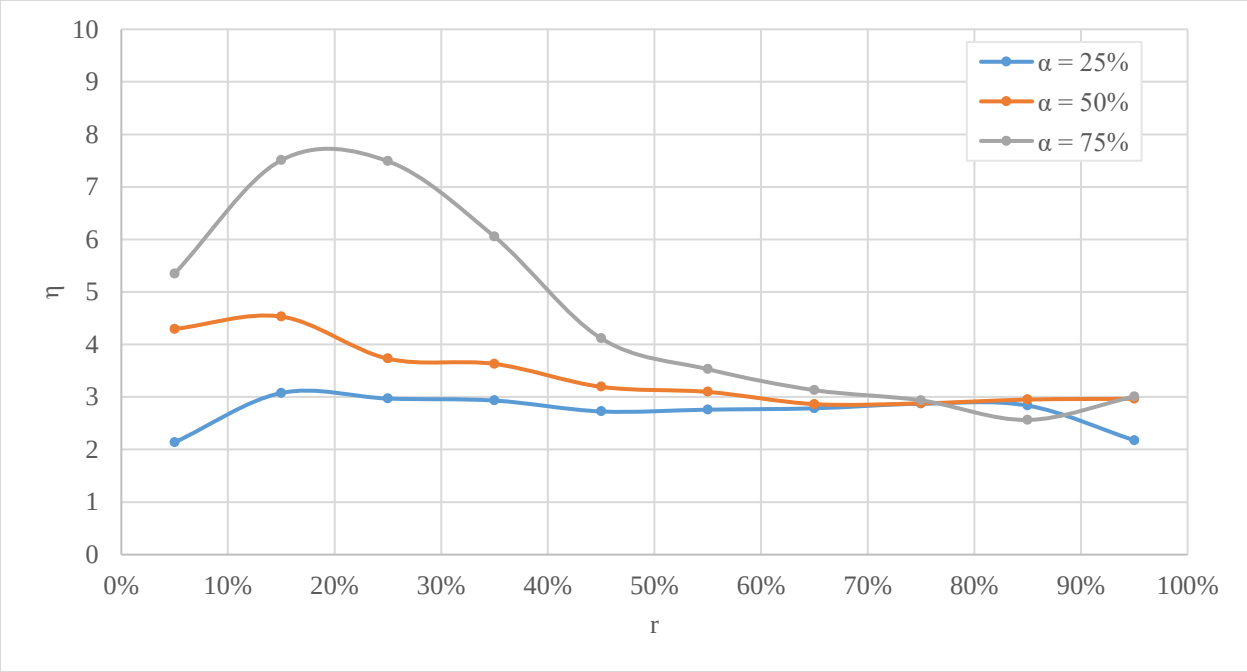

Figure 16 Summary of average η for α = 25%, 50% and 75%.

Table 1 reveals interesting trends. First, all three α fill ratios show a common average length near η = 3.0 at some point in their r distribution. The η = 3.0 value was most consistent throughout the α = 25% tests, and seemed to get pushed to the right for the α = 50 and 75% tests. During the tests, it seemed that once the initial liquid segments introduced to the tube had traveled to the end of the tube near the crimp, the remaining liquid being injected had a much greater variability in length, and a higher average length. The critical fill ratio at which the liquid reached the far end of the tube appeared to be between α = 25 and 50%, after which point any

new liquid introduced was longer on average with a wider distribution in length. This was observed in the earlier location of the tube (lower r values) of the higher α tests. This was observed on Figure 13-15, and can be described as a "compression effect" of liquid and vapor segments further down-tube, resulting in higher η values of newly-entering liquid, starting at low r and moving from left to right as α increases.

Described in Figure 16, a different way to compare the η distributions across α can be to think of the last two-thirds of the α = 75% tests representing the entirety of the α = 50% tests, and the last one-third of the α = 75% tests representing the α = 25% results. Similarly, the last half of the α = 50% tests represent the entirety of the α = 25% tests. From this interpretation, increasing α makes the tube appear effectively shorter.

The higher η values and greater variability at higher fill ratios near the entrance region may have occurred due to the vapor springs throughout the tube beginning to compress between the liquid segments, affecting the dynamics of the liquid segment formation near the entrance of the tube. The regular, consistent production of the liquid-vapor segments, resulting in a train, may have been affected as a force on the far end of the tube pushed back on the train. Though an increase in pressure in the vapor segments as the tube fills may be discernable by observing the menisci evolution throughout the injection, we did not measure this directly during each test. Practically, it appears that fill ratios at or below 25% can be modeled with an η value near 3.0 throughout the entirety of the channels, and fill ratios greater than 50% should consider using a variable distribution of liquid segment lengths that changes based the fluid's r location in the channel.

Also, at higher fill ratios once the vapor segments began to compress, the liquid segments did not collapse and join together. In one test that filled the tube to α of 100%, the vapor segments maintained their individual original length throughout the duration of the test until α of 100% was approached, where the vapor segments gradually became smaller and smaller, and eventually collapsed as α approached 100%.

A more detailed comparison of the η values for each α is shown below in Figure 17-19.

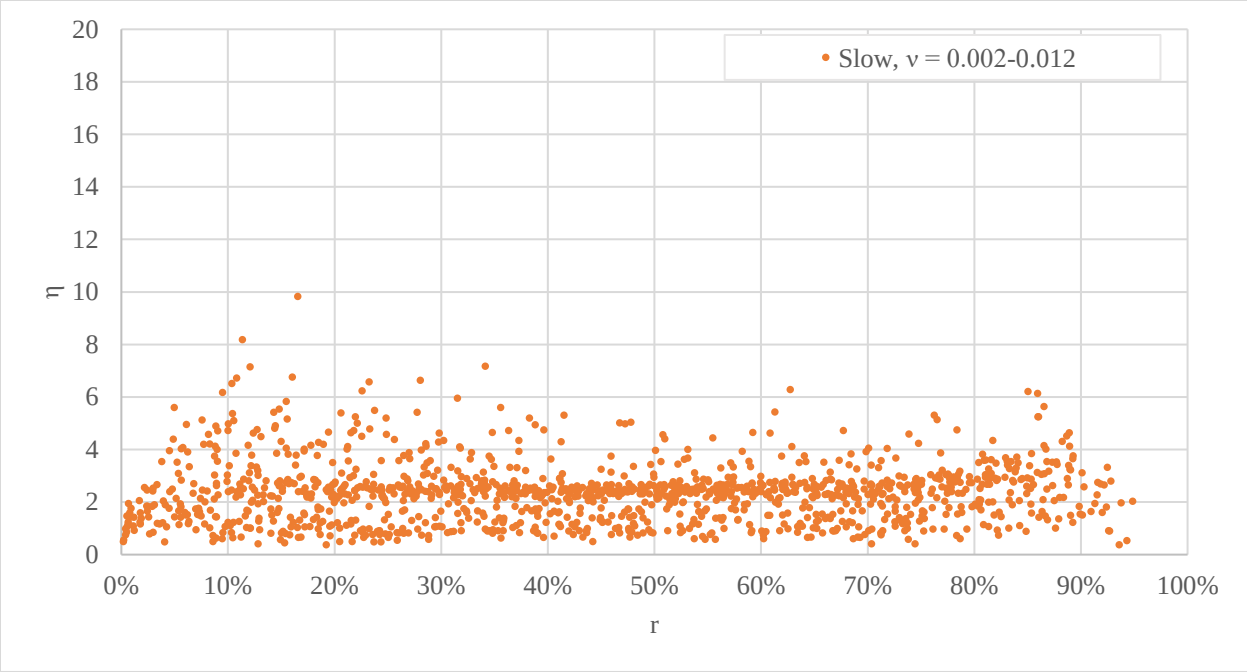

(a)

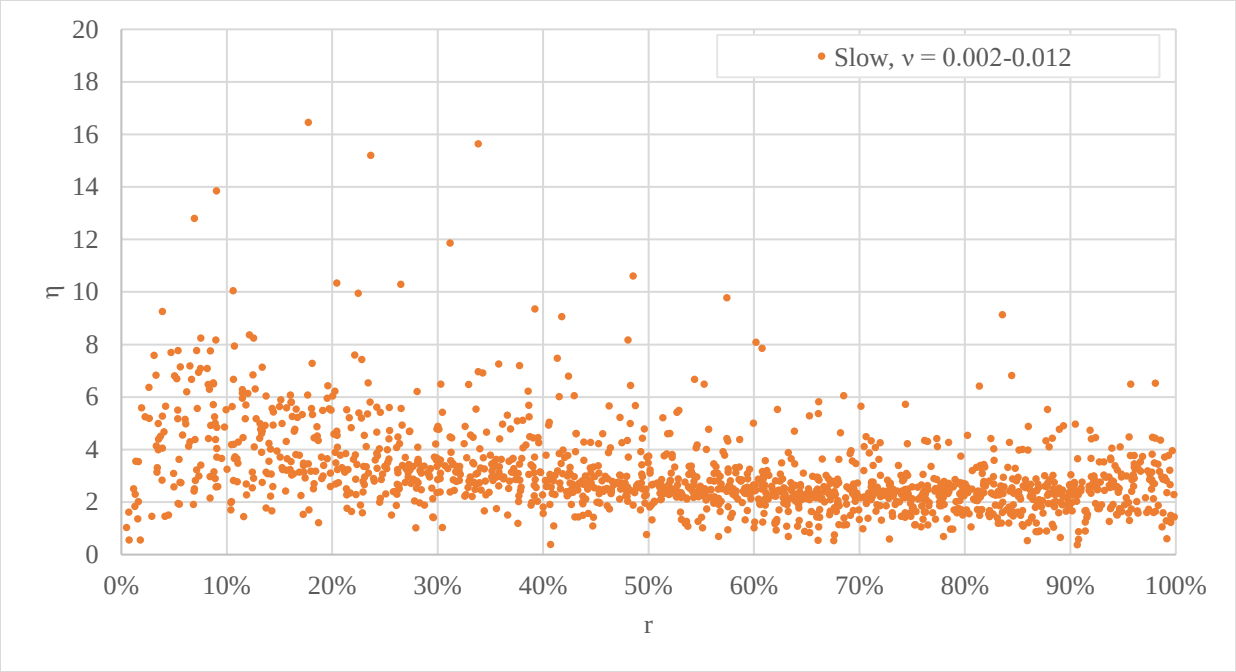

(b)

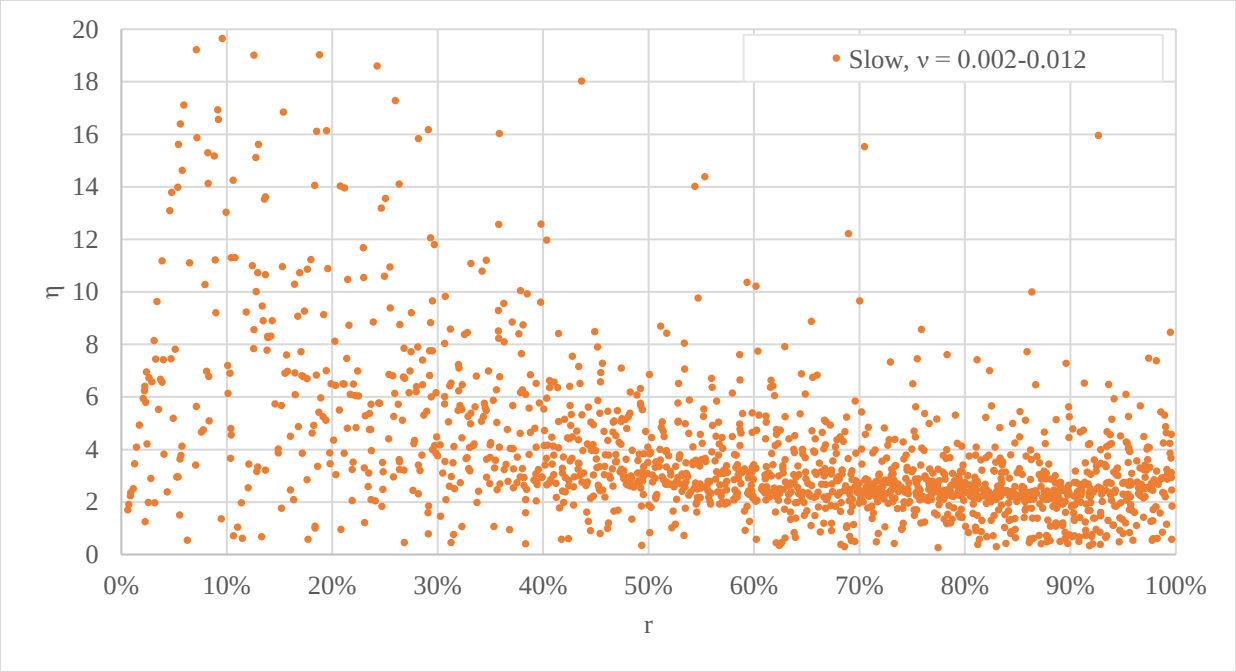

(c)

Figure 17 η distributions at the Slow (ν = 0.002-0.012) injection rate for (a α) = 25%, (b) α = 50%, and (c) α = 75%.

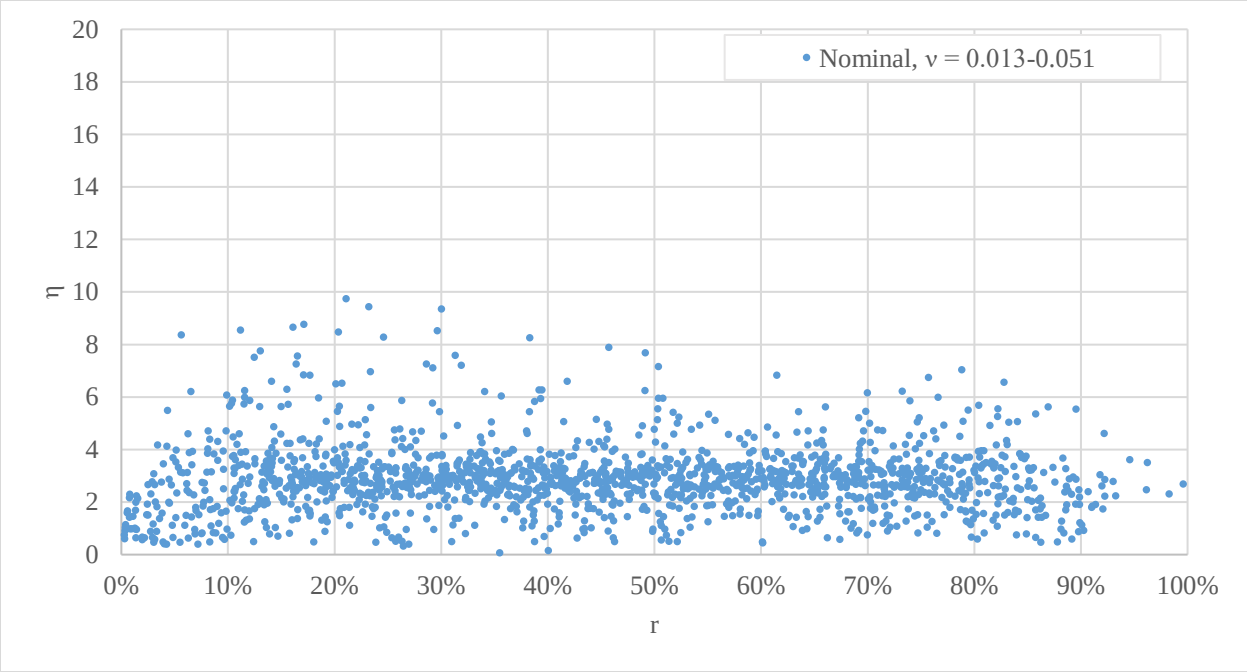
Nominal, ν = 0.013-0.051
η
r
0
2
4
6
8
10
12
14
16
18
20
0%
10%
20%
30%
40%
50%
60%
70%
80%
90%
100%

(a)

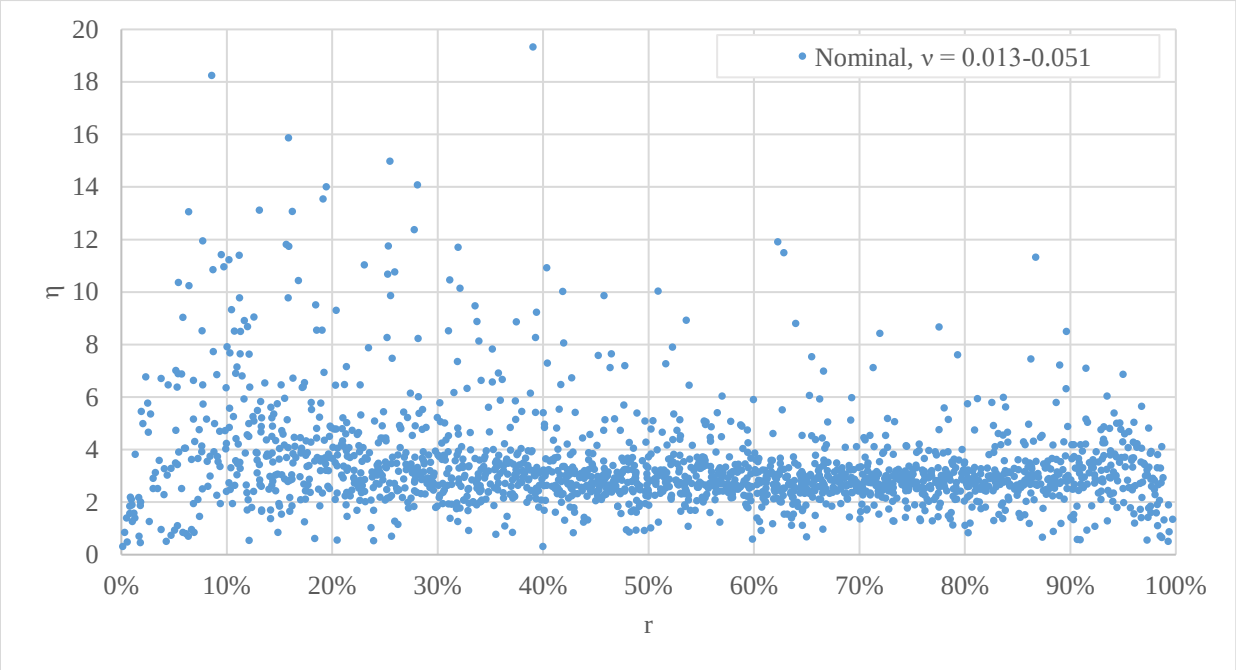
Nominal, ν = 0.013-0.051
η
r
0
2
4
6
8
10
12
14
16
18
20
0%
10%
20%
30%
40%
50%
60%
70%
80%
90%
100%

(b)

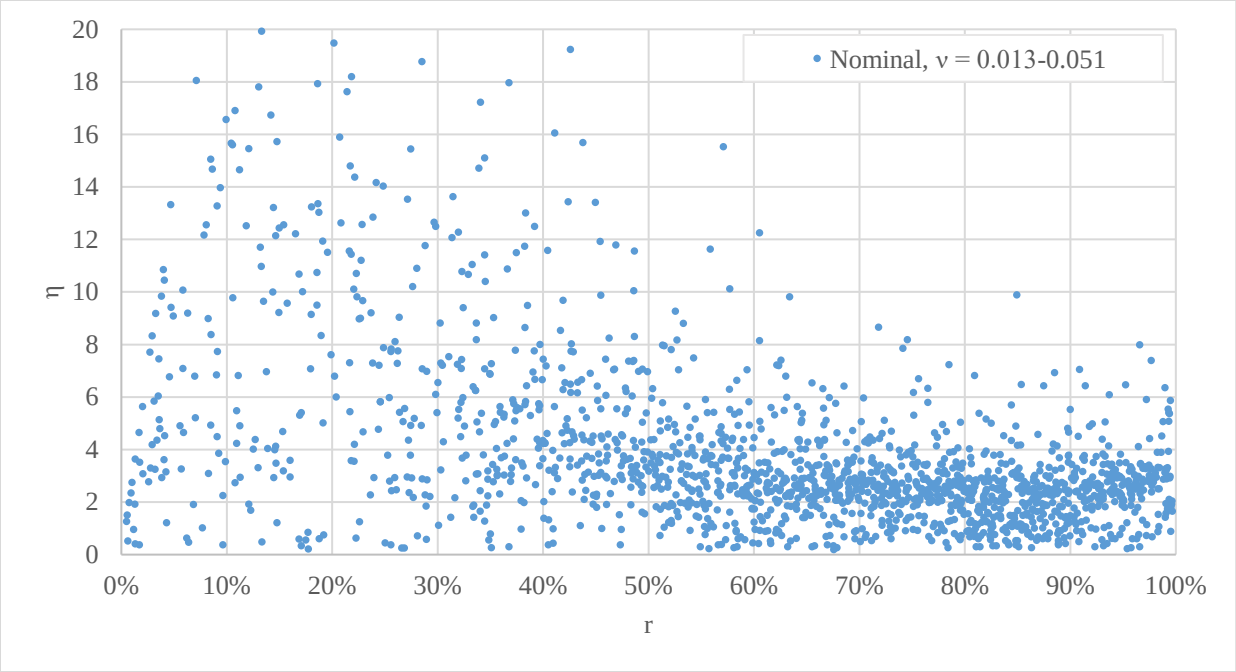

(c)

Figure 18 η distributions at the Nominal (ν = 0.013-0.051) injection rate for (a) α = 25%, (b) α = 50%, and (c) α = 75%.

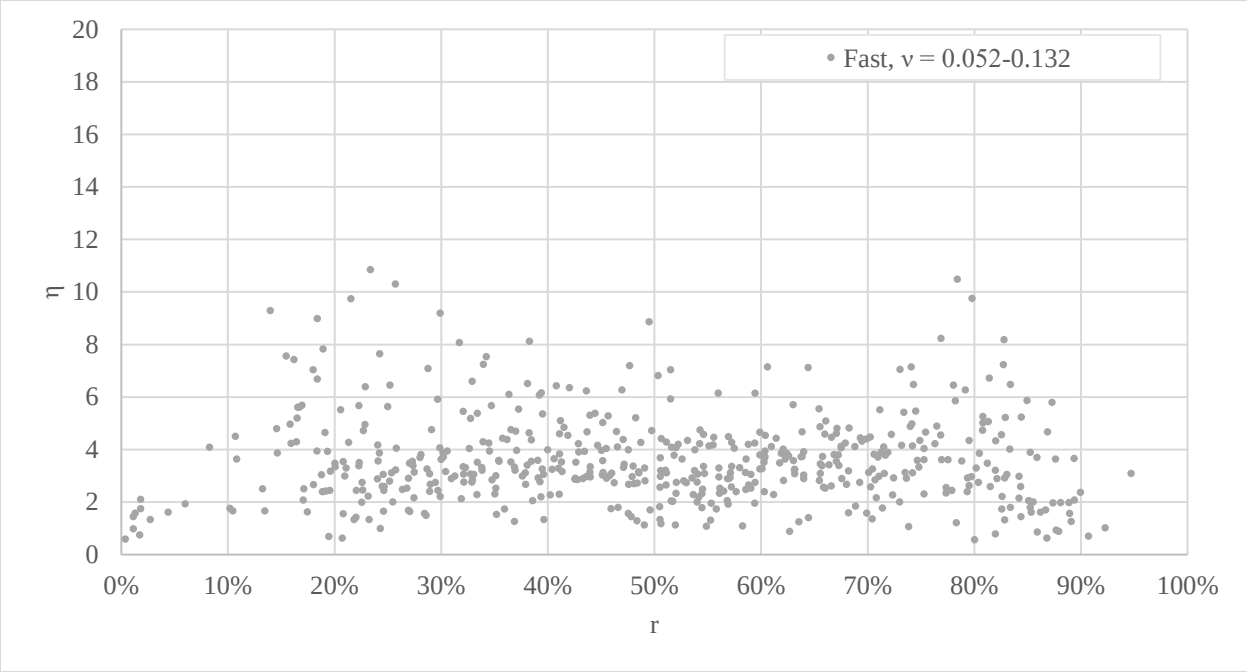
Fast, ν = 0.052-0.132
η
r
0
2
4
6
8
10
12
14
16
18
20
0%
10%
20%
30%
40%
50%
60%
70%
80%
90%
100%

(a)

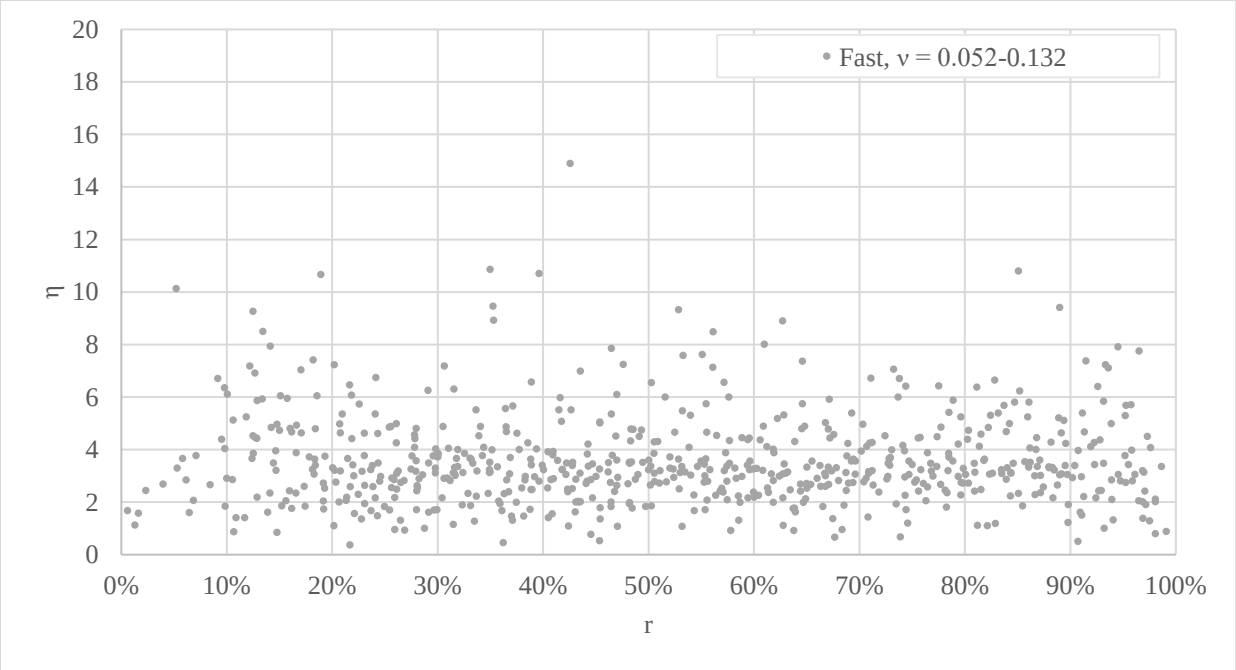
Fast, ν = 0.052-0.132
η
r
0
2
4
6
8
10
12
14
16
18
20
0%
10%
20%
30%
40%
50%
60%
70%
80%
90%
100%

(b)

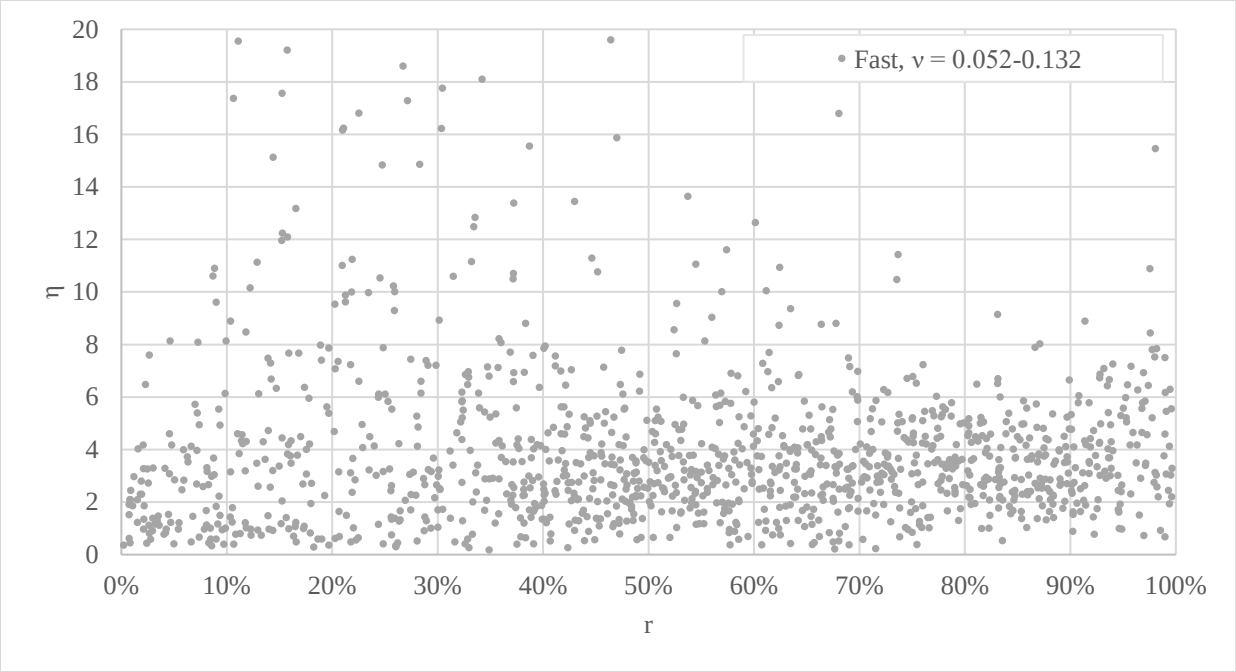

(c)

Figure 19 η distributions at the Fast (ν = 0.052-0.132) injection rate for (a) α = 25%, (b) α = 50%, and (c) α = 75%.

These graphs show in more detail the trends of average η values for the given ν. Slower ν values lead to less variability and shorter average η values, and faster ν values lead to greater variability and longer average η values. The "compression effect" is somewhat less evident in the higher ν tests due to greater overall variability in the results.

3.1.2 Distribution of Lengths

The distribution of η for all liquid slugs in the tube was also compared for each fill ratio and ν, as shown in Figure 20. The percent distribution of η was not symmetric around the

highest probability case, but instead showed a more right-skew distribution, as can be expected since negative values are not allowed.

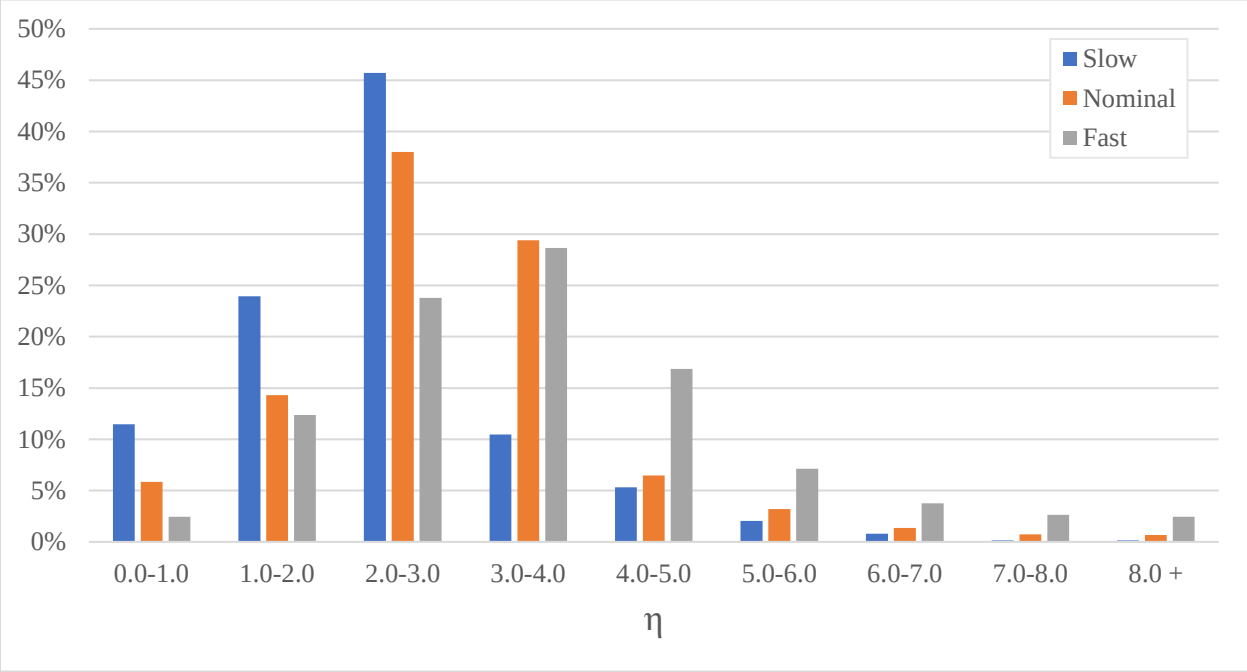

(a)

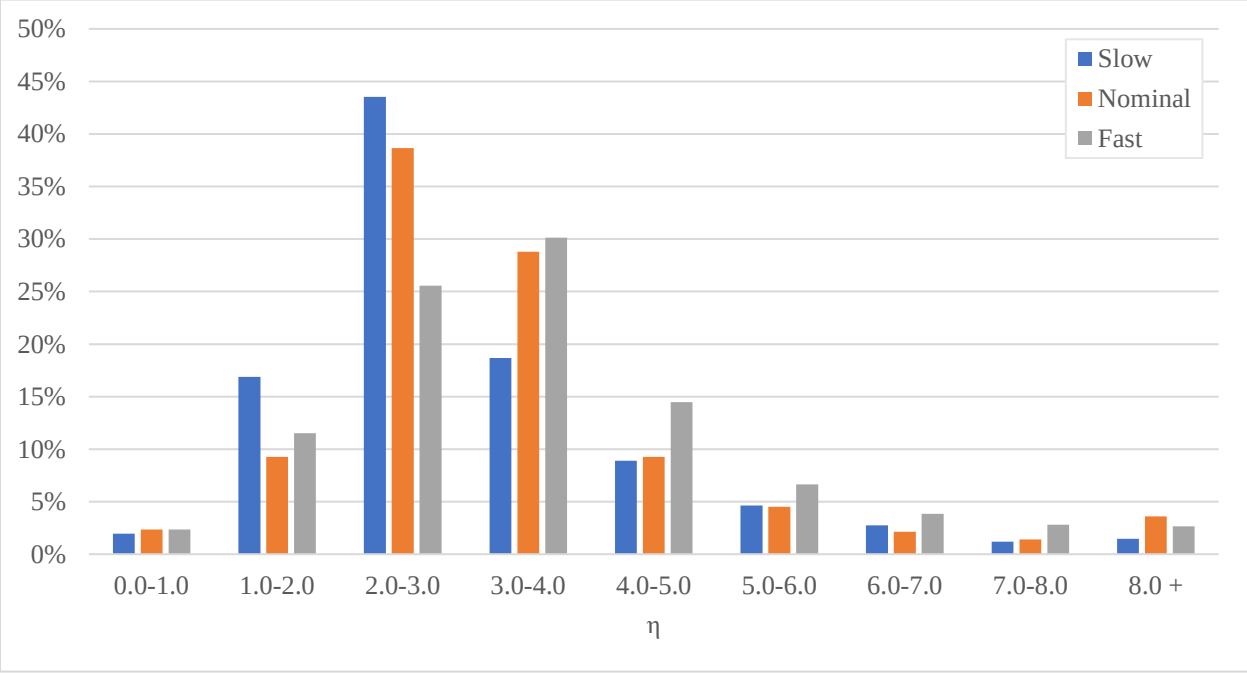

(b)

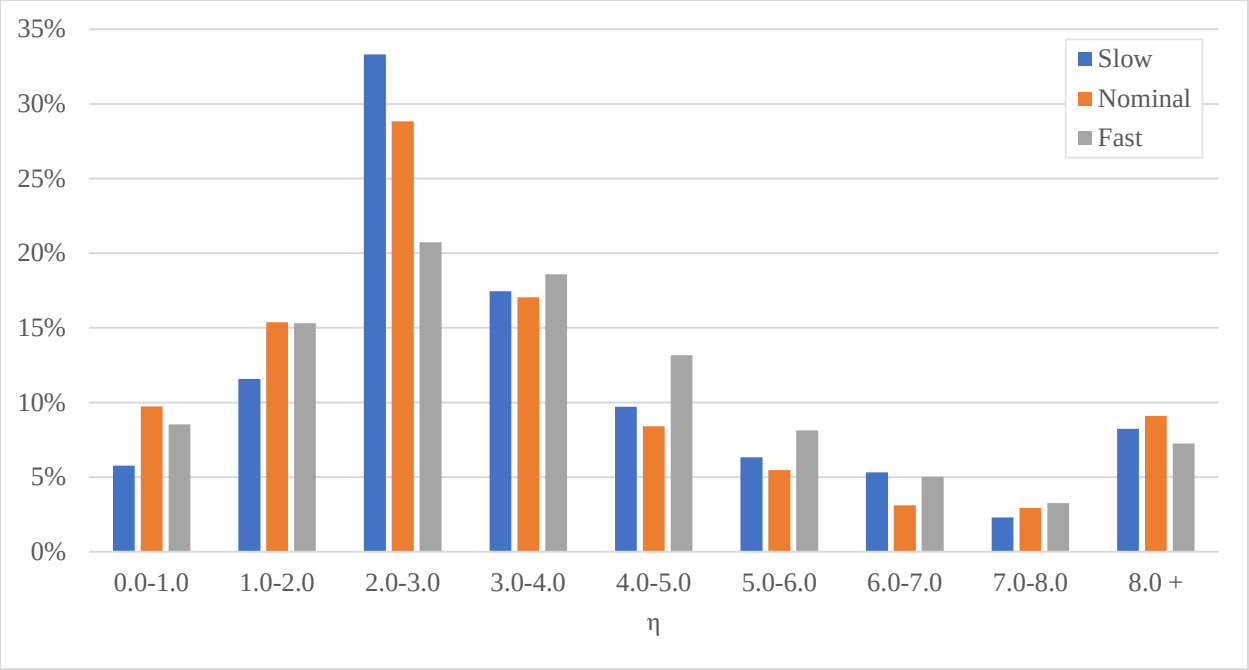

(c)

Figure 20 η distributions for (a) α = 25%, (b) α = 50%, and (c) α = 75%.

As discussed earlier, the lower α tests show a relatively tighter distribution of η, and the higher α show a somewhat flatter distribution of η. The trend shown in

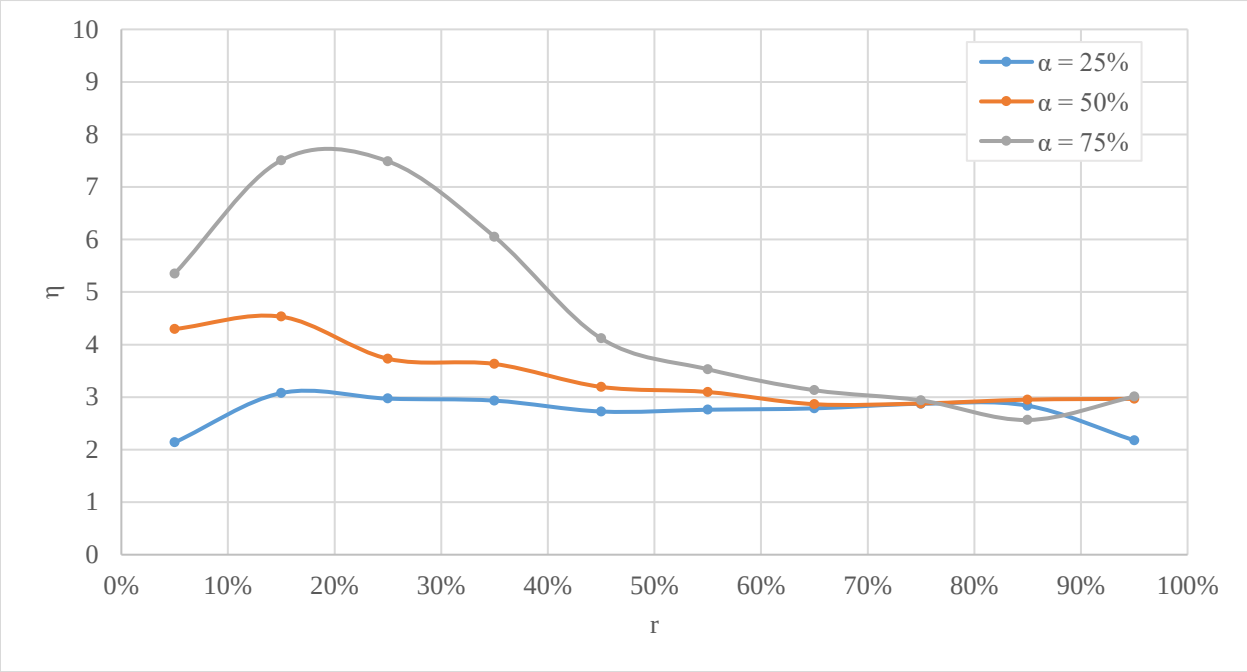

Figure 16 Summary of average η for α = 25%, 50% and 75%.

Table 1 describes increasing average η with ν and α, and is shown here with more clarity here. There were no η values greater than 7.0 in the α = 25% tests, though the quantity of η values in this range increased for the α = 50 and 75% tests. Figure 20 shows how the presence of longer liquid segments (η = 8.0+) in the higher α tests affect the distribution and relative averages for the Slow, Nominal, and Fast injection rates over the three fill ratios. There are consistently higher percentages of low- η lengths in the lower α tests. The peak in the distribution for the higher α tests is between η = 2.0-4.0, though the average for the higher fill ratios is somewhat higher than the peak due to the presence of longer η segments.

Additional distributions for each 10% increment along r can be found in the appendices A.1 Distribution of $\boldsymbol{\eta}$ per 10% increments of $\boldsymbol{r}$ for $\boldsymbol{\alpha}$ = 25%. These distributions display which r locations in the tube have different distributions of η values. It is evident from these graphs that there is a point in the tube where consistent segment formation is achieved, i.e., a high peak in the distribution of η values appears, especially for the α = 25% tests after r = 40%. The diminishing of this peak for the α = 50% and 75% tests should not be ignored, however, since the longer liquid segments observed with the higher fill ratios are a very real consideration that appears when the later-most liquid is entering the channel. These longer η values should be considered in any practical aspects of modeling an OHP.

Comparisons of each α against each ν are shown in Figure 21 below. This arrangement of the data shows relative trends that the α has for each ν. Again, here it is observed that the presence of longer η values in the higher fill ratio tests smooths out the distribution of liquid segment lengths in the tube.

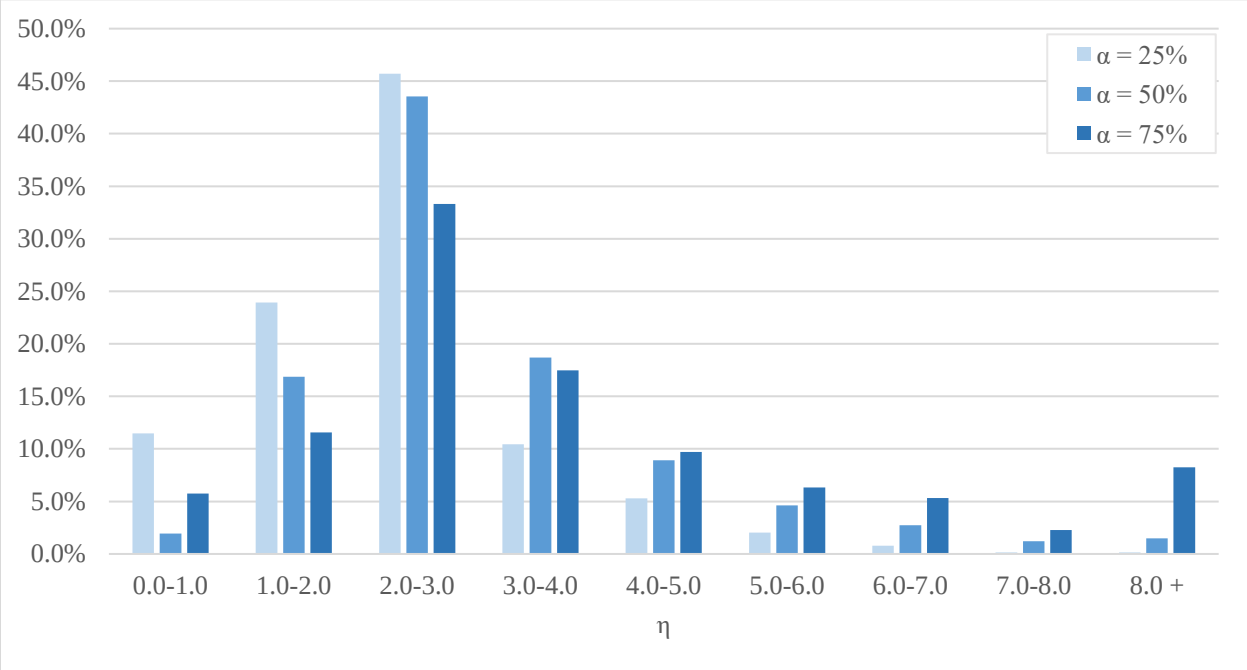

(a)

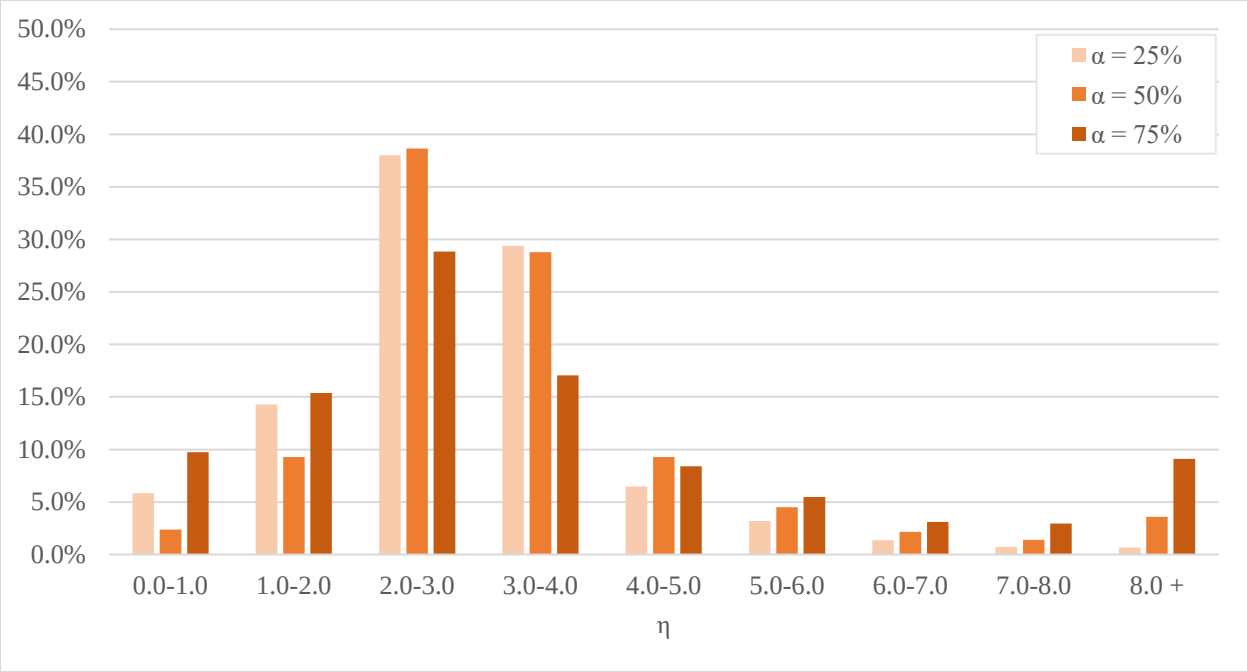
50.0%
45.0%
40.0%
35.0%
30.0%
25.0%
20.0%
15.0%
10.0%
5.0%
0.0%
α = 25%
α = 50%
α = 75%
0.0-1.0
1.0-2.0
2.0-3.0
3.0-4.0
4.0-5.0
5.0-6.0
6.0-7.0
7.0-8.0
8.0 +
η

(b)

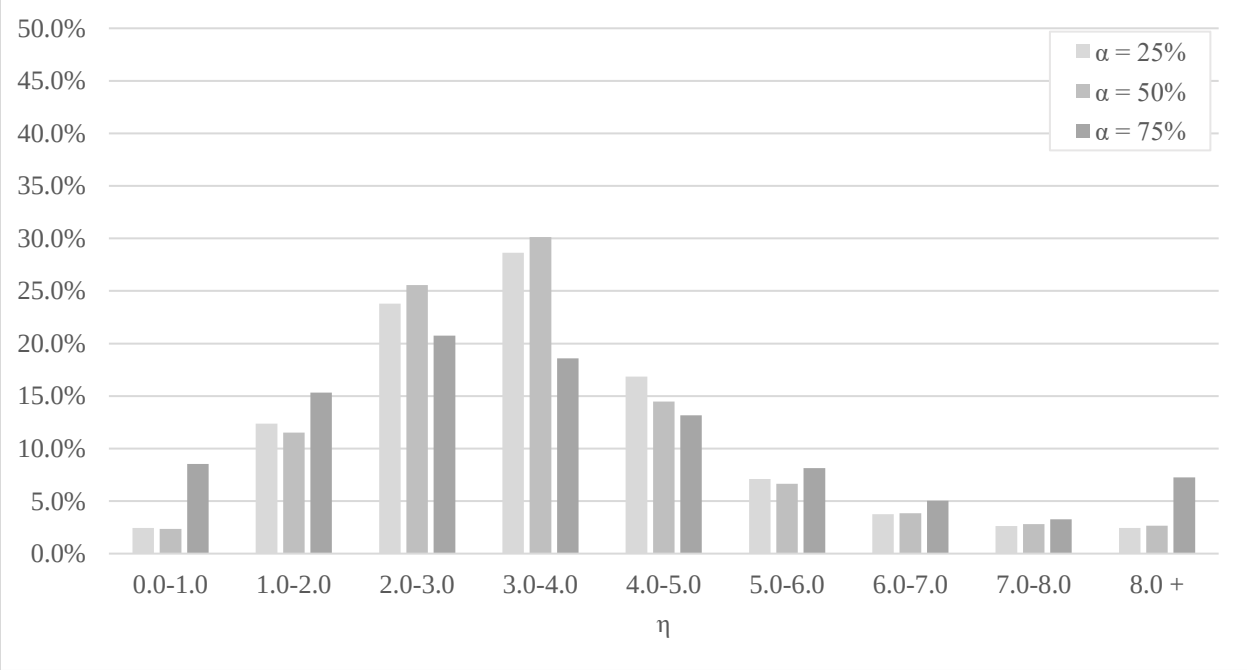
50.0%
45.0%
40.0%
35.0%
30.0%
25.0%
20.0%
15.0%
10.0%
5.0%
0.0%
α = 25%
α = 50%
α = 75%
0.0-1.0
1.0-2.0
2.0-3.0
3.0-4.0
4.0-5.0
5.0-6.0
6.0-7.0
7.0-8.0
8.0 +
η

(c)

Figure 21 Distribution of η comparing α = 25%, 50%, and 75% for (a) Slow ν = 0.002-0.012 (b) Nominal ν = 0.013-0.051 (c) Fast ν = 0.052-0.132.

3.1.3 Length vs Injection Rate

The average liquid length η and standard deviation is plotted vs ν in this section to clearly show the behavior with respect to injection rate.

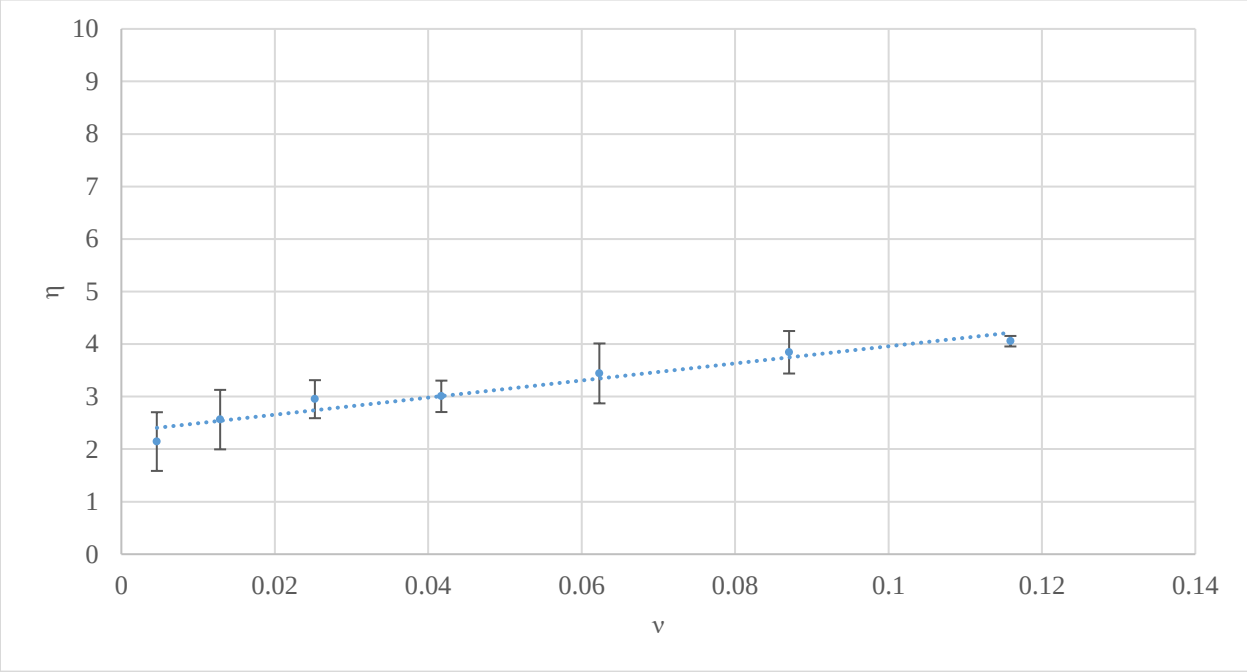

(a)

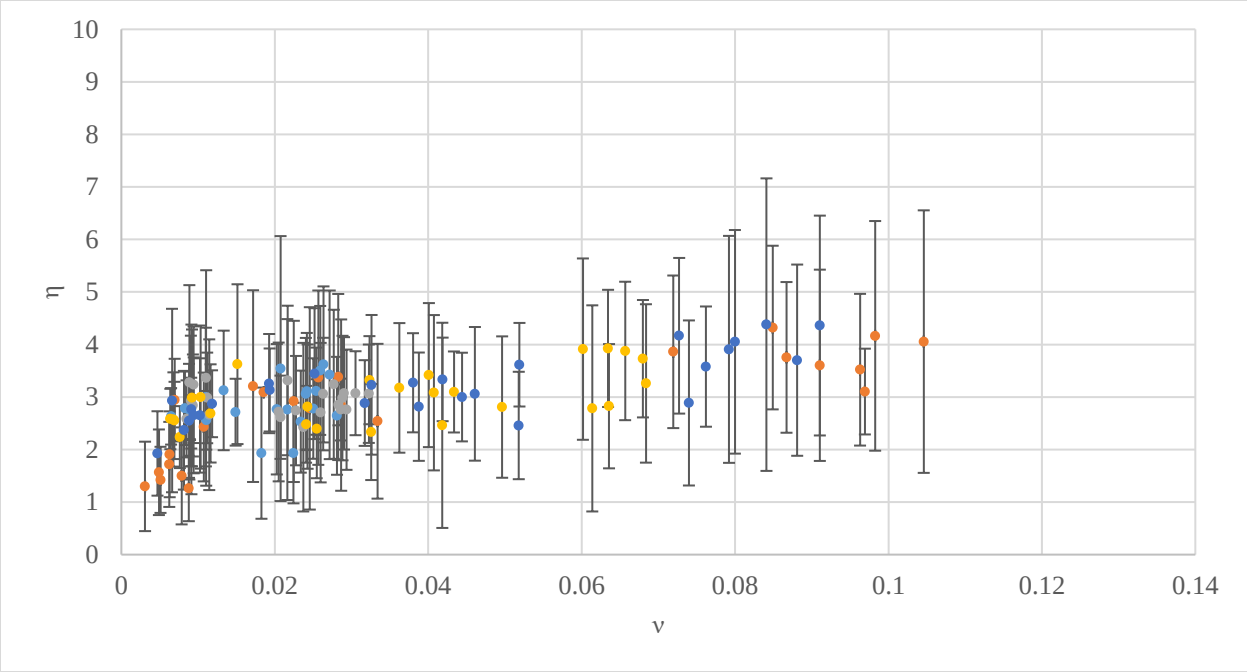

(b)

Figure 22 η vs. ν for α = 25% (a) average η and standard deviation per increments of 0.02, and (b) average η and standard deviation per individual ν tests.

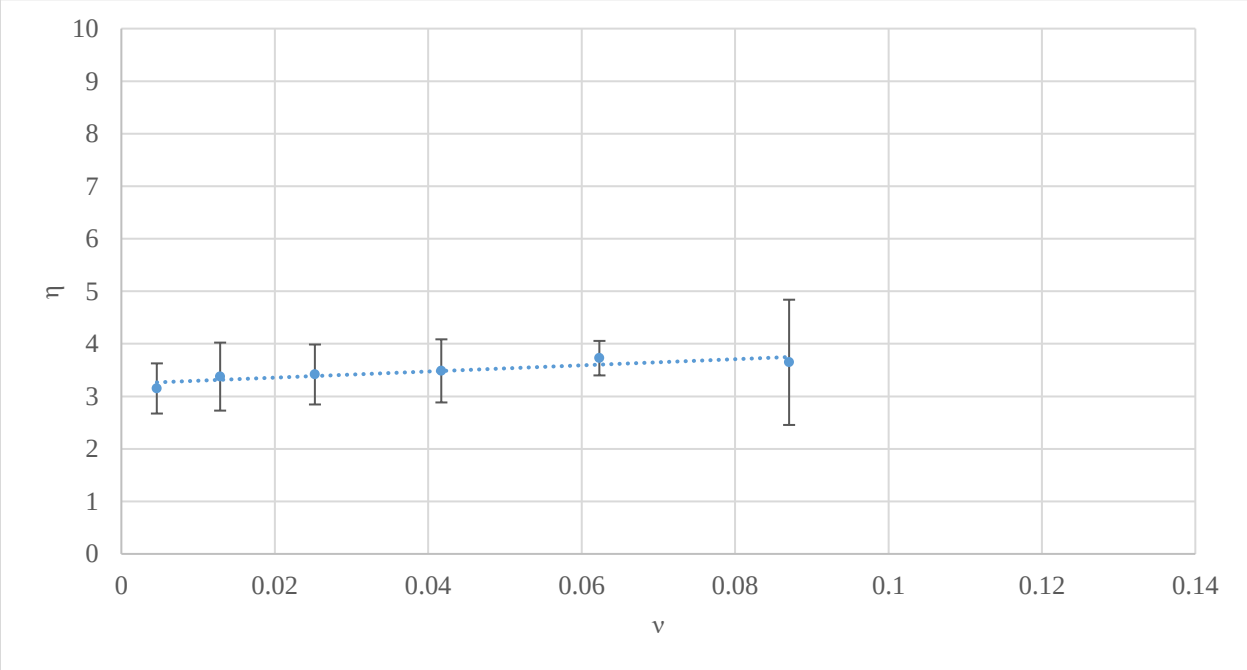

(a)

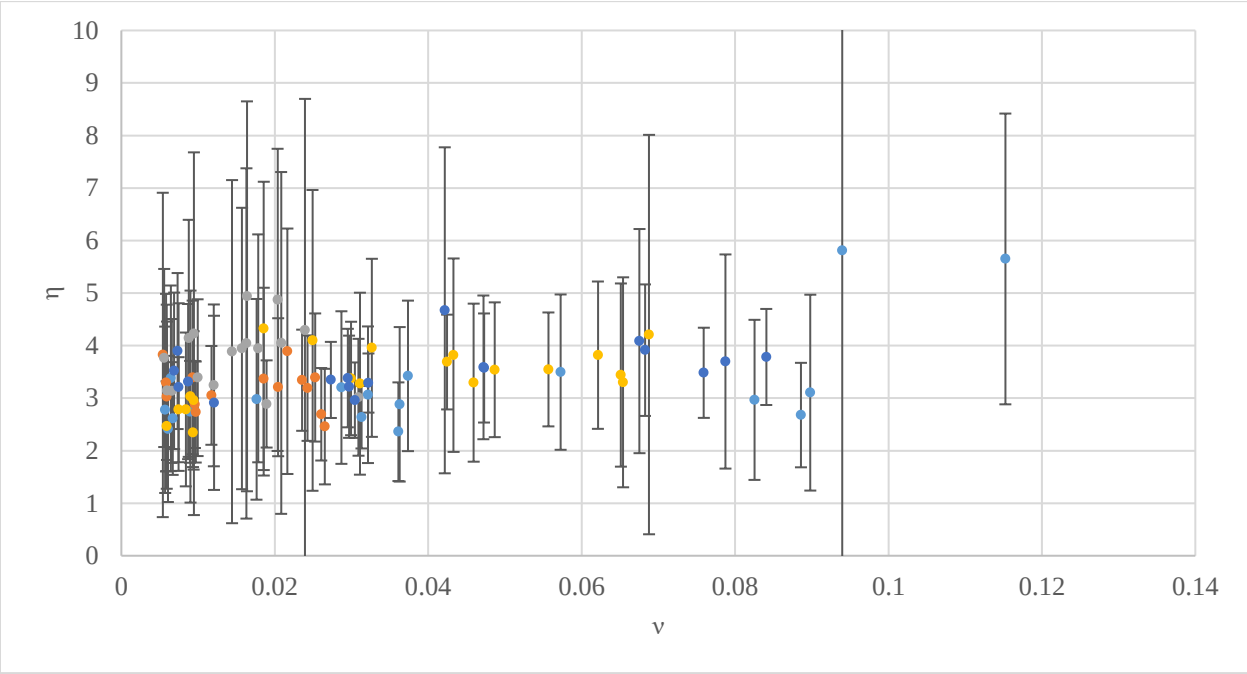

(b)

Figure 23 η vs. ν for α = 50% (a) average η and standard deviation per increments of 0.02, and (b) average η and standard deviation per individual ν tests.

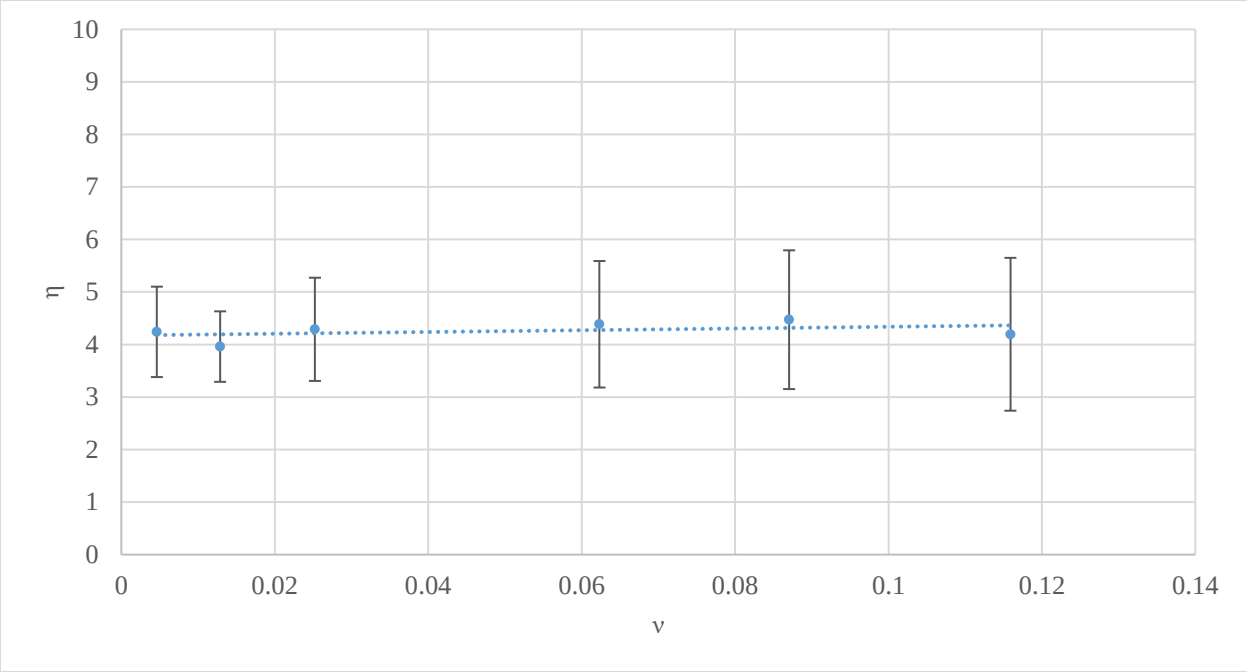

(a)

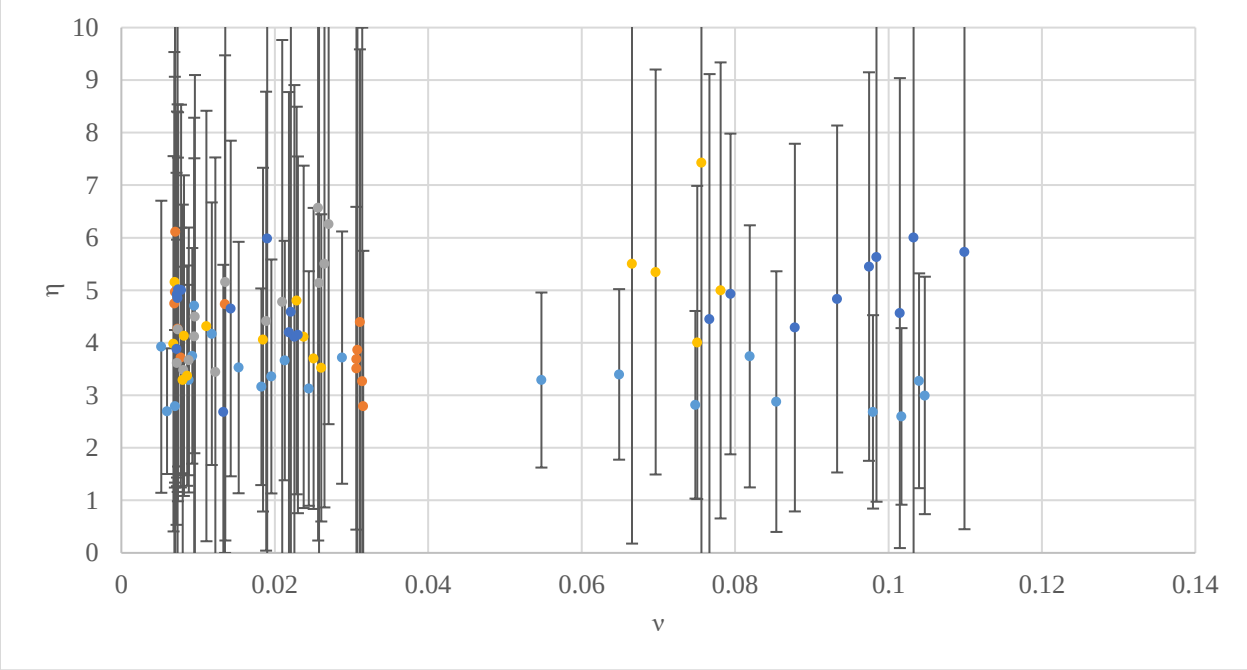

(b)

Figure 24 η vs. ν for α = 75% (a) average η and standard deviation per increments of 0.02, and (b) average η and standard deviation per individual ν tests.

As is seen here, the injection rate plays a noticeable role in the average η values, but primarily for the lower α cases. The average η is relatively flat for the α = 75% tests, though this can be explained by the compression effect of the longer liquid lengths after the critical fill ratio described in section 3.1.1.

3.1.4 Count vs Injection Rate

The count of liquid segments, k, in the device was also assessed. The average count of liquid segments can be determined from the aspect ratio of the channel and the ratio of α to the average $\bar{\eta}$ as follows,

$$C = \frac{L_{TLIQ}}{L_{avg}} = \frac{L_{TLIQ}}{\frac{L_{avg}}{D_h} D_h} = \frac{L_{TCHAN}\ \alpha}{\bar{\eta}\ D_h}$$

$$k = \frac{\alpha}{\bar{\eta}} \qquad [4]$$

$$C = \frac{L_{TCHAN}}{D_h}\ k$$

Here C is the count of liquid segments in the OHP, L_{TLIQ} is the total length of liquid segments in the OHP, L_{avg} is the average length of liquid segments, L_{TCHAN} is the total length of channels in the OHP, D_h is hydraulic diameter of channels, α is the fill ratio and $\bar{\eta}$ is the average nondimensional liquid segment length. The k-factor can be multiplied by a given OHP's aspect ratio to calculate the total number of liquid segments in the device. The distribution of this count should be considered with respect to r, described by the distributions shown in Figure 16.

The k values with respect to ν and α are shown in Figure 25, where higher k values represent higher counts of liquid and therefore shorter average η values.

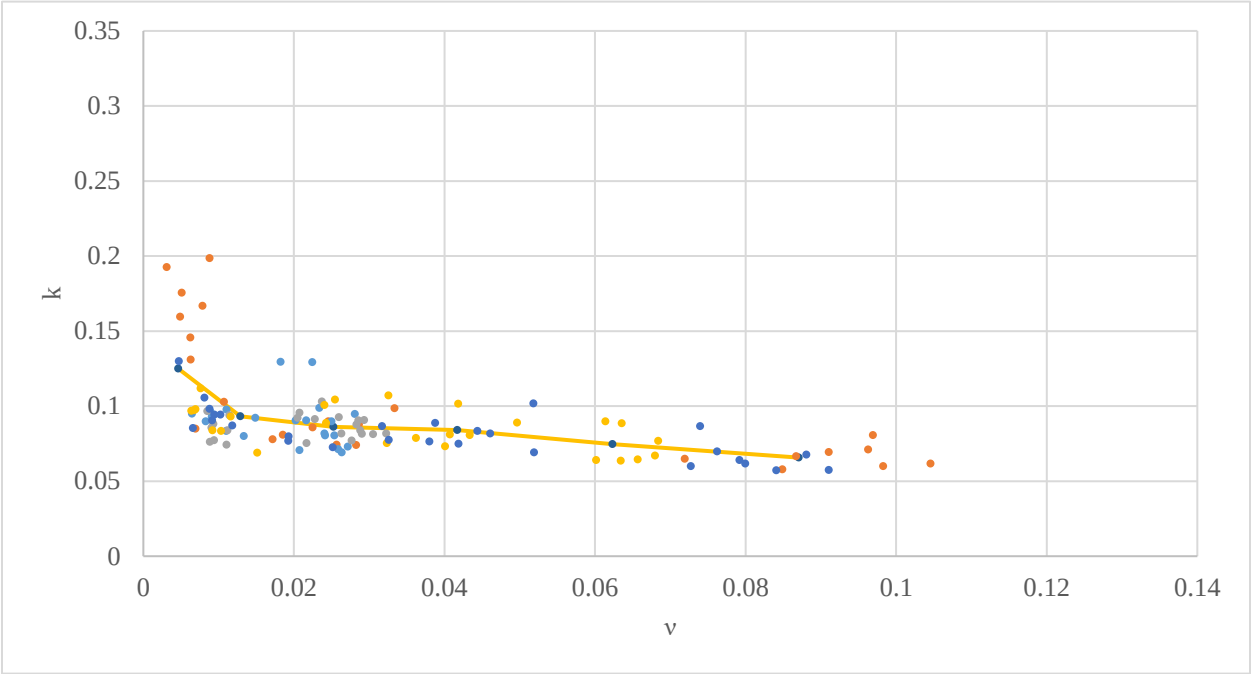
0.35
0.3
0.25
0.2
0.15
0.1
0.05
0
k
0
0.02
0.04
0.06
0.08
0.1
0.12
0.14
ν

(a)

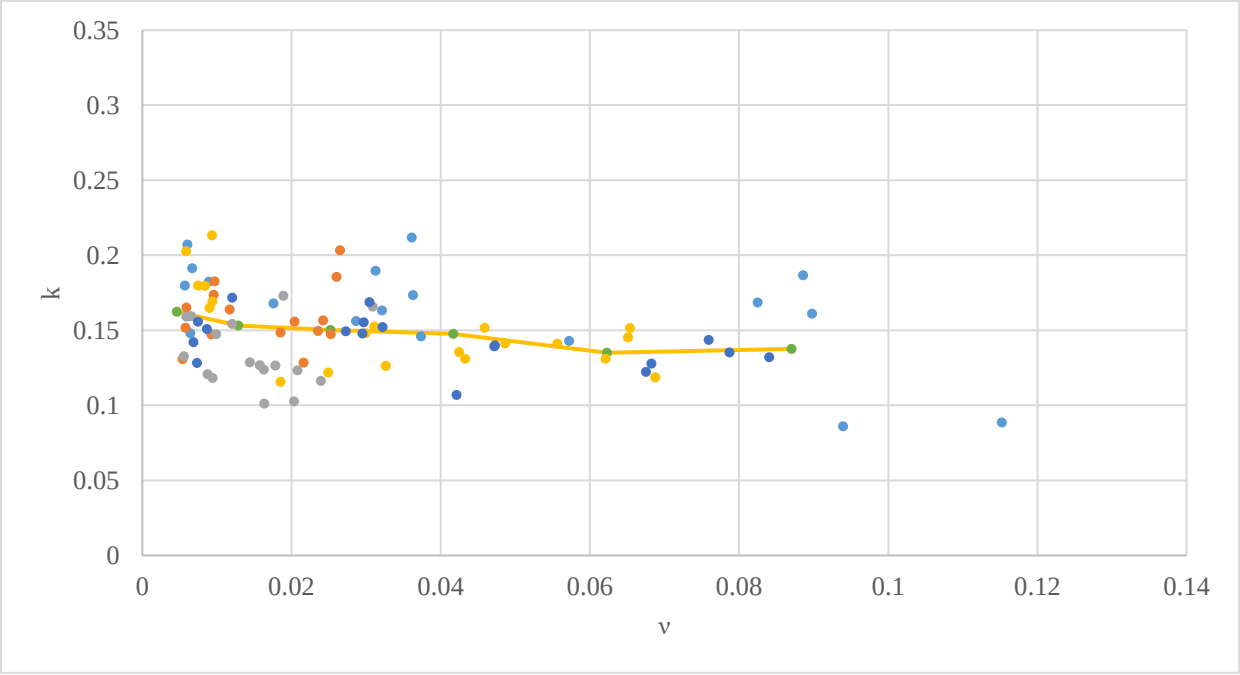
0.35
0.3
0.25
0.2
0.15
0.1
0.05
0
k
0
0.02
0.04
0.06
0.08
0.1
0.12
0.14
ν

(b)

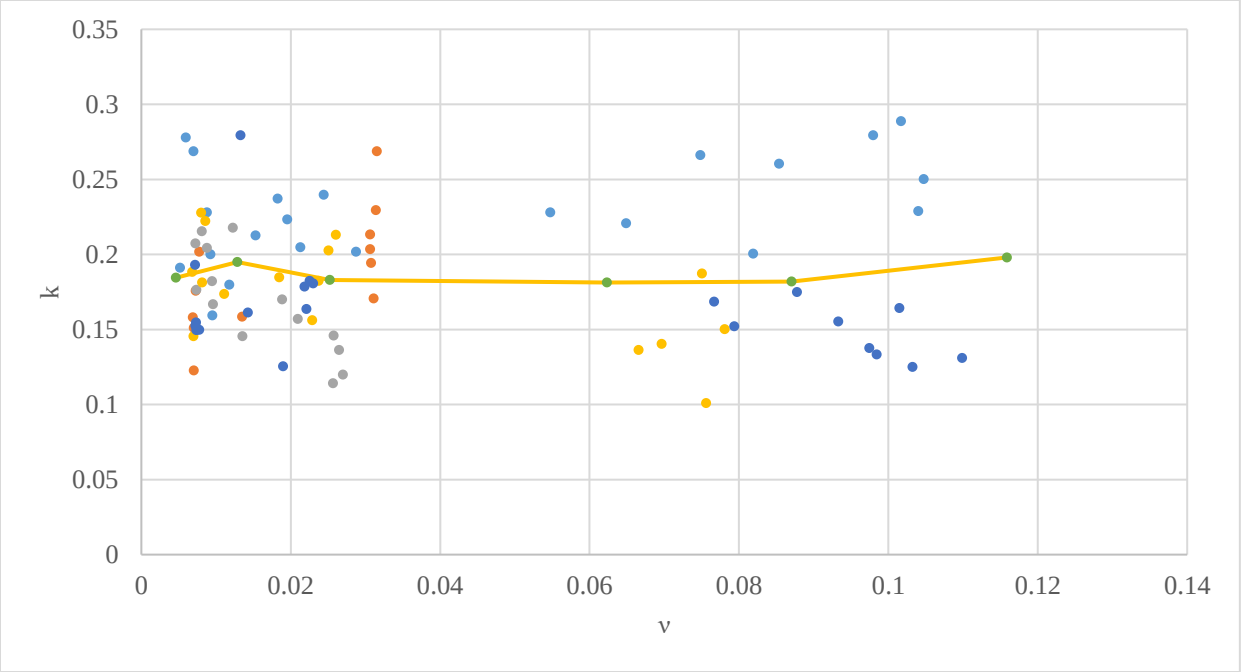

(c)

Figure 25 k vs ν for (a) α = 25%, (b) α = 50%, and (c) α = 75%. The yellow line represents the average value for each 0.02 increment of ν.

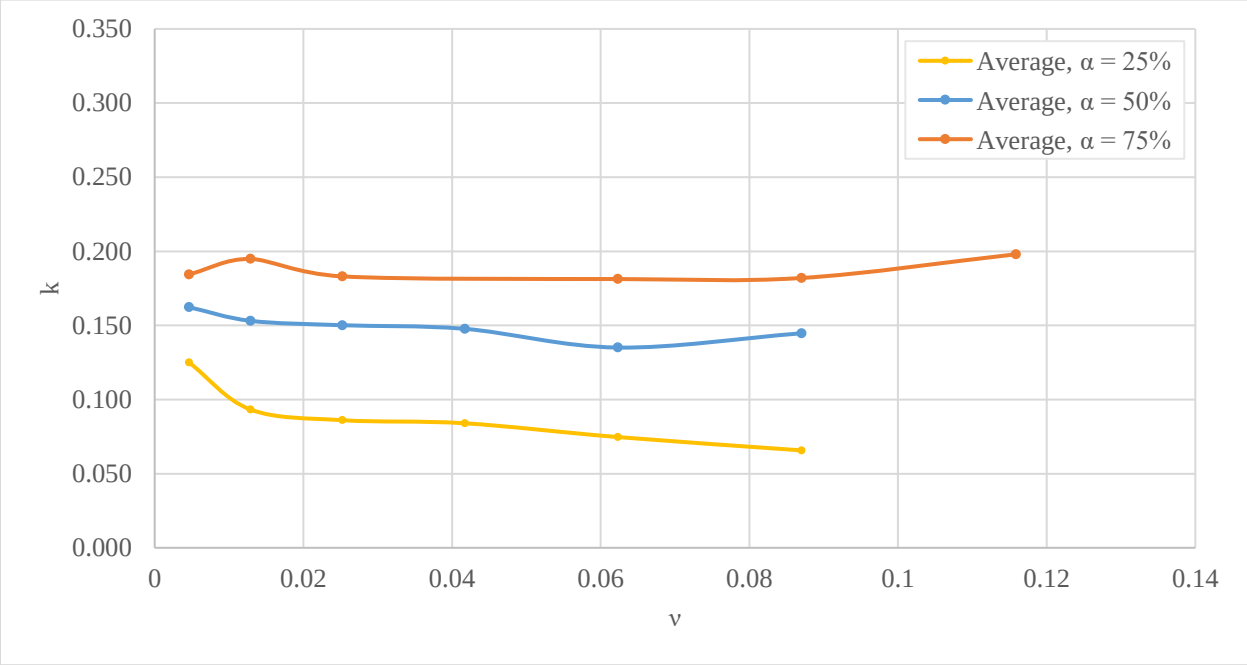

Figure 26 Comparison of average k vs ν for α = 25%, 50%, and 75%.

The k value correlates with the physical system's liquid segment count, and has an inverse relationship with η, meaning that the lower the k value, the fewer liquid segments exist and the longer the average η for the given condition. These results were corroborated in Section 3.1.1 which showed a shorter average η value during the lower α tests and longer average η values for higher α tests. This can be explained by the compression effect, also described in section 3.1.1, where longer liquid segments appear later in the filling process for higher fill ratios. These longer liquid segments occur at higher fill ratios even during slower injection rates and bring down the normalized liquid segment count.

The average k value per α is shown below in Table 2. Note that due to the injection rate targets aimed for during the tests, there was no data collected for the ν = 0.40-0.50 mL/sec injection rate for the α = 75% tests.

Table 2 Average k and standard deviation of ν ranges per α.

ν range	α = 25% Avg k / std dev	α = 50% Avg k / std dev	α = 75% Avg k / std dev
0.002-0.008	0.125 / 0.035	0.162 / 0.025	0.184 / 0.041
0.008-0.019	0.093 / 0.023	0.153 / 0.028	0.195 / 0.035
0.019-0.033	0.086 / 0.012	0.150 / 0.024	0.183 / 0.039
0.033-0.052	0.084 / 0.009	0.148 / 0.028	0.181 / 0.050
0.052-0.074	0.075 / 0.014	0.135 / 0.012	-
0.074-0.101	0.066 / 0.007	0.138 / 0.032	0.182 / 0.055
0.101-0.132	0.062 / 0.000	0.088 / 0.000	0.198 / 0.068
All	0.089 / 0.024	0.150 / 0.027	0.201 / 0.044

3.2 Additional Analysis and Discussion

In addition to analyzing the data collected, there were a number of other qualitative observations from the tests.

3.2.1 Observations on Fluid Entering Tube and Liquid Segment Formation

While the fluid was entering the tube from the syringe and through the valve, the way the liquid formed into liquid segments was examined. The liquid, at all injection rates, would travel along the bottom of the tube until some critical point in the glass tube, approximately 100 mm from the valve entrance, when it would suddenly form a liquid segment spanning the entire cross

section of the tube. This was observed for all vapor segments, from the first that were formed to the last. The first one or two liquid segments that entered the tube would form but later vaporize as they traveled down the tube, about halfway and for all α values.

Subsequent liquid traveling behind the most recently-formed liquid segment would continue joining the newly formed liquid segment as it continued to grow in the direction of fluid entering the tube, until it would detach and become separated by a vapor plug and travel along the length of the tube in a train of other liquid-vapor segments. This detached liquid segment was followed by the sudden formation of a new liquid segment as the process repeated.

It was also interesting to note that a swirling eddy of much smaller bubbles in some of the newly formed liquid segments could be observed, and occasionally led to the formation of a vapor bubble within the liquid segment after it had detached, and occasionally formed into a vapor segment of its own, splitting the liquid segment into two, as it traveled down the length of the tube.

One additional observation worth noting was right as the micro-metering valve was opened but prior to any liquid entering the tube, the interior of the tube appeared to fog during each test. It appeared that the leading-most fluid vaporized and condensed on the interior of the glass tube. This did not seem to have any effect on the subsequent formation of liquid and vapor segments.

3.2.2 Variability between Valves and Tube Positions

Some variability in liquid length and distribution was also observed between each of the five tube assemblies, or “tube positions”. A set of experiments was conducted to determine the major factor in these differences, which included physically moving the tubes to different

vertical positions in the test set up, changing the adapting hardware to the syringe between valves and tubes, changing the glass tubes, and changing the valves in each set up. This set of experiments ultimately concluded that the valve itself was the main reason for the variability.

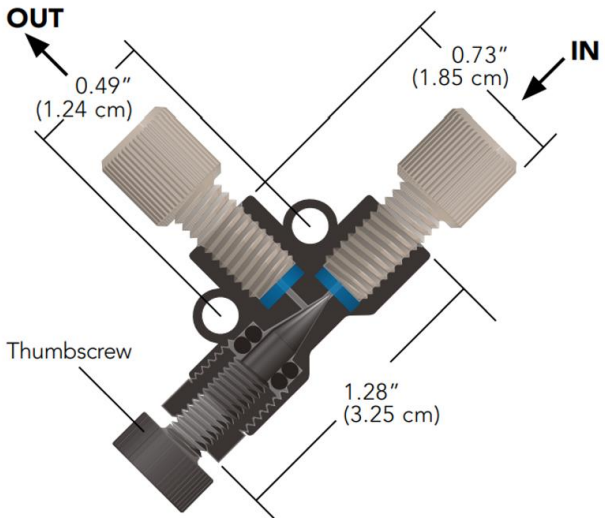

Figure 27 Cross Section of IDEX P-447 Micro-Metering Valve.

The valve is a micro-metering needle valve, which consists of a pointed needle actuated by a thumbscrew controlling two .020” thru-holes on either side, shown in Figure 27. A number of different types of valves were tested, and this valve showed the best success in maintaining hermeticity during pump down and with metering the introduction of fluid into the tube. The original reason for having five tubes and valves in this set up was for more rapid data collection and throughput reasons, however the small differences between the otherwise identical valves seems to have also provided more realistic random variability in the data, thus providing at a data distribution more likely to mirror variations expected in a real-world setting containing inherent differences between devices.

It should also be noted that positions 3 and 4 were not able to achieve the fast injection rate range (ν = 0.052-0.132), the cause of which remains undetermined and is assumed to be related to variability valve to differences in valve behavior at these positions. An example of the variation between the five valves can be seen in Figure 28 which represents all of the α = 50% data. Each point on the graph represents an η length at a given r in the tube, and each color represents a unique test.

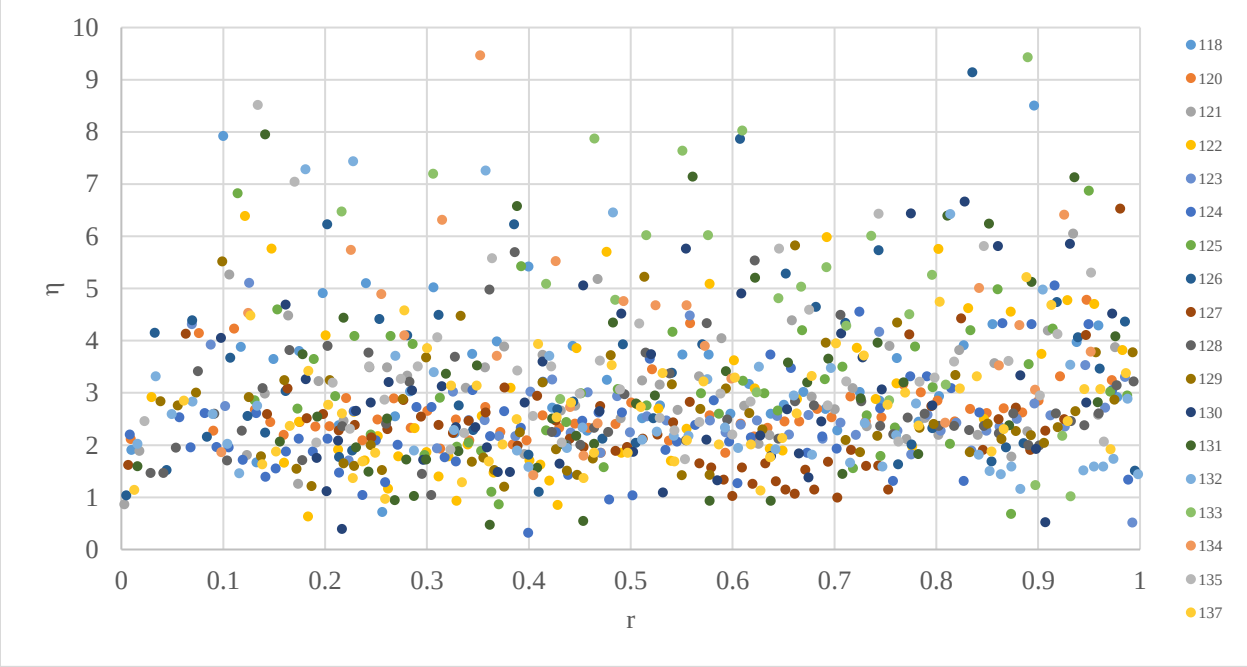

(a)

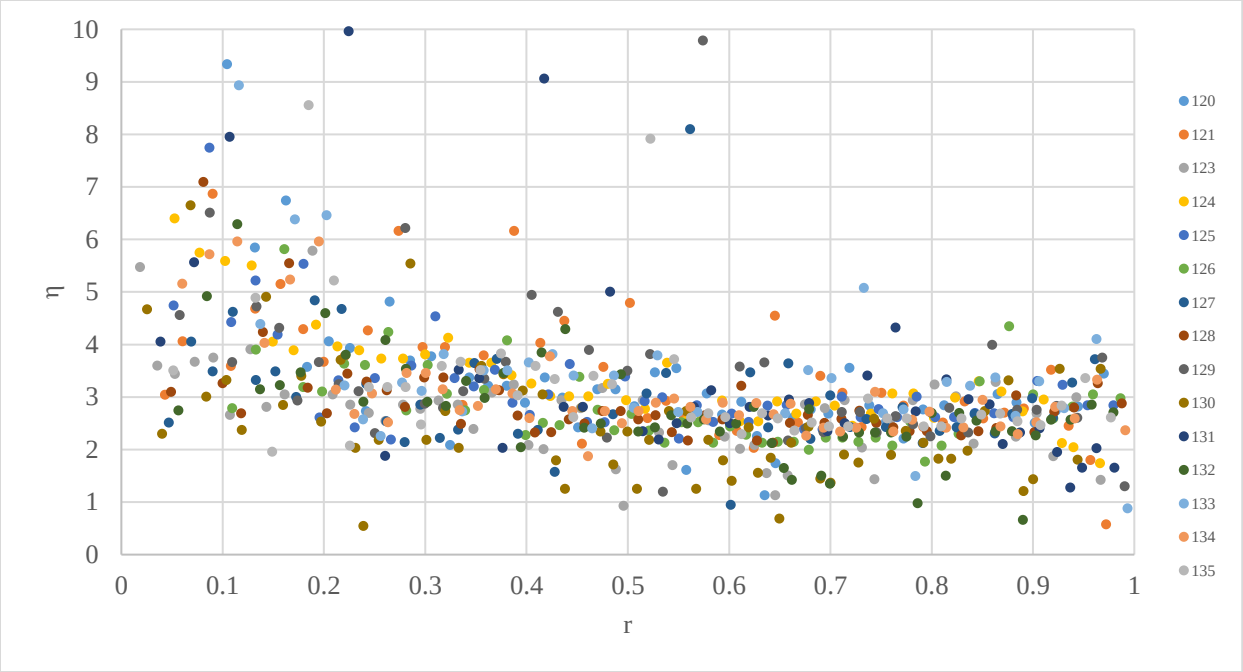
10
9
8
7
6
5
4
3
2
1
0
η
0
0.1
0.2
0.3
0.4
0.5
0.6
0.7
0.8
0.9
1
r
120
121
123
124
125
126
127
128
129
130
131
132
133
134
135

(b)

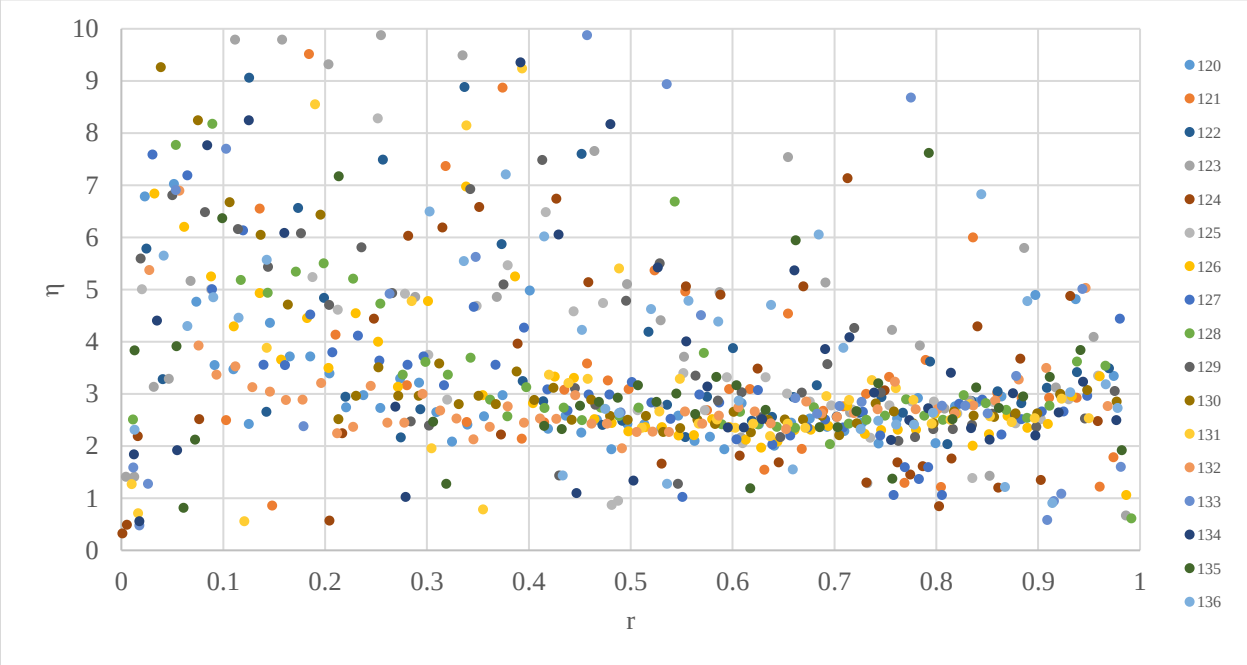
10
9
8
7
6
5
4
3
2
1
0
η
0
0.1
0.2
0.3
0.4
0.5
0.6
0.7
0.8
0.9
1
r
120
121
122
123
124
125
126
127
128
129
130
131
132
133
134
135
136

(c)

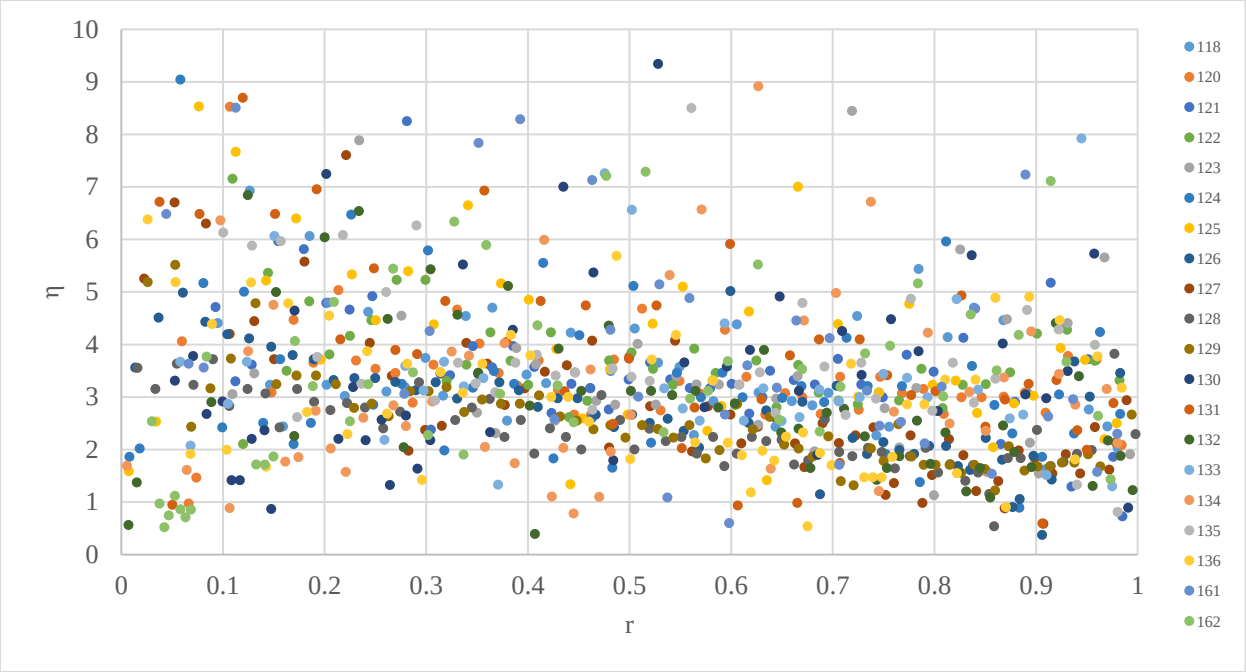

(d)

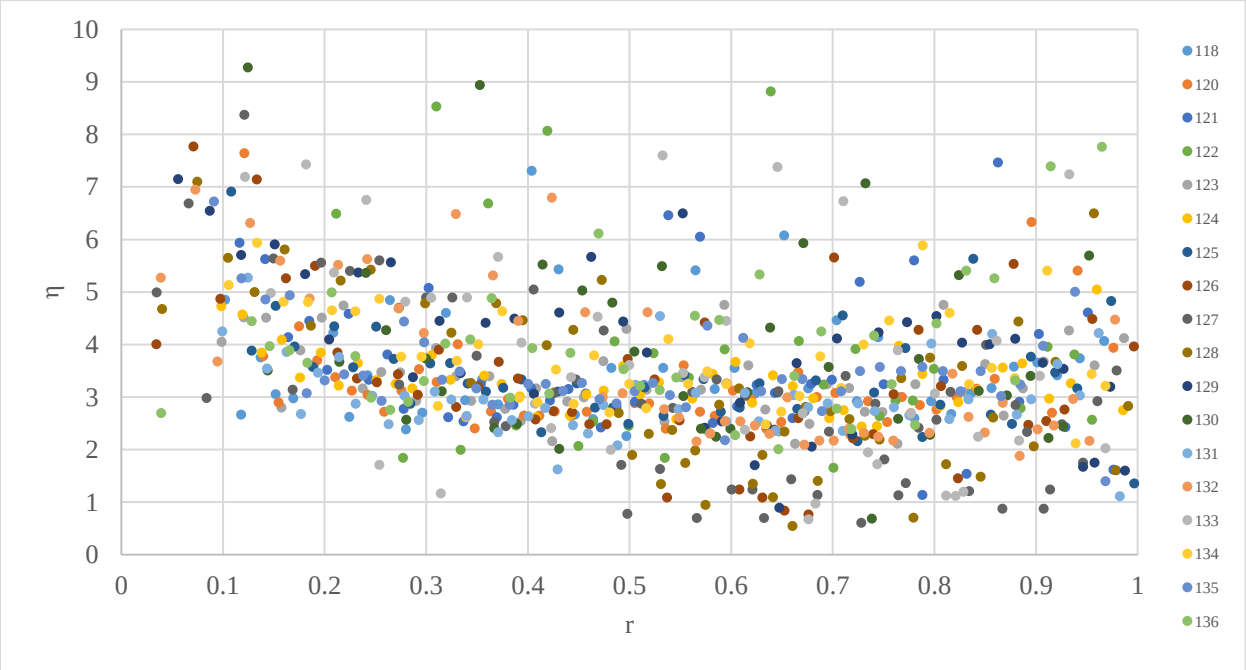

(e)

Figure 28 Variability of η vs r for all ν rates at α = 50%; (a) position 1/bottom tube, (b) position 2, (c) position 3, (d) position 4, (e) position 5/top tube.

Though there were some differences in the distribution of η between tube positions and valves, the underlying average η value was very similar throughout. This ultimately provided more confidence in a composite average of the five valves and positions for practical industrial application.

3.2.3 Injection Rate Throughout Each Test

As noted in section 2.3, the injection rate slowed slightly as more fluid was introduced into the tube, as may be expected. Specifically, it stands to reason that the flow rate would slow down as the vapor segments downstream in the tube reached ambient vapor pressure, and additional filling of the tube required compression of the vapor at the end of the tube, though this effect was not as dramatic as expected. The subtleness of the decline may be explained by the small orifices and/or needle controlling the flow resistance and flow rate more than the vapor pressure changes downstream in the tube. The trend in injection rate is shown in Figure 29 for a representative α = 50% test in the Slow injection rate range (ν = 0.002-0.012).

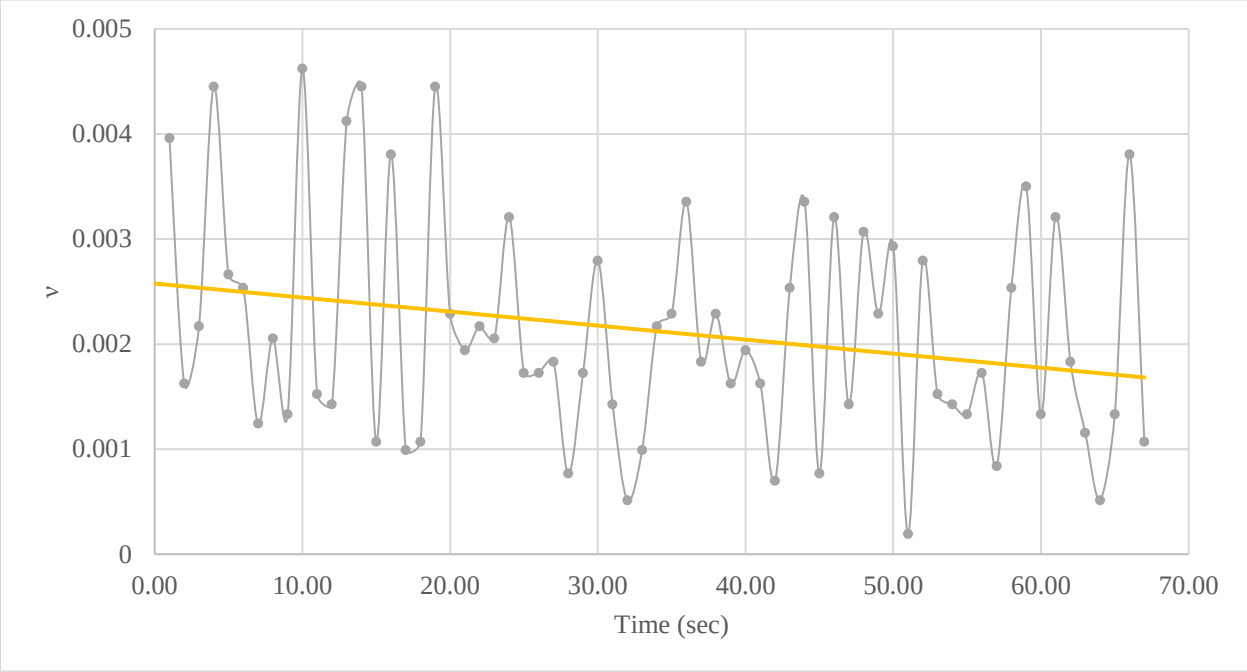

Figure 29 Exemplary Injection Rate Change as Linear Trendline, α = 50%.

As shown, the average injection rate was relatively steady but does show a decreasing trend from approximately ν = 0.00260 to 0.00180, with an average of 0.00212. This phenomenon is not expected to have had any major impact on the results of these tests, though this may be a consideration when filling future OHP devices with longer channel lengths and timescales. Because the change in injection rate during a test was small, only the average values achieved during a test were reported.

3.2.4 Effect of Gravity and Externally Applied Forces

The gravity dependency of the distribution and effect of other externally applied forces were also of interest but not tested in detail in this work. As discussed earlier, a typical

commercial devices' dependency on gravity is reduced with an increase in the number of serpentine channel passes [21], [22]. The device developed and tested in this work represented a single channel pass, and the effect of gravity on the distribution was briefly examined.

In an exploratory test, the device was tested per the method described in 2.3 at the α = 50% condition and Slow injection rate (ν = 0.002-0.012) and filled in the horizontal position. The single tube was then gently tilted at a 45 degree angle counter-clockwise, then a 45 degree angle clockwise, then returned horizontally. During the test, as the tube was tilted counter-clockwise, the liquid segments slid in the direction of gravity and bounced slightly as they settled against the numerous vapor springs separating them from each other. As the tube was tilted in the opposite direction, the liquid segments slid in the opposite direction with gravity until they bounced gently and settled again. Upon returning to horizontal, the liquid segment count was reduced from 30 (k = 0.094) to 28 (k = 0.088). The exact locations and distribution did change slightly from when the tube was in its original horizontal position.

Another test looked at vigorously shaking the tube by hand up and down in the vertical orientation for 30 seconds, which resulted in greater consolidation of liquid and vapor segments (an average liquid segment count 33% lower than what was originally injected) and a different distribution than was originally observed. Anecdotal accounts from industry partners described vibration and motion applied to OHPs with several serpentine channel passes having a similar effect of consolidating liquid segments into fewer longer segments than originally injected.

It is evident that movement following the initial injection has some effect on the initial distribution of the liquid and vapor segments, though the relative scale of this effect seems to vary with the force applied to the system. This should be studied more closely for devices that will be charged and sealed with a working fluid and shipped to another location. This effect

should also be studied and considered for OHP devices that have been integrated into their respective assemblies and exposed to vibration and other external forces. The research conducted in this work should be expanded to develop stronger analytical models in a lab environment, and future work should study the effect of external forces on the consolidation of liquid segments in OHPs.

3.2.5 Comparisons to Initial Conditions Used in Models

When the results from these tests were compared to methods used for determining initial liquid-vapor lengths and distributions in models, some interesting comparisons were made that illustrate opportunities for generating more accurate initial conditions in first principles discrete modeling of OHP behavior.

Shafii, et al. [32] developed an explicit finite difference scheme to predict the behavior of liquid-vapor interaction in an OHP, and used water with 1.50 mm ID channels at α = 61.4% in an open-loop OHP in the vertical top-heating position. The total length of channel was 1140 mm, and the model assumed an initial liquid distribution of two equally sized liquid segments, each 350 mm long, or η = 233.3, located partially in the condensing and adiabatic regions, as shown in Figure 30 Shafii, et al. [32], Initial Liquid Vapor Distribution in Unlooped OHPFigure 30. The model also explored different initial numbers of identical liquid and vapor segments, ranging from 20-76. A separate model assumed that the number of vapor segments would equal the number of heating sections over time, which was three in this case. Three liquid segments were ultimately used in the model, though the author goes on to describe an alternate method of estimating the initial liquid vapor distribution in a partially-filled small diameter channel using instability theory of condensate films.

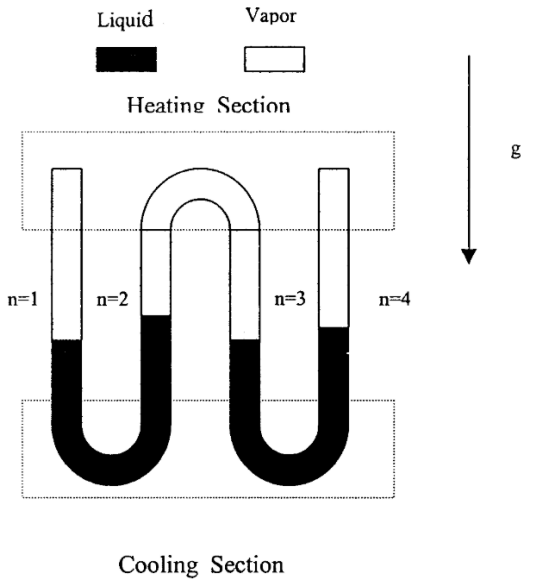

Figure 30 Shafii, et al. [32], Initial Liquid Vapor Distribution in Unlooped OHP.

Analysis of the instability theory of condensate films yields

$$\lambda_m = \sqrt{8}\,\pi a \qquad [5]$$

where $\lambda_m$is the most-unstable wavelength of the condensate film, and a is the undisturbed radius of the condensate film inner surface, which is assumed to be half the size of the tube radius [41]. Assuming the film instability drives the breakup of liquid segments gives an initial liquid segment length of 3.33 mm, which has an equivalent η value of 2.22. This method of estimating the initial liquid lengths does not consider other important factors about the device, such as its fill ratio, properties of the working fluid, or the injection rate of the fluid. Results from the present investigation suggest that other important physics may also need to be considered, specifically with respect to the eddy formation observed during the liquid-vapor formation into the channel, as discussed in section 3.2.1.

Alternatively, based on the results of the work conducted in this study, the initial liquid segment length and distribution could be found by interpolating for the desired fill ratio from Figure 16 and Table 1. This gives average η values for α = 61.4% between approximately 3.0 and 6.0, depending on the liquid segment's position r throughout the tube. Higher accuracy of lengths could be obtained if the device's injection rate were considered. A similar analysis using Figure 26 Comparison of average k vs ν for α = 25%, 50%, and 75%. could be conducted by interpolating for the given fill ratio and assuming an injection rate to determine the count of liquid segments. Doing so would provide a k value between approximately .150-.201. Applying these values for the given OHP aspect ratio presented in Shafii et al. [32] would produce a range of liquid segment lengths between 4.50-9.00 mm, with the longer liquid segments closer to the injection location, and a quantity of 114-153 liquid segments. The distribution of liquid segments could be interpolated throughout the channels per Figure 20. These results suggest that either the condensate film instability theory is not the primary driving factor for determination of the liquid slug lengths, or that condensate film instability is influenced by factors not included in the analysis resulting in equation [5].

Mameli, et al. [2] developed an numerical model to estimate the behavior of an OHP using Ethanol with 3 and 9-turn devices having 2.00 mm ID channels. The device was closed-loop, filled to α = 60%, and tested in the horizontal, 45 degree, and vertical positions. The 3 turn device had a total length of 440 mm, and the 9 turn device had a total length of 1100 mm. The model assumed an initial distribution of three equally sized and spaced liquid segments for each device, though the author states that "further work is mandatory to define this initial condition with a statistical approach".

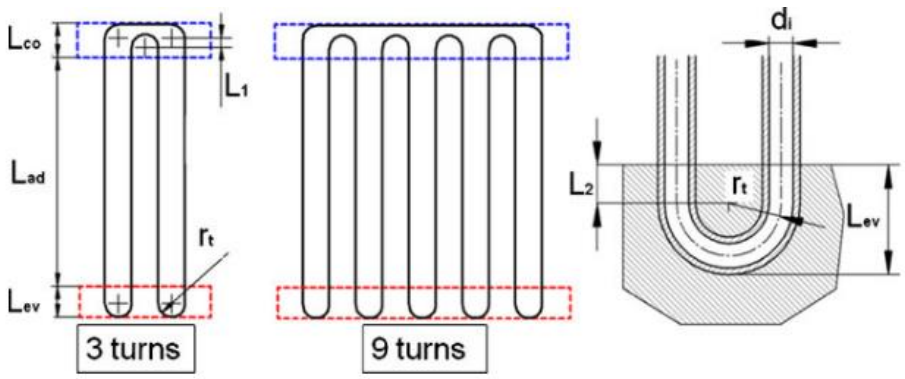

Figure 31 Mameli, et al., CLPHP geometry input parameters, 3 and 9 turns [2] .

The 3-turn device resulted in liquid segment lengths of 88 mm, or η = 174, and the 9-turn device resulted in liquid segment lengths of 220 mm, or η = 440. If the data on initial distributions of liquid and vapor segments presented in this research with water were applicable to other working fluids such as Ethanol, which remains to be shown, the resulting average η values for α = 60% would be between approximately 3.0 and 6.0, depending on the liquid segment's position r throughout the tube. Higher accuracy of lengths could be obtained if the device's injection rate were considered. A similar analysis using Figure 26 Comparison of average k vs ν for α = 25%, 50%, and 75%. could be conducted by interpolating for the given fill ratio and assuming an injection rate to determine the count of liquid segments. Doing so would provide a k value between approximately .150-.201.

Applying these η and k values for the 3-turn OHP channel geometry would equate to a distribution of liquid segment lengths between 6.00-12.00 mm, with the longer liquid segments closer to the injection location, and a quantity of 33-44 liquid segments. The 9-turn OHP channel

geometry would result in the same η distribution of liquid segment lengths but with a higher quantity between 82-110 liquid segments.

Daimaru, et al. [3] built on the work from Mameli, et al. [2] and used a similar model and device to explore the effects of the initial distribution of liquid segments on startup behavior. The author stated that "no study has investigated the effects of the initial distribution of the working fluid in the startup motion of OHPs", and compared a mathematical model of three initial liquid distributions against experimental results, though direct observation of the experimental distribution of liquid segments was not able to be observed (i.e., the initial distribution of liquid segments in the experimental device was not able to be validated, and only computational and experimental performance was compared). The three initial liquid distribution initial conditions are shown in Figure 32, and were compared with respect to the actual startup characteristics of the experimental device.

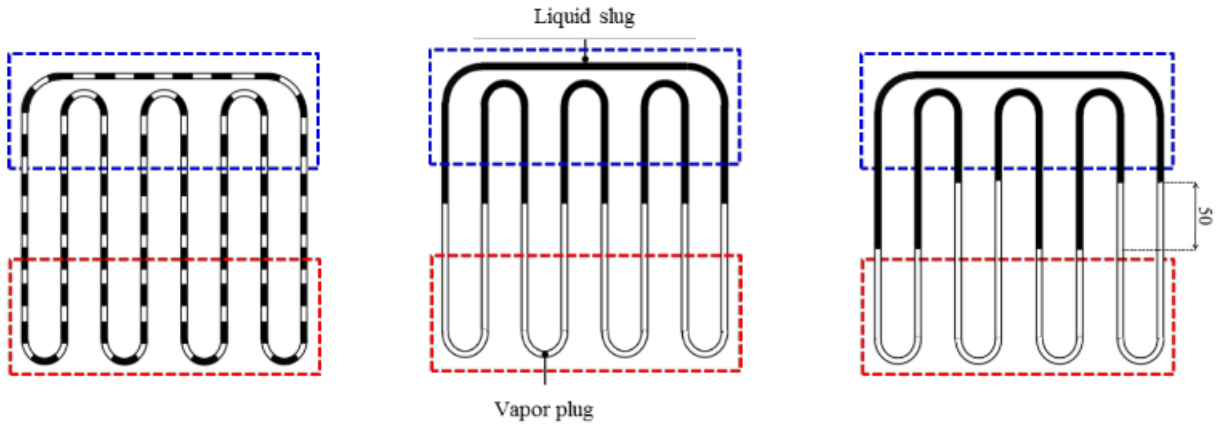

(a) (b) (c)

Case	Initial distribution pattern		Heat input [W]
1	Equal distribution	$N_{l,int}$: 100	80
2	Localization in cooling section	$N_{l,int}$: 8	80
3	Localization with gaps	$N_{l,int}$: 8, 50-mm gaps in each turn	80

(d)

Figure 32 Daimaru, et al. [3], Schematics of initial distribution pattern (a) equal distribution, (b) localization in cooling section, (c) localization with gaps; and (d) number of liquid segments.

Daimaru, et al. [3], used Ethanol with a 2.00 mm ID channel at α = 55% in a closed-loop OHP in the horizontal position. The total length of the channel was 5605 mm, and the model assumed three initial liquid segment distributions described in Figure 32, with conditions (b) and (c) showing the same count and length of liquid segments [3]. For condition (a), the liquid segment length was assumed to be 31 mm, or η = 15.5. Conditions (b) and (c) assume a liquid segment length of 770.70 mm, or η = 385.35.

Again, if the data on initial distributions of liquid and vapor segments presented in this research with water were applicable to other working fluids such as Ethanol, which remains to be shown, the resulting η values for α = 55% would be between approximately 3.0 and 5.0, given the liquid segment's position r throughout the tube. Higher accuracy of lengths could be obtained if the device's injection rate were considered. A similar analysis using Figure 26 Comparison of average k vs ν for α = 25%, 50%, and 75%. could be conducted by interpolating for the given fill ratio and assuming an injection rate to determine the count of liquid segments. Doing so would provide a k value between approximately .130-.170.

Applying these η and k values would equate to a distribution of liquid segment lengths between 6.00-10.00 mm, with the longer liquid segments closer to the injection location, and a quantity of 364-476 liquid segments.

3.3 Summary Analysis

OHPs with a lower fill ratio and slower injection rate of fluid resulted in the shortest η and the greatest consistency. As the fill ratio increased past some critical fill ratio, between α = 25% and 50%, and the first liquid introduced to the channels reached the end of the tube, the subsequent liquid entering the tube grew in average η length (the "compression effect") and increased in variability. For all fill ratios, faster injection rates resulted in greater average length and variability in η.

Broadly speaking, shorter liquid segment lengths are desirable to assist in easier startup of the OHP. Though it remains to be seen if the same η and k values hold for other working fluids and channel diameters, the compression effect and resulting distribution after some critical fill ratio is expected to present itself in a similar fashion, due to the compression of vapor segments once a certain volume of fluid reaches the end of the channel and begins affecting the newly-entering fluid's formation of liquid segments.

For industrial applications, the location of the fill port may be of key importance for achieving a desired average liquid segment length at critical locations in the device. The location of where the fluid is introduced to the device should be positioned with respect to where the shortest liquid segments are desired. The device's fill ratio should also be considered in accordance with the fluid distributions presented. Generally speaking, shorter liquid segments may be desirable near evaporator locations to assist with evaporation of the liquid segment's menisci, and should be placed with respect to the distribution of η values in terms of r. This liquid segment length can also be controlled somewhat by adjusting the injection rate of the working fluid into the device.

It is also expected that similar trends of liquid-vapor distributions described in this work will be observed with OHP configurations containing several realistic turns and serpentine passes. This is due to the fact that the liquid-vapor segments were maintained as they traveled along the length of the tube, and turns are not expected to consolidate or separate liquid segments that have already formed.

Similarly, the distributions and trends observed in this straight open-loop configuration are expected to be observed in closed-loop OHPs as well. It is expected that the working fluid will split evenly from the injection location, and as the fluid meets in the middle of the close-loop configuration's channels, it is expected that the η distribution will begin to change similar to when the liquid segments met the end of the single tube described in this work's configuration. This would initiate the same compression effect where longer average liquid segments and a greater variability will begin to present itself at the injection location where new fluid is entering the device.

CHAPTER 4.

ECONOMICS

4.1 OHP Market

The market for Oscillating Heat Pipes has been expanding in recent years and the growing market presence was a key motivator for this work. According to knowledge from those in the industry, the open market opportunity of OHPs is estimated to be between $2.3-2.5 billion USD, based on existing markets using traditional heat pipes[1]. These markets include the automotive, aerospace and defense, medical, telecommunications, consumer electronics, power and energy, and food and beverages industries. Currently, OHPs make up a small percentage of these markets, though their adoption has continued to grow in recent years as the technology becomes better understood and more easily modeled by the practicing community.

The true market size of OHPs is challenging to determine, however, since this market value only captures discrete OHP and wicked Heat Pipe sales, and does not capture OHPs and wicked HPs that are sold as integrated units in larger devices. Since new areas and applications are hindered by the lack of known modeling practices, the true size of the market is unknown, though it is expected to be substantial based on the current size of the market.

To assess the OHP industry as a whole, a Porter's Five Forces analysis is conducted below in

[1] Personal conversation with Joe Boswell, ThermAvant Technologies.

Table 3, which describes that one of the major barriers to growth of the technology in industry centers around modeling the device's behavior.

Table 3 Porter's Five Forces analysis of OHP industry.

	Rating	Rationale
Rivalry Amongst Industry	Low	Currently there is very limited rivalry in the OHP industry. One dominant player, ThermAvant Technologies, leads the industry, and few if any other comparable contenders exist in the market. Other sources developing the technology primarily involve academic research from around the world.
Threat of New Entrants	Low	A major barrier to entry for new entrants is primarily centered around the ease and confidence in modeling the complex nature of the OHP. Currently, the most mature models in industry rely on correlations developed over several years and considerable investment, which would be challenging to overcome by a new entrant.
Threat of Substitutes	Medium-High	Alternative, incumbent technologies to OHPs exist. Though alternative technologies may score lower on the Size, Weight, and Power scale comparatively, alternatives such as wicked copper-water heat pipes and pyrolytic graphite may continue to be used in place of OHPs due to simpler and better understood modeling of the technology.
Bargaining Power of Buyers	Low	Limited quantity of OHP suppliers in the industry makes competitive sourcing of OHPs challenging for buyers.
Bargaining Power of Suppliers	Low	OHP devices can be made in a number of materials and working fluids, and limited specialty equipment is required in their design, fabrication, and testing.

Though the OHP industry is growing as a whole due to the success of a small number of existing OHP suppliers, the technology as a whole may be adopted more rapidly if more OHP suppliers existed. The major barrier to entry for new entrants to the OHP supplier industry is the lack of a comprehensive theoretical model, with accurate inputs, to simulate the device's

performance. Currently a number of models exist that simulate specific regimes of the device's performance and physical performance with varying degrees of accuracy, but all rely on assumptions, empirical input, or correlations.

Wider adoption of the technology by users may also be hindered without a comprehensive model. If users, or buyers, of OHP technology must continue to rely on industry suppliers with proprietary models built on experimentally validated correlations to design and predict the device's performance, the rate of wider adoption may be hindered. Alternatively, models that are available for users to design their own devices and compare performance against competing technologies may be a bridge to wider adoption of the technology. This would also likely lead to novel designs that further improve the case for using OHPs over competing technologies. Competitive advantage of industrial OHP suppliers could be maintained in the fabrication and general manufacturing of the devices, specifically in specialty materials, designs, and operating environments and conditions.

For example, the industry know-how for wicked copper-water heat pipes, whose underlying physics is relatively better understood and able to be modeled, is in the manufacturing method of the wick structure and general manufacturing of the device. The ability to accurately model traditional heat wicked pipe devices, including capillary pumping, evaporation, vapor transport, and condensation, has resulted in an explosion of adoption over the past decades, where these devices are operating daily in applications ranging from space to personal computing. Similar adoption could be attained with OHPs, though there is a steeper curve to climb in understanding the underlying physics governing their operation and modeling the device's behavior.

As understanding of the OHP's mechanics improves, work towards a comprehensive theoretical model will lower the barrier to entry for new entrants and wider adoption by users in the industry. Furthermore, accurate inputs and initial conditions for these models should exist, such as the initial conditions presented in this work. Using known initial conditions will enable refinement and validation of more accurate models and in turn accelerate the adoption of OHP technology in practice.

4.2 Value of a Known Fill Ratio

Other advantages resulting from this and future related work include models that can predict a more accurate and optimal fill ratio for a given device and its operating conditions. Models that use more accurate initial conditions can be used to refine and validate performance and behavior of models more quickly and produce more accurate results from the model. These more accurate models can, in turn, be used to save time and equipment cost during the integration. For example, the current state of the art practice is to estimate the proper fill ratio for the desired performance, and then validate with tests at other fill ratios in a given range around the estimate to refine the optimal fill ratio. This can take on the order of weeks, which negatively affects the product's time to market and ties up resources. An estimate of labor and equipment costs per new device are below in

Table 4.

Table 4 Cost estimate of OHP integration in industry.

	Hours (hrs)	Rate ($/hr)	Cost ($)	Total ($)
Current Labor	80	250	-	20,000
Current Equipment	-	-	20,000	20,000
Current Sum				**40,000**
New Labor	40	250	-	10,000
New Equipment	-	-	10,000	10,000
New Sum				**20,000**

By knowing the optimal fill ratio of the device via the model and accurate initial conditions, less labor will be required during integration of new devices and less equipment will be required as throughput improves. An estimate of 50% savings in each category is described above with the knowledge accurate initial conditions and models to predict the device's optimal fill ratio. Currently, there are approximately 10s-100s of new OHP devices integrated per year, which means this knowledge could yield $0.2M-$2.0M of savings per year toward a given company's bottom line[2]. This value would scale with the growth of OHPs in the future, and have multiplying effects as faster trades between working fluids and the faster down-selection of optimal fill ratios are arrived at.

4.3 New Charging Method

The liquid injection, or charging, method described in this work also has an impact on the industry. The current state of the art charging method is to fill the device to 100%, verify the mass of the system to identify the fill ratio, and then bleed liquid out until the desired fill ratio is measured or if overfilled [8]. Though this method may be acceptable for arriving at the desired

[2] Per conversation with Joe Boswell, ThermAvant Technologies.

fill ratio for lab test units or short production runs, it may prove undesirable for higher quantity serial production of OHPs, resulting in a more time-consuming process and with more wasted working fluid, especially if custom or uncommon working fluids are used. Alternatively, the procedure for charging the device described in this work would allow for a one-shot injection of the working fluid at the known fill ratio, saving time and material cost for each recurring production unit. This recurring savings may have a substantial impact on a company's bottom line as it would affect each device fabricated for development and production.

CHAPTER 5.

CONCLUSIONS AND FUTURE RESEARCH

5.1 Summary of Findings and Conclusions

A method of introducing and measuring a controlled volume of fluid into an evacuated small diameter channel, representative of an Oscillating Heat Pipe, was presented. Measurements related to liquid segment length, count, and distribution were taken over three fill ratios, α = 25%, 50%, and 75%, and over three injection rate ranges, ν = 0.002-0.012 (Slow), 0.013-0.051 (Nominal), and 0.052-0.132 (Fast).

It was observed that the initial distribution of the ratio of liquid lengths to tube diameter, η, changed with respect to changes in α and ν values. Specifically, tests with a lower fill ratio and slower injection rate resulted in the most consistent and shortest η liquid segments, which may lend to the most desirable conditions for startup. A critical fill ratio was also observed, between α = 25% and 50%, where new liquid entering the channel began growing in average length once the first-most liquid-vapor segments had reached the far-end of the channels and began providing a spring-like resistance for new liquid entering the channel. This was described as the compression effect, referring to the increase in η values of new liquid entering the channels for higher α tests, shown in Figure 16. The rate at which the working fluid was introduced into the device, ν, was also found to have an impact on the resulting distribution, with slower ν rates having a more consistent distribution and lower average η value, and faster ν rates having a wider distribution and higher average η value.

This work may be used to validate and mature different analytical models of OHP devices in lab environments. These more robust models can then be applied to other initial

conditions of liquid distributions in the channels, such as after a device has been charged, sealed, and shipped, which may have affected the distribution of liquid within the device. Additionally, though the exact lengths and distributions of liquid may change with different working fluids and channel diameters, the general compression effect of η as α increases is expected to present itself, and increases in ν are expected to affect length and consistency in the resulting distribution. The location of the OHP's fill port should also be considered with respect to where the evaporating and condensing section(s) are in the device, since an adverse placement of working fluid, i.e., longer liquid segments near evaporating sections, may impact startup. This should place an increased focus on charging methods' impact on lab and industrial-scale production of OHPs.

The trends in η distribution shown in this single straight channel are expected to be similar in realistic devices with several serpentine turns, due to the fact that the liquid-vapor segments were maintained as they traveled along the length of the single tube and turns are not expected to consolidate or separate liquid segments that have already formed. Furthermore, similar trends are expected to be observed in closed-loop OHPs as well, and that the working fluid will split evenly in both directions from the injection location throughout the channel. As the fluid meets in the middle of the close-loop configuration's channels, the η distribution should present a similar compression effect in the new fluid entering the device. Future research should validate these hypotheses, and explore other related topics.

5.2 Future Research

Future work should expand on the topics introduced in this work, and may involve exploring η distributions with respect to changing the following variables:

- Different inner diameter tubing with water (e.g., 2 mm, 3 mm, 5 mm, etc.), to observe changes in liquid length distribution with respect to Bond number limit changes for the same working fluid ($Bo = 2.07$ for 4 mm diameter tubing discussed in this work).
- Different working fluids (e.g., alcohols, refrigerants, etc.), to observe the effect of different surface tension and other fluid properties have on the distribution of liquid segment formation. This may track with Bond number, or may present new results.
- Different channel substrates (e.g., hydrophobic, hydrophilic), to better understand how different surface energies affect liquid-vapor formation, and how this relates to different Bond number combinations.
- Visual recording of liquid entering and progressing throughout the channel, to better observe the liquid-vapor formation process, specifically with respect to the eddies observed and discussed in chapter 3.2.1, and to document if and how the radius of the leading meniscus evolves as the liquid progresses down the channel to obtain a better understanding of what we refer to as the compression effect and the role vapor pressure during filling may play in this.
- Alternative charging methods (e.g., methods described by Ma [8], etc.) may affect the initial lengths and distribution of liquid in the device.
- Different charging orientations (e.g., vertical, 45 degrees, etc.) and other externally applied forces (e.g., vibration from shipping, shock, etc.) may affect the initial lengths and distribution, as was qualitatively shown in this work. This should be better understood for practical applications and may include comparing the externally applied

forces with vapor spring magnitude and the resulting consolidation or count, and/or the distribution of resulting liquid segments.

- Effect of serpentine turns in the channel layout, and a close-loop layout, should be characterized to validate the hypothesis that this will not affect the initial distribution of liquid segments presented in this work.
- Effect of multiple operational start-stop/heating-cooling cycles should be characterized to validate what the resulting liquid-vapor distribution(s) become over the life of the device.

APPENDIX

A.1 Distribution of η per 10% increments of r for α = 25%

A.1.1 Distribution of η for r = 0-10% for α = 25%

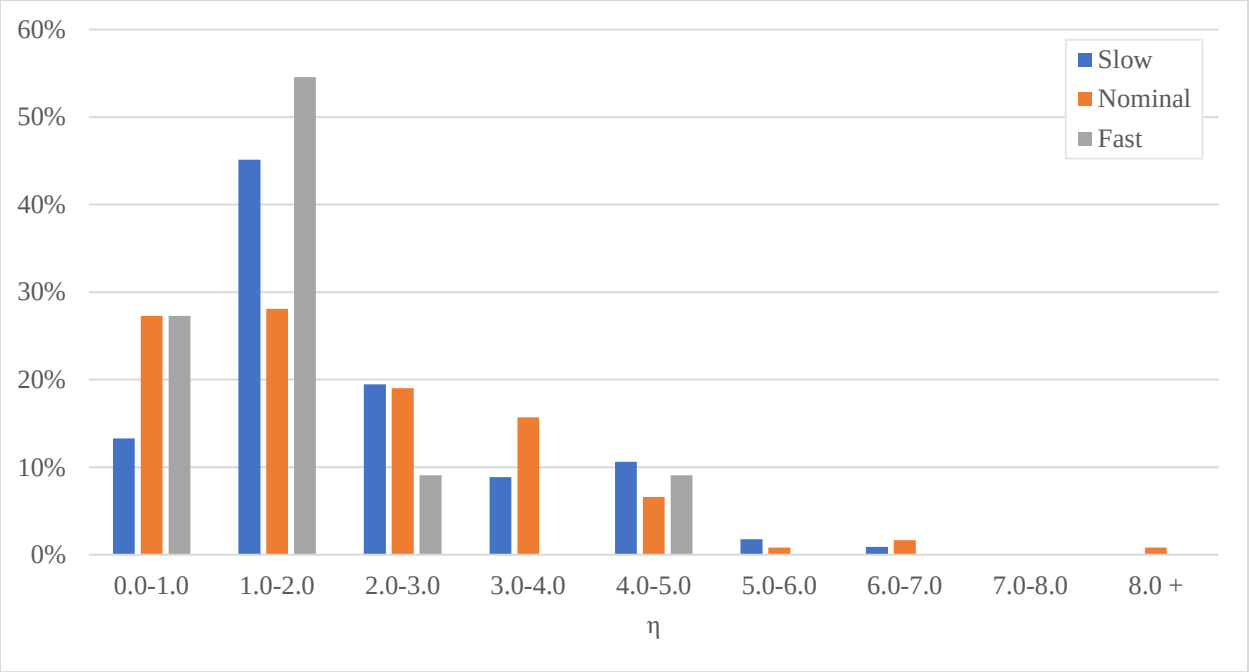

A.1.2 Distribution of η for r = 10-20% for α = 25%

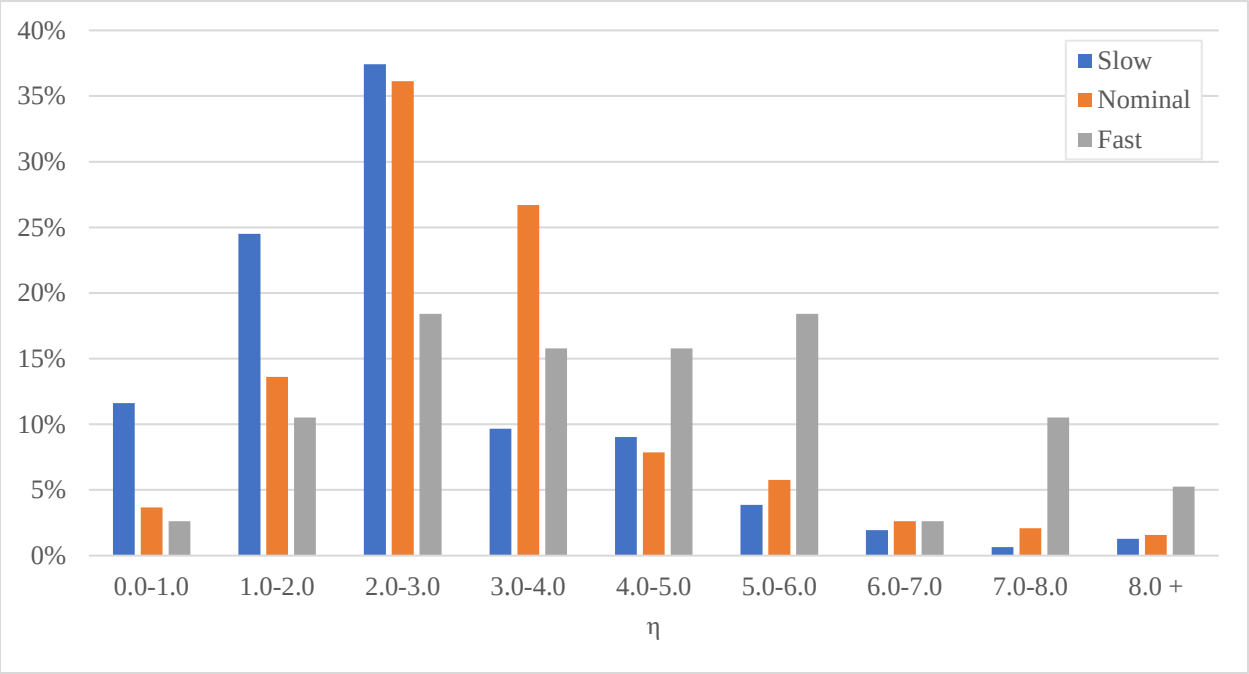

A.1.3 Distribution of η for r = 20-30% for α = 25%

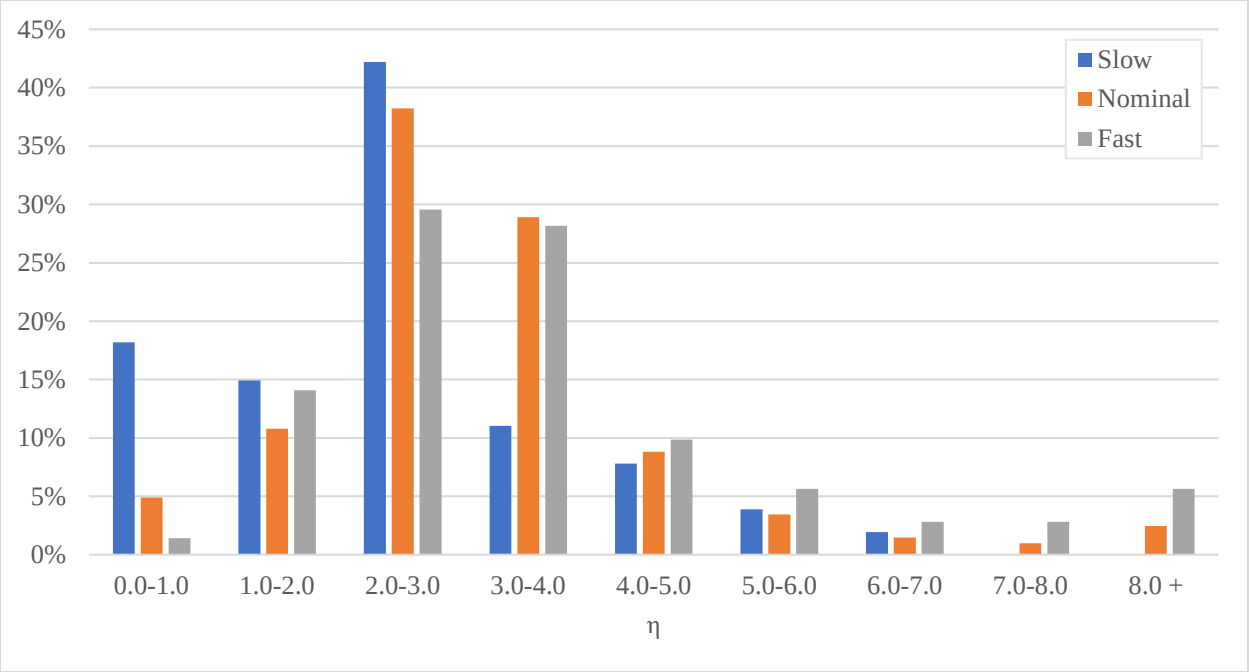

A.1.4 Distribution of η for r = 30-40% for α = 25%

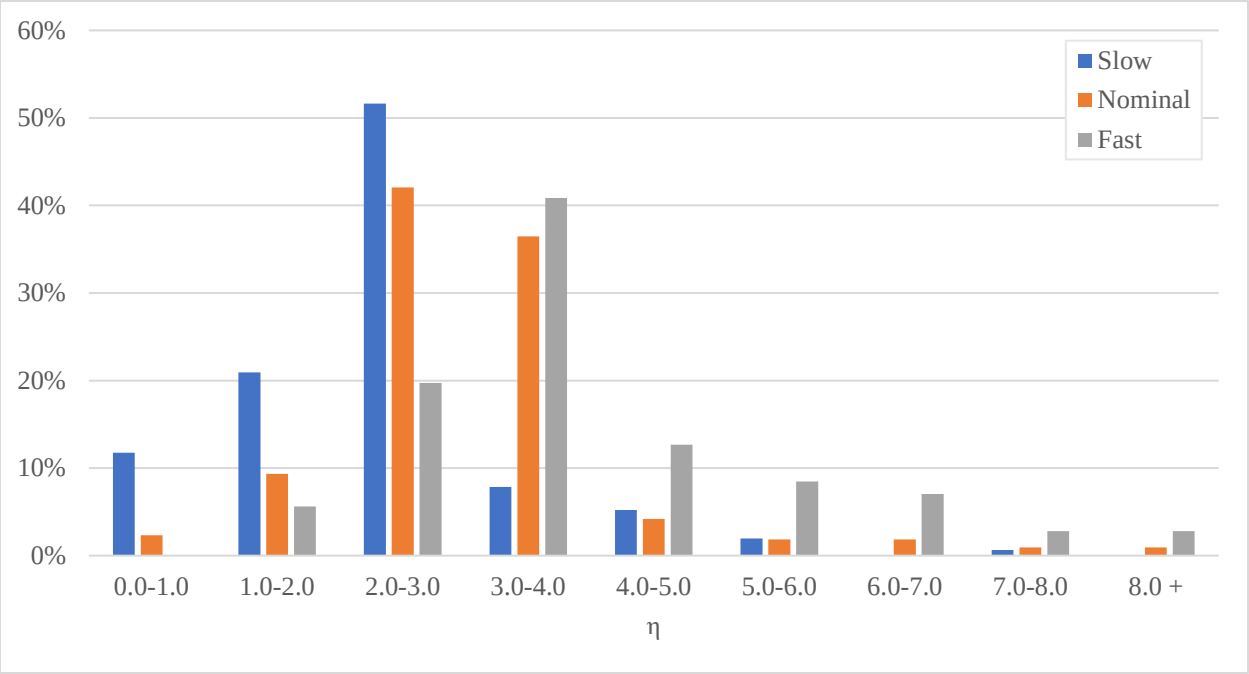

A.1.5 Distribution of η for r = 40-50% for α = 25%

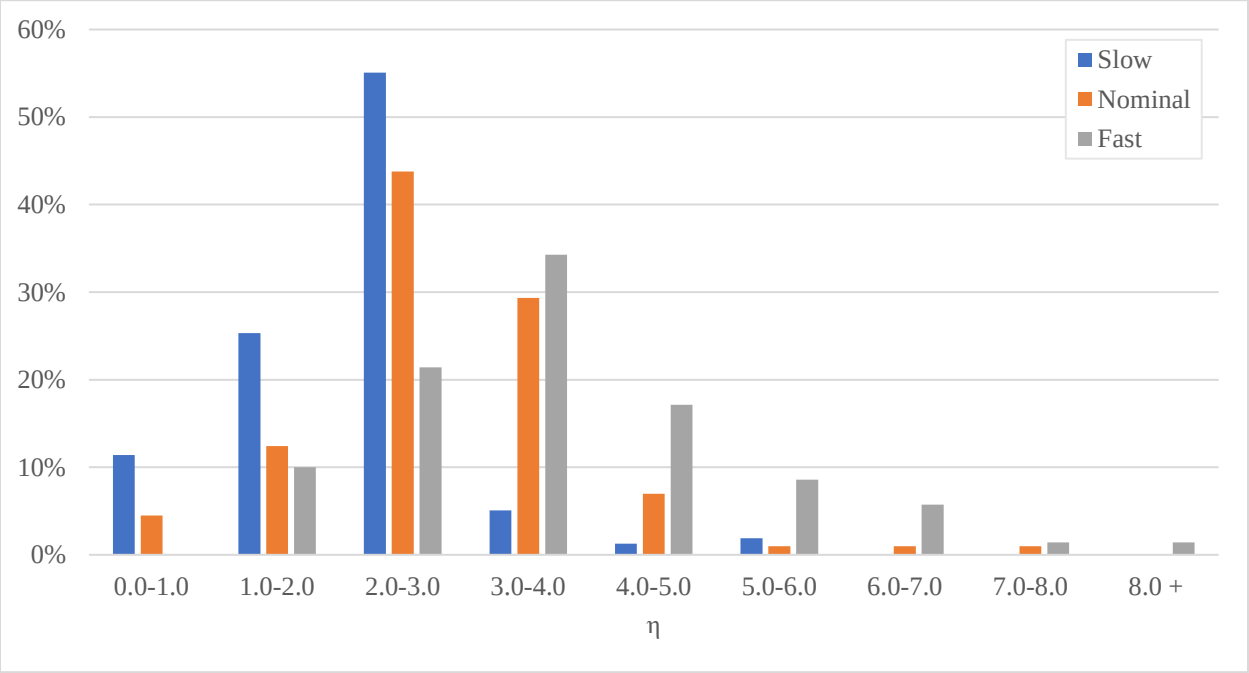

A.1.6 Distribution of η for r = 50-60% for α = 25%

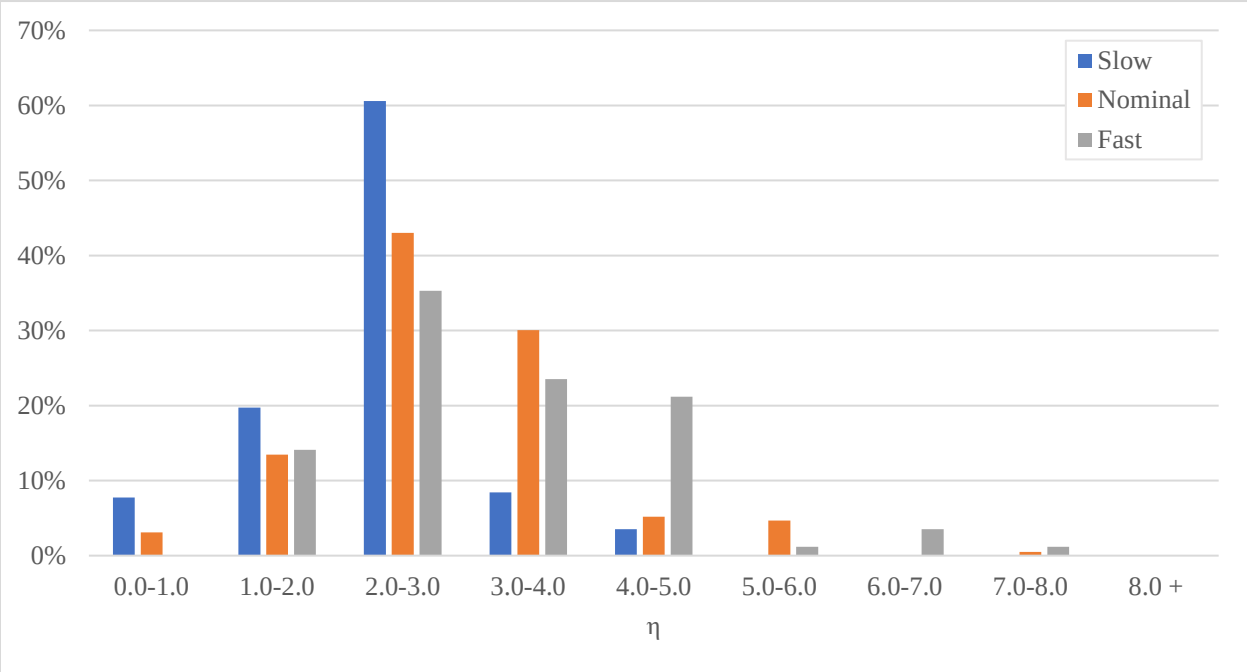

A.1.7 Distribution of η for r = 60-70% for α = 25%

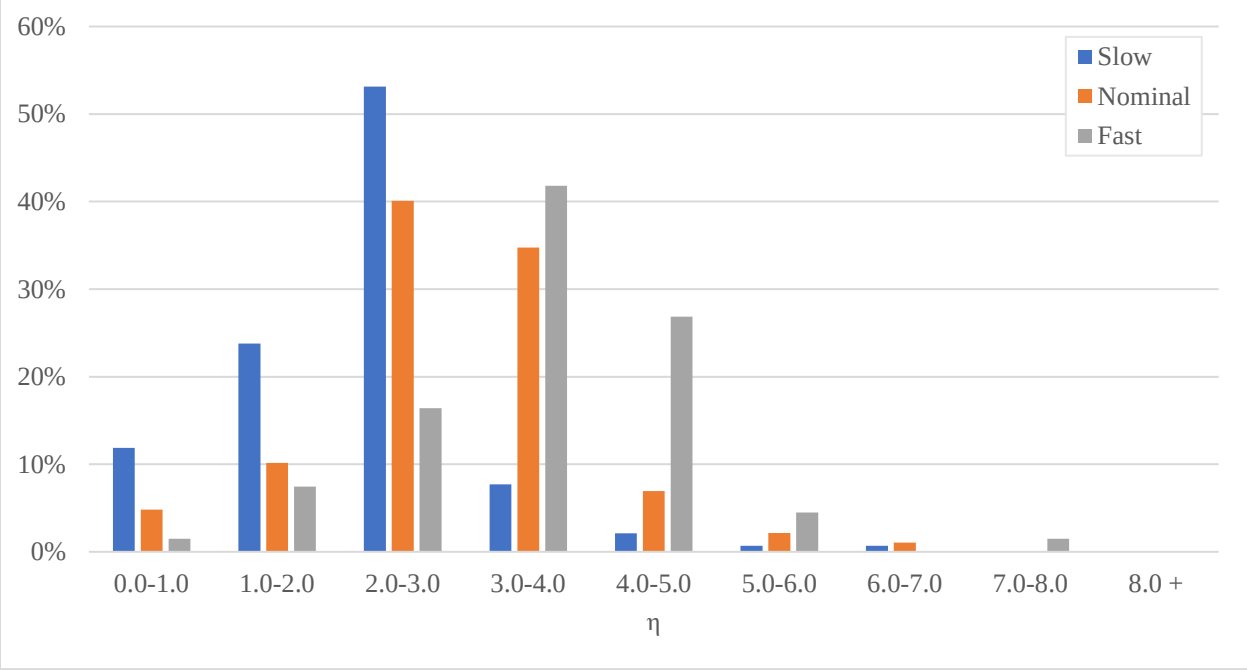

A.1.8 Distribution of η for r = 70-80% for α = 25%

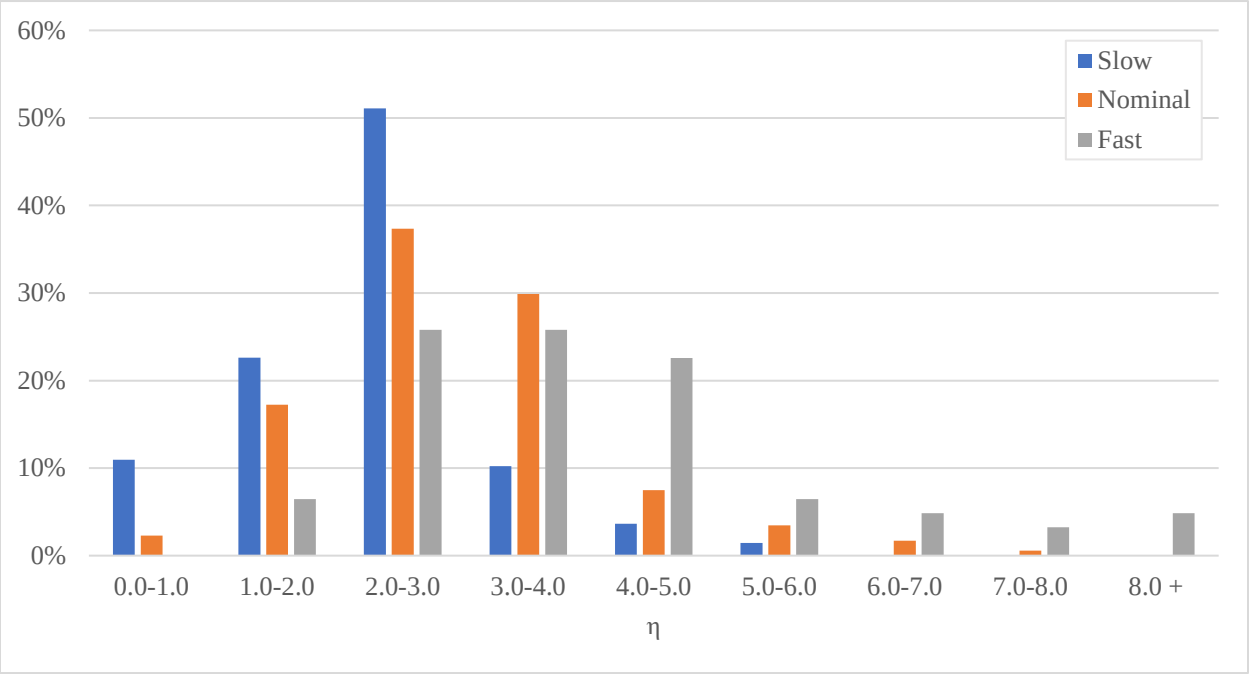

A.1.9 Distribution of η for r = 80-90% for α = 25%

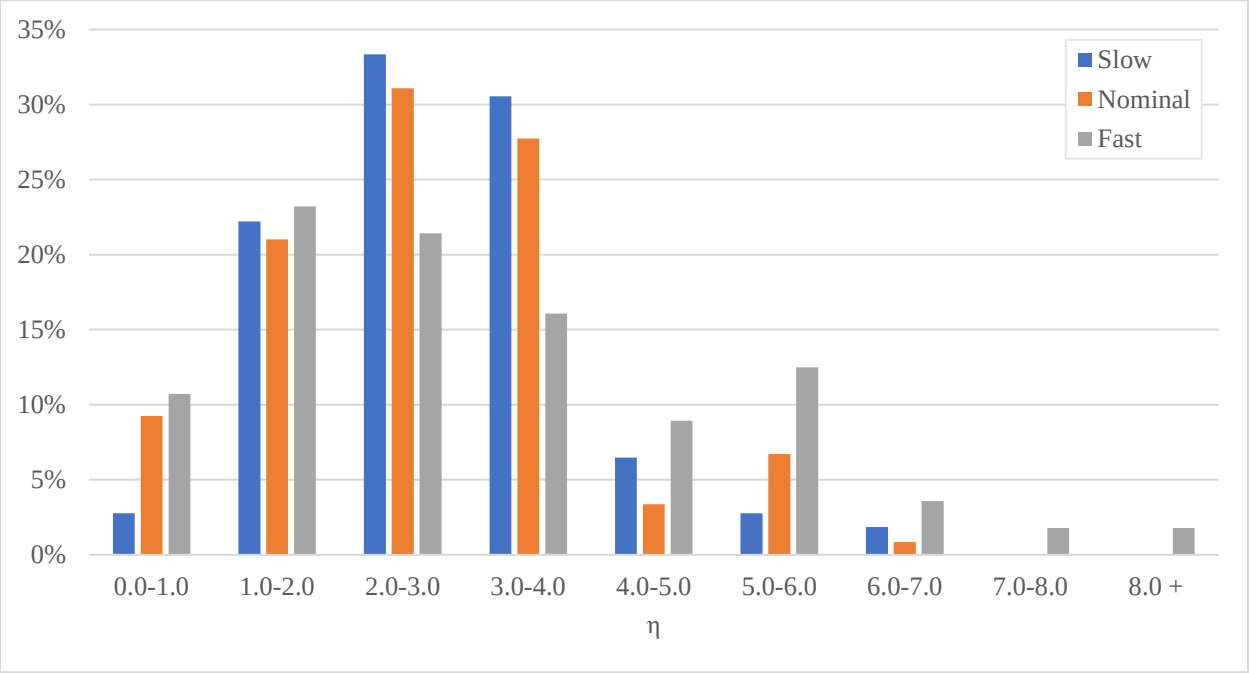

A.1.10 Distribution of η for r = 90-100% for α = 25%

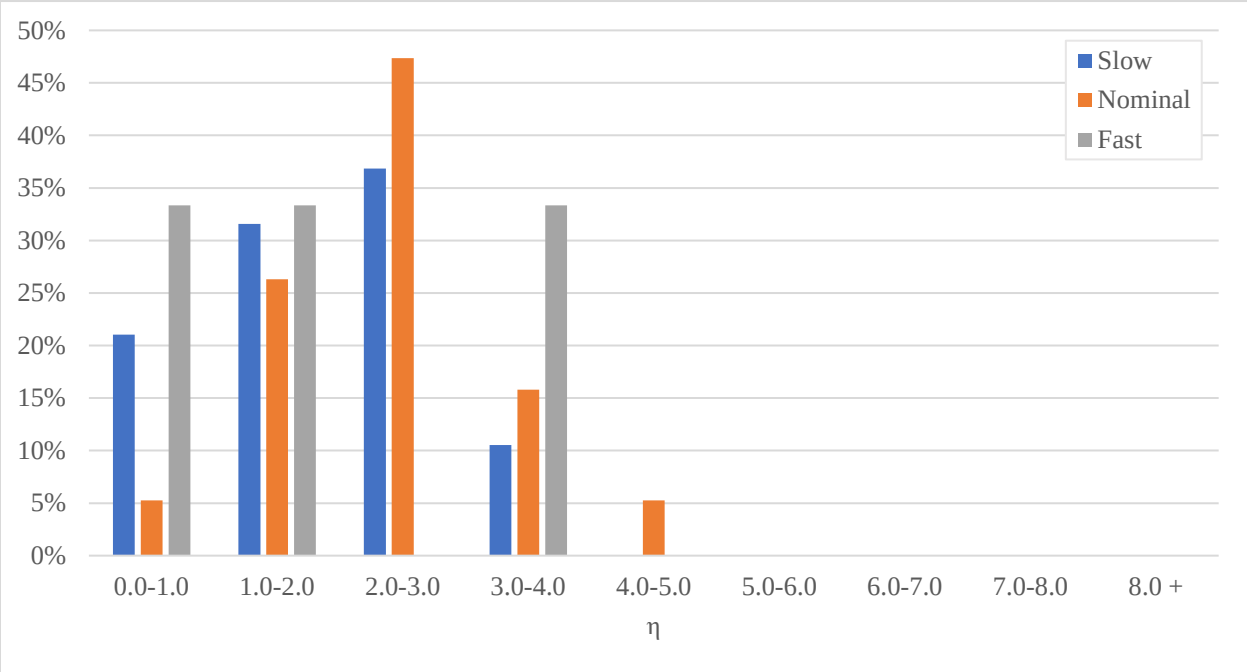

A.2 Distribution of η per 10% increments of r for α = 50%

A.2.1 Distribution of η for r = 0-10% for α = 50%

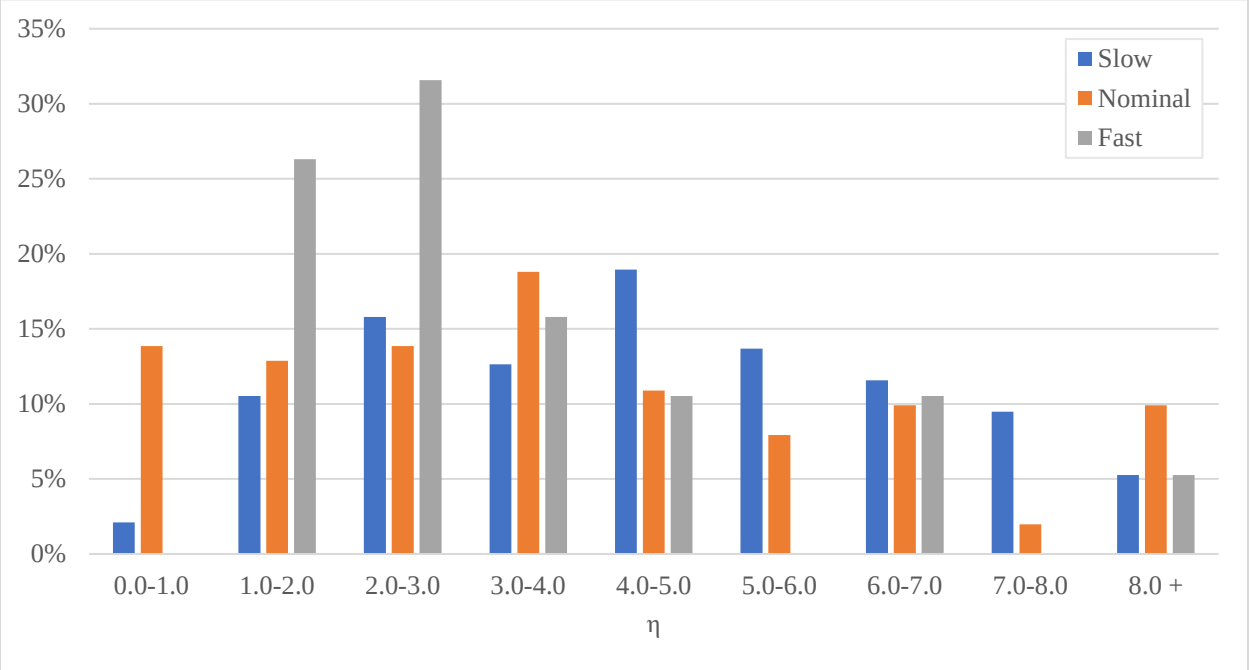

A.2.2 Distribution of η for r = 10-20% for α = 50%

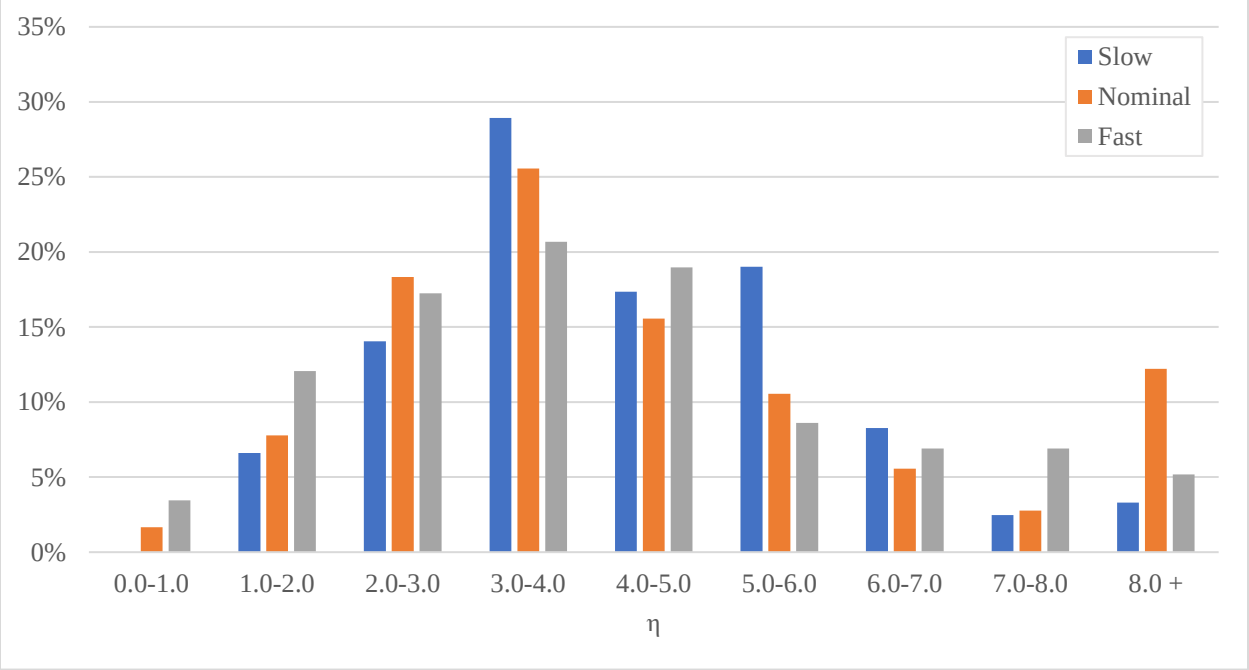

A.2.3 Distribution of η for r = 20-30% for α = 50%

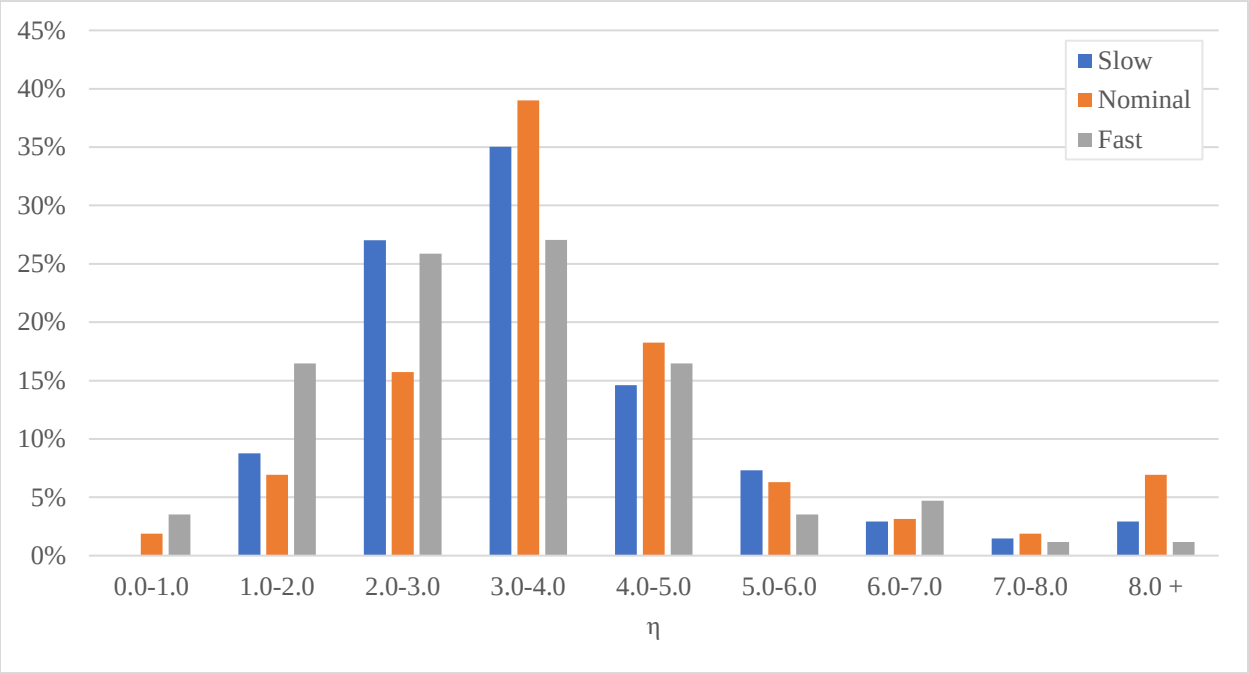

A.2.4 Distribution of η for r = 30-40% for α = 50%

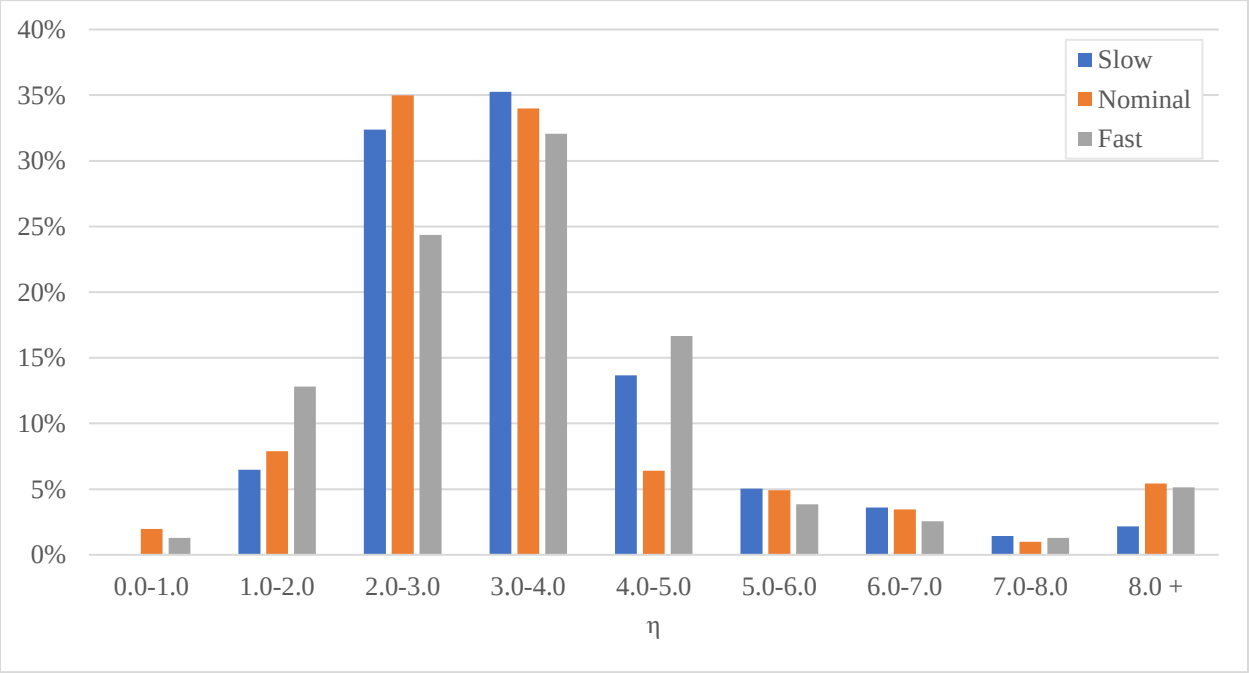

A.2.5 Distribution of η for r = 40-50% for α = 50%

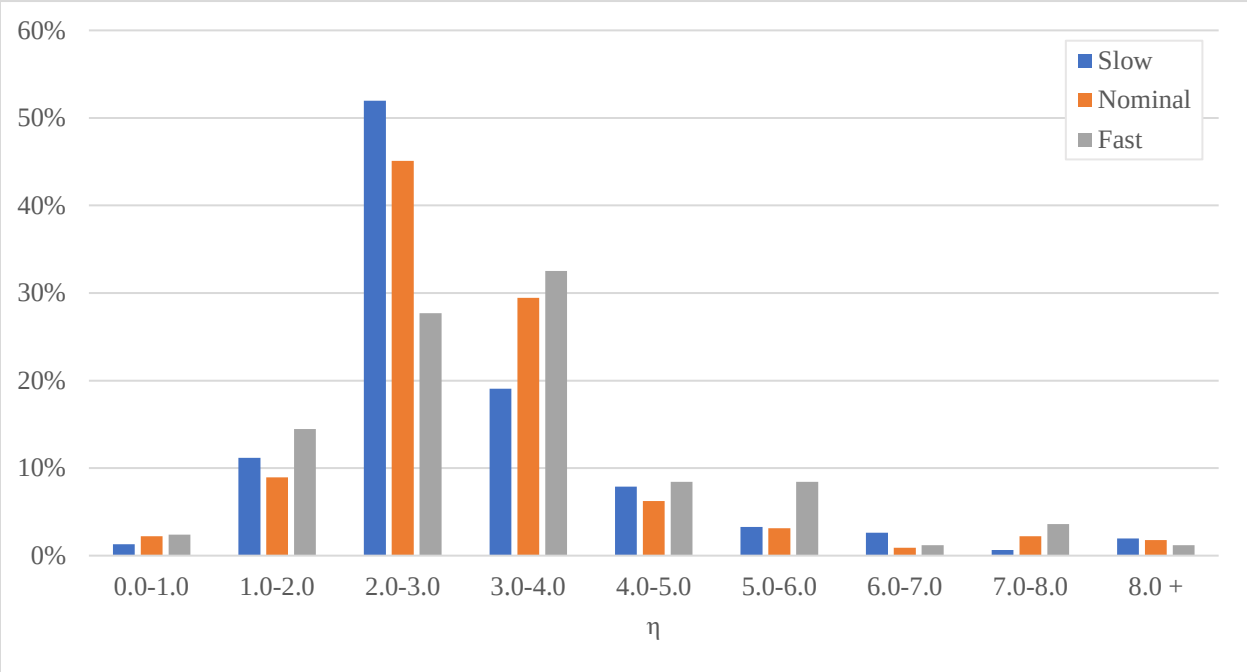

A.2.6 Distribution of η for r = 50-60% for α = 50%

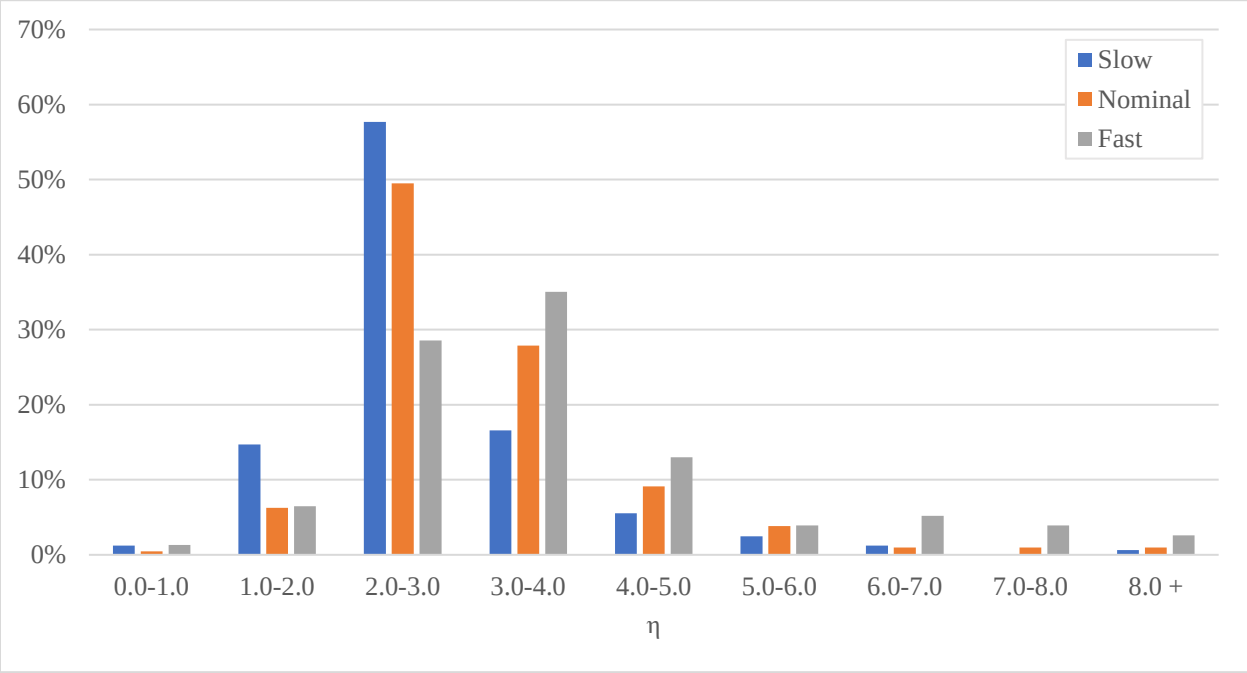

A.2.7 Distribution of η for r = 60-70% for α = 50%

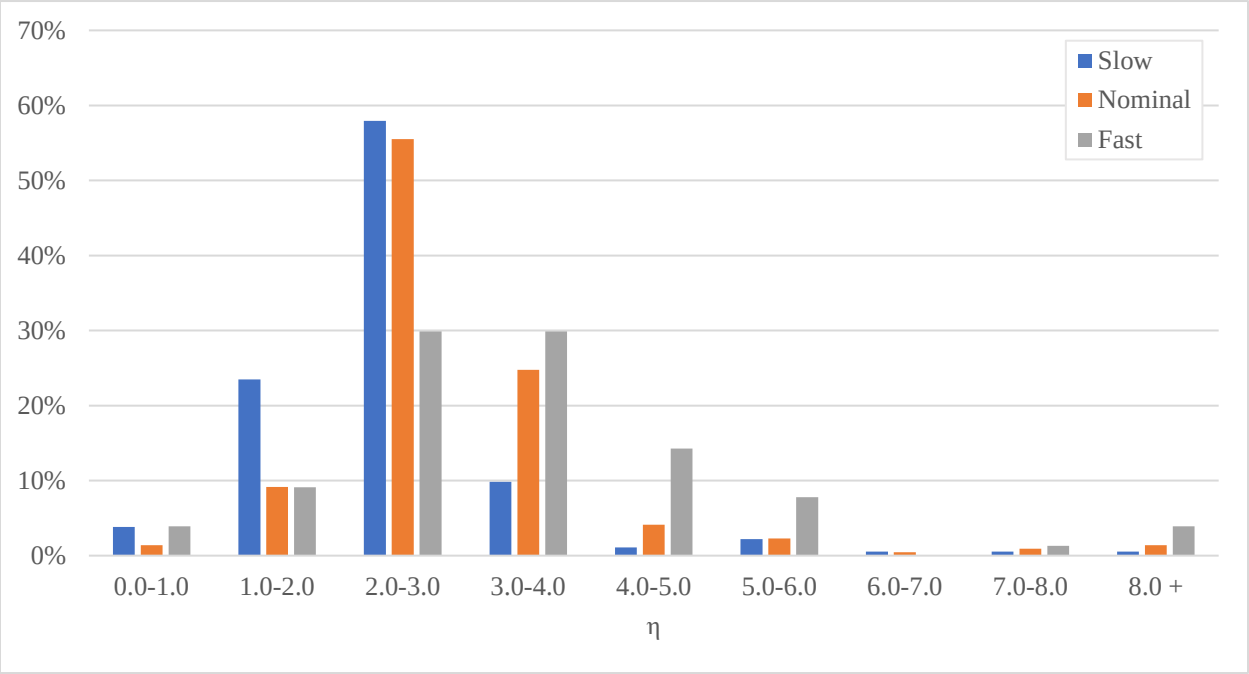

A.2.8 Distribution of η for r = 70-80% for α = 50%

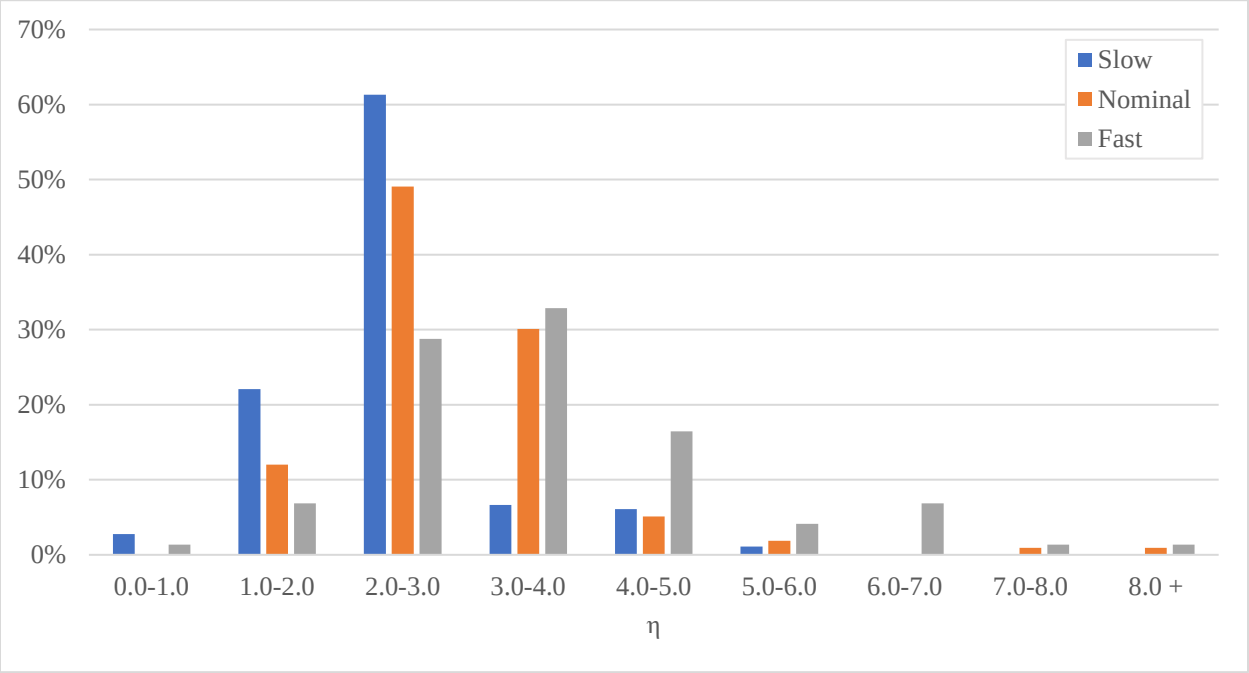

A.2.9 Distribution of η for r = 80-90% for α = 50%

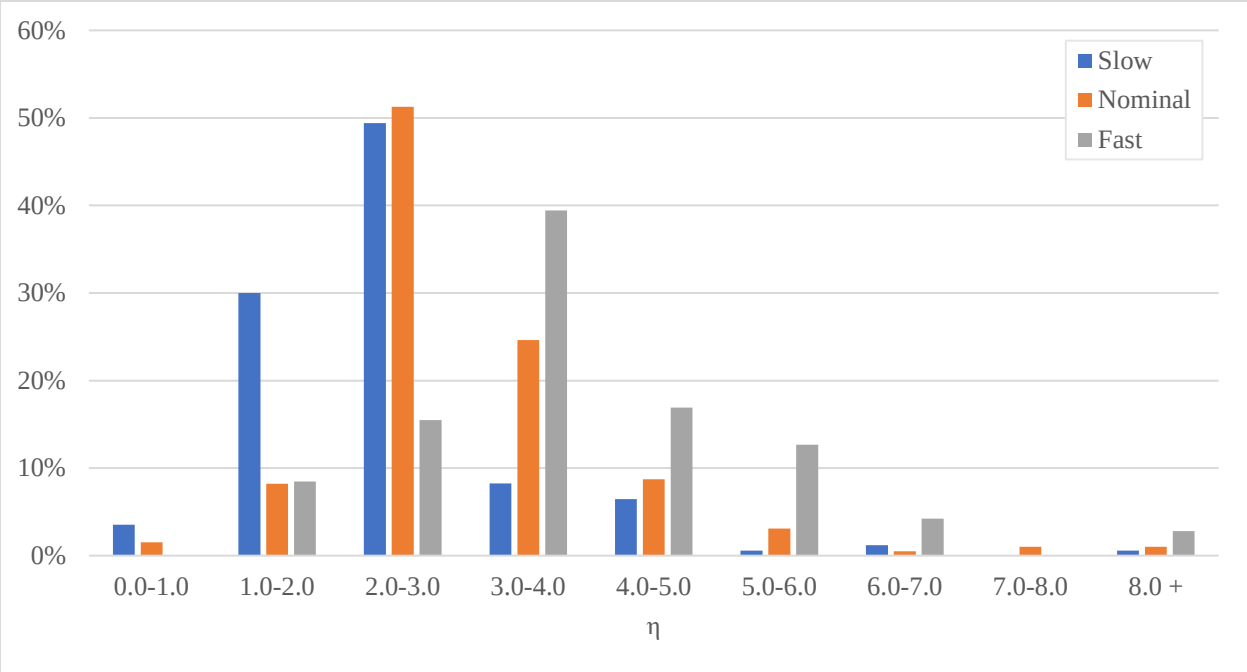

A.2.10 Distribution of η for r = 90-100% for α = 50%

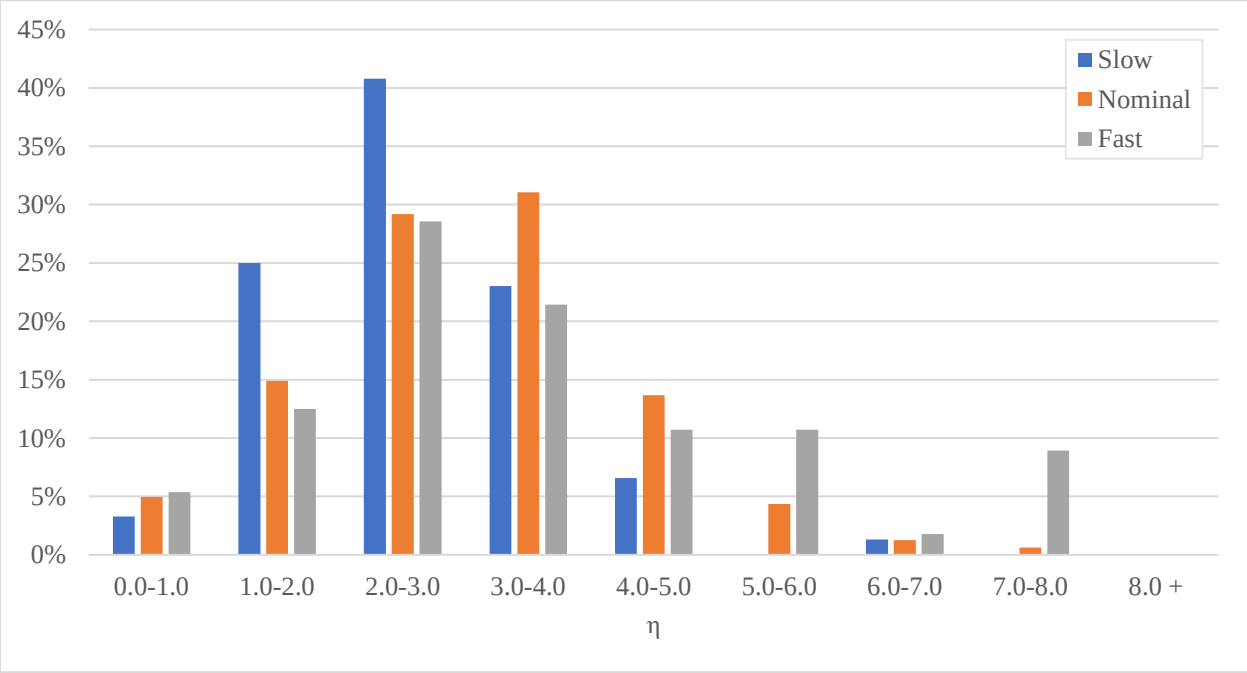

A.3 Distribution of η per 10% increments of r for α = 75%

A.3.1 Distribution of η for r = 0-10% for α = 75%

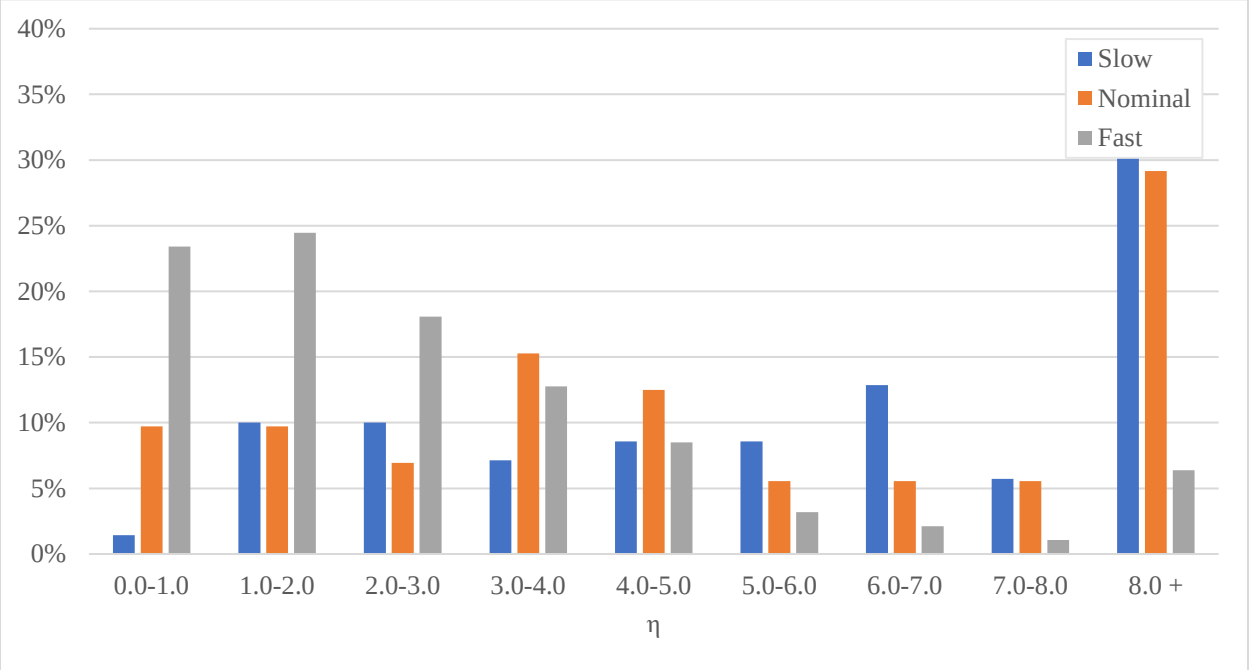

A.3.2 Distribution of η for r = 10-20% for α = 75%

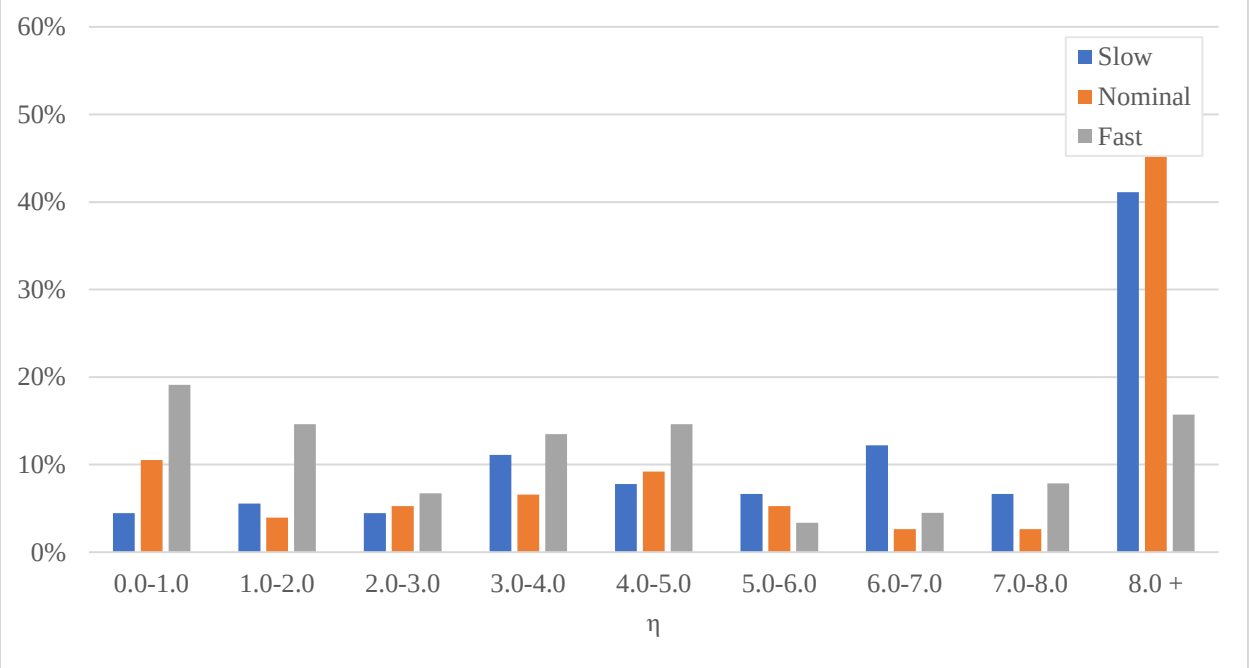

A.3.3 Distribution of η for r = 20-30% for α = 75%

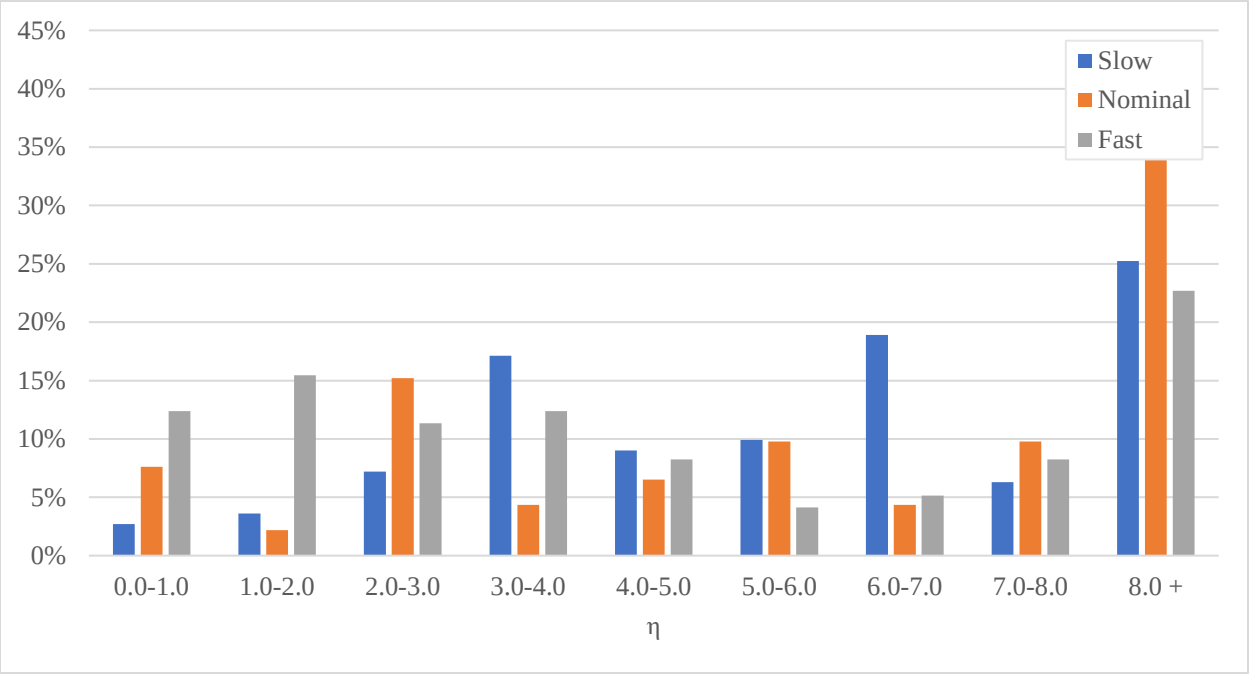

A.3.4 Distribution of η for r = 30-40% for α = 75%

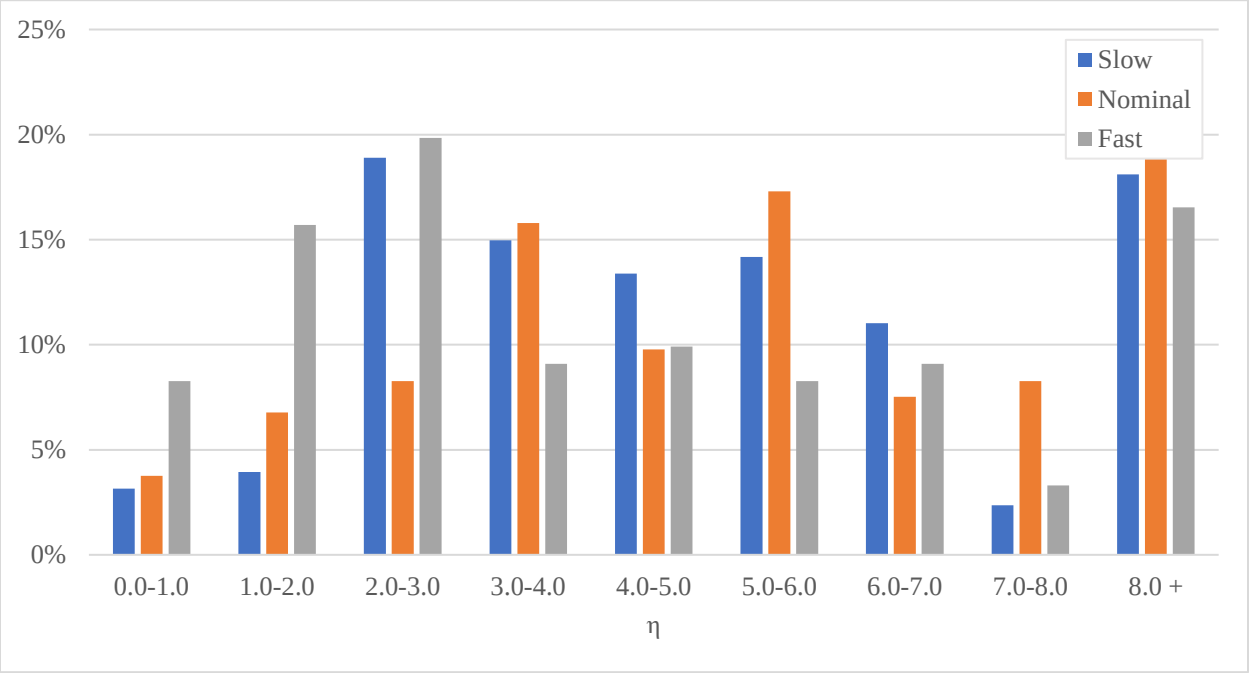

A.3.5 Distribution of η for r = 40-50% for α = 75%

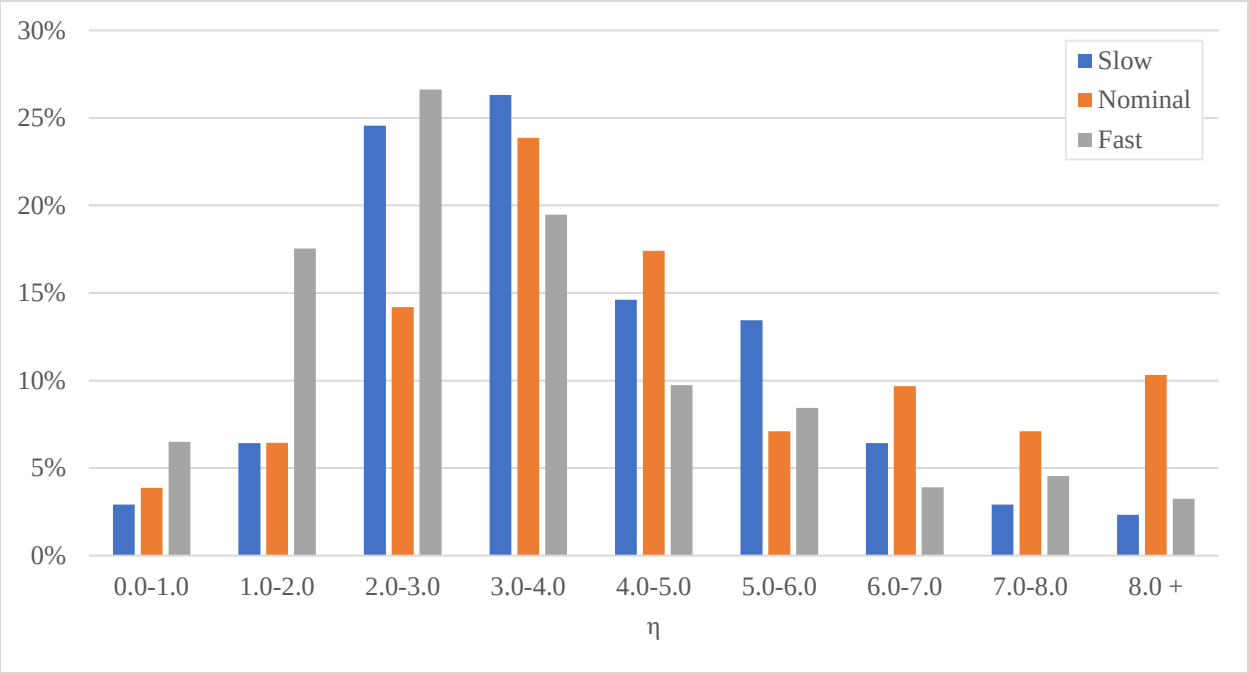

A.3.6 Distribution of η for r = 50-60% for α = 75%

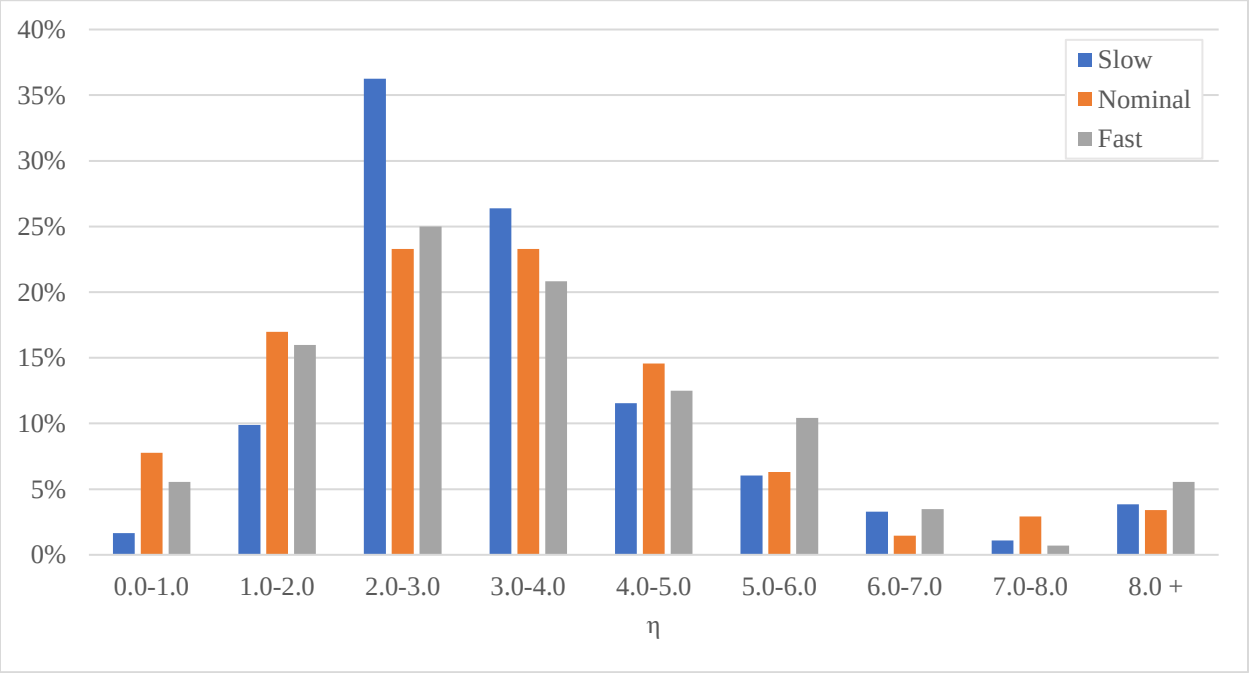

A.3.7 Distribution of η for r = 60-70% for α = 75%

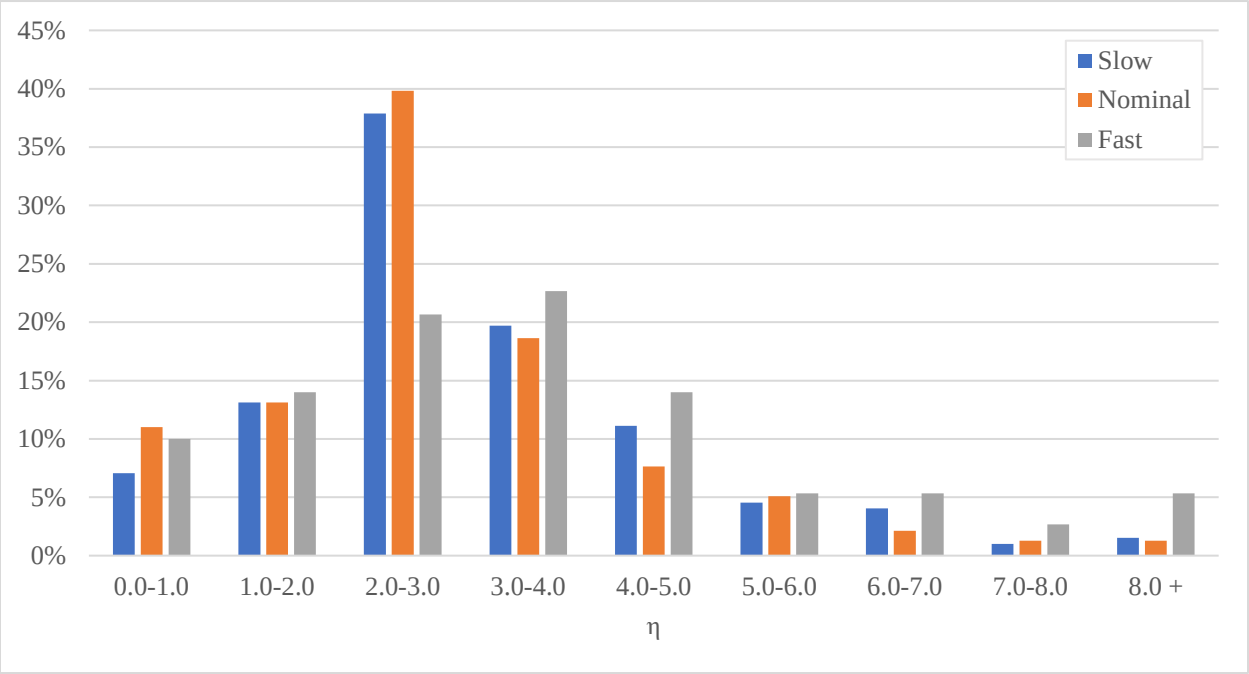

A.3.8 Distribution of η for r = 70-80% for α = 75%

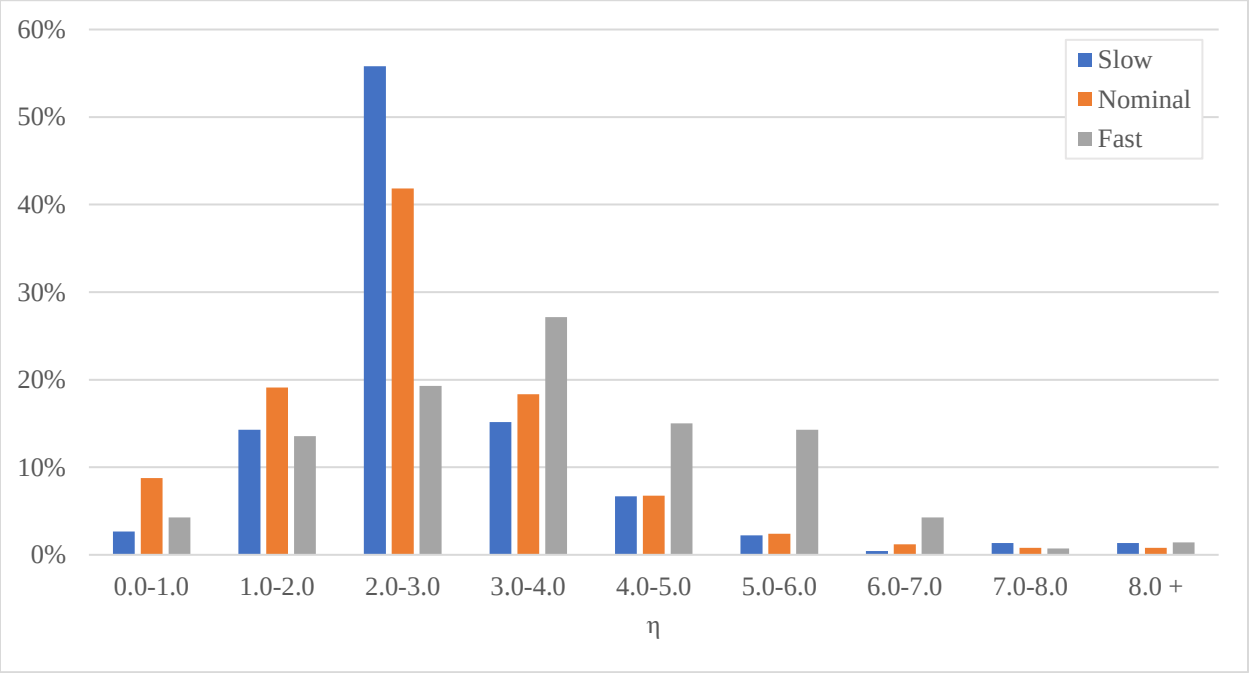

A.3.9 Distribution of η for r = 80-90% for α = 75%

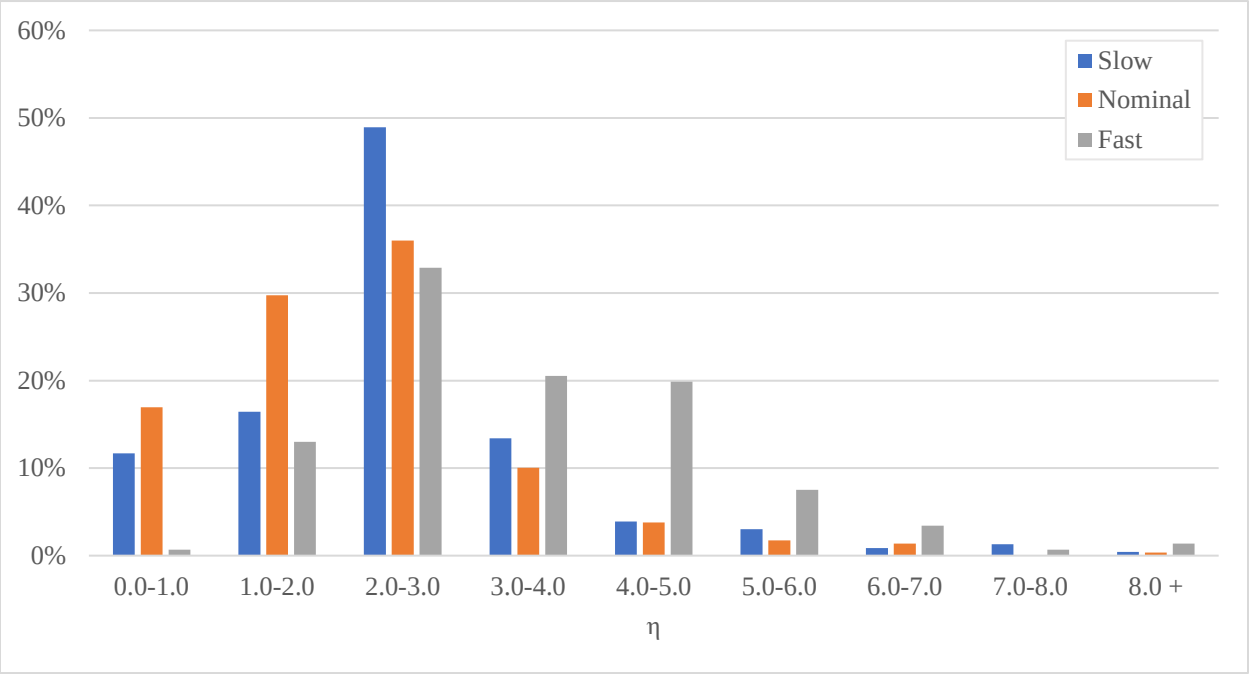

A.3.10 Distribution of η for r = 90-100% for α = 75%

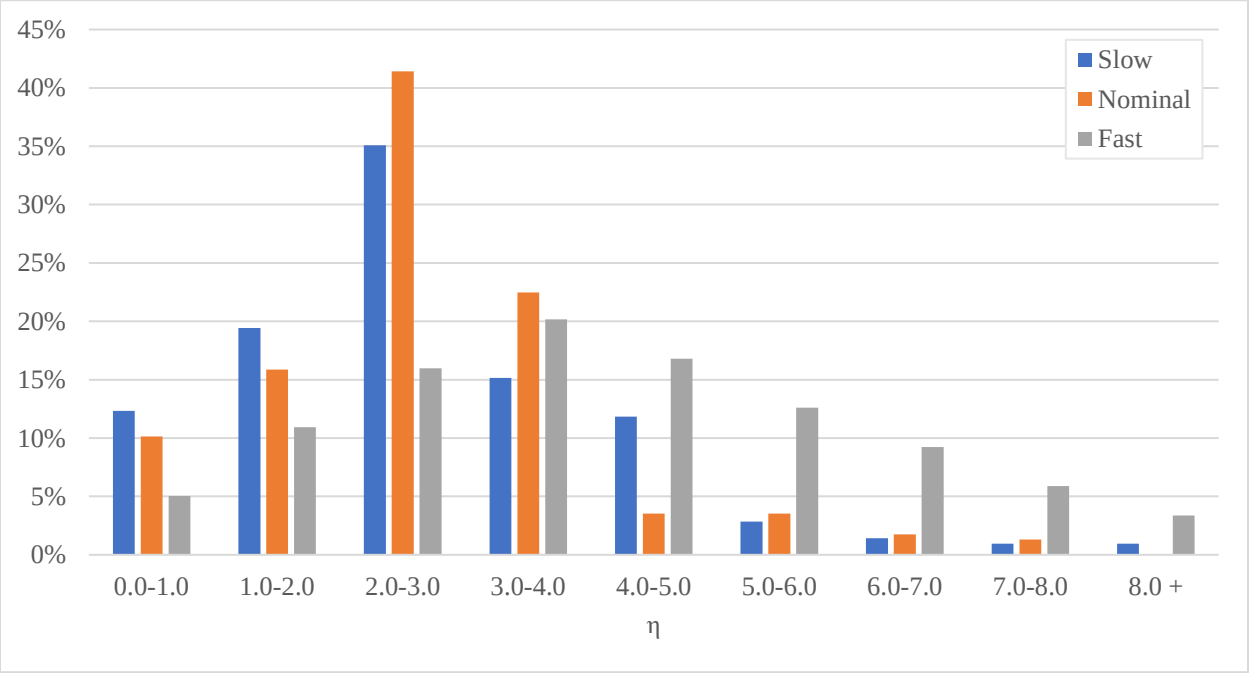

BIBLIOGRAPHY

[1] H. Akachi, “Structure of a heat pipe,” US Patent No. 4921041, 1990.

[2] M. Mameli, M. Marengo, and S. Zinna, “Numerical investigation of the effects of orientation and gravity in a closed loop pulsating heat pipe,” *Microgravity Sci. Technol.*, vol. 24, no. 2, pp. 79–92, 2012.

[3] T. Daimaru, S. Yoshida, H. Nagai, A. Okamoto, M. Ando, and H. Sugita, “Mathematical Modeling and Experimental Validation of Oscillating Heat Pipes,” in *44th International Conference on Environmental Systems*, 2014, pp. 1–14.

[4] S. Khandekar, N. Dollinger, and M. Groll, “Understanding operational regimes of closed loop pulsating heat pipes: An experimental study,” *Appl. Therm. Eng.*, vol. 23, no. 6, pp. 707–719, 2003.

[5] P. Angeli and A. Gavriilidis, “Taylor Flow in Microchannels,” *Encyclopedia of Microfluidics and Nanofluidics2*. Springer, pp. 1–9, 2014.

[6] B. Mehta and S. Khandekar, “Taylor bubble-train flows and heat transfer in the context of Pulsating Heat Pipes,” *Int. J. Heat Mass Transf.*, vol. 79, pp. 279–290, 2014.

[7] R. Gupta, D. Fletcher, and B. Haynes, “Taylor flow in microchannels: A review of experimental and computational work,” *J. Comput. Multiph. Flows*, vol. 2, no. 1, pp. 1–31, 2010.

[8] H. Ma, *Oscillating Heat Pipes*. Springer, 2015.

[9] Y. Zhang and A. Faghri, “Heat transfer in a pulsating heat pipe with open end,” *Int. J.*

Heat Mass Transf., vol. 45, pp. 755–764, 2002.

[10] H. B. Ma, B. Borgmeyer, P. Cheng, and Y. Zhang, "Heat transport capability in an oscillating heat pipe," *J. Heat Transfer*, vol. 130, no. 8, pp. 1–7, 2008.

[11] S. Lips, A. Bensalem, Y. Bertin, V. Ayel, C. Romestant, and J. Bonjour, "Experimental evidences of distinct heat transfer regimes in pulsating heat pipes (PHP)," *Appl. Therm. Eng.*, vol. 30, pp. 900–907, 2010.

[12] J.-S. Kim, N. H. Bui, H.-S. Jung, W.-H. Lee, and H. Bui, "The Study on Pressure Oscillation and Heat Transfer Characteristics of Oscillating Capillary Tube Heat Pipe," *KSME Int. J.*, vol. 17, no. 10, 2003.

[13] J. Jo, J. Kim, and S. J. Kim, "Experimental investigations of heat transfer mechanisms of a pulsating heat pipe," *Energy Convers. Manag.*, vol. 181, no. December 2018, pp. 331–341, 2019.

[14] V. S. Nikolayev, "A dynamic film model of the pulsating heat pipe," *J. Heat Transfer*, vol. 133, p. 081504, 2011.

[15] H. Onishi, K. Sawairi, and Y. Tada, "Numerical study on heat transport characteristics in oscillating heat pipe under small temperature difference," *Proc. First Pacific Rim Therm. Eng. Conf.*, 2016.

[16] B. L. Drolen and C. D. Smoot, "Performance Limits of Oscillating Heat Pipes: Theory and Validation," *J. Thermophys. Heat Transf.*, pp. 1–17, 2017.

[17] B. S. Taft, A. D. Williams, and B. L. Drolen, "Review of Pulsating Heat Pipe Working Fluid Selection," *J. Thermophys. Heat Transf.*, vol. 26, no. 4, 2012.

[18] V. M. Patel and H. B. Mehta, “Influence of working fluids on startup mechanism and thermal performance of a closed loop pulsating heat pipe,” *Appl. Therm. Eng.*, vol. 110, pp. 1568–1577, 2017.

[19] Y. Zhang and A. Faghri, “Advances and Unsolved Issues in Pulsating Heat Pipes,” *Heat Transf. Eng.*, vol. 29, no. 1, pp. 20–44, 2008.

[20] S. Khandekar and M. Groll, “An insight into thermo-hydrodynamic coupling in closed loop pulsating heat pipes,” *Int. J. Therm. Sci.*, vol. 43, no. 1, pp. 13–20, 2004.

[21] H. Yang, S. Khandekar, and M. Groll, “Performance characteristics of pulsating heat pipes as integral thermal spreaders,” *Int. J. Therm. Sci.*, vol. 48, no. 4, pp. 815–824, 2009.

[22] Z. Lin, S. Wang, and W. Zhang, “Experimental study on microcapsule fluid oscillating heat pipe,” *Sci. China, Ser. E Technol. Sci.*, vol. 52, no. 6, pp. 1601–1606, 2009.

[23] M. Mameli, V. Manno, S. Filippeschi, and M. Marengo, “Thermal instability of a Closed Loop Pulsating Heat Pipe: Combined effect of orientation and filling ratio,” 2014.

[24] D. A. Chavan and V. M. Kale, “Understanding Effect of Operating Parameters on Thermal Performance of Closed Loop Pulsating Heat Pipe: An Experimental Study,” *Int. J. Curr. Eng. Technol. E-ISSN INPRESSCO IJCET Spec. Issue*, vol. 4106, no. 5, pp. 2347–5161, 2016.

[25] R. R. Riehl, “Characteristics of an Open Loop Pulsating Heat Pipe,” in *National Institute for Space Research - INPE/DMC/Satelite*, 2004.

[26] B. S. Taft, “Non-Condensable Gases and Oscillating Heat Pipe Operation,” *Front. Heat Pipes*, vol. 4, no. 1, pp. 1–6, 2013.

[27] D. Yin, H. Wang, H. B. Ma, and Y. L. Ji, “Operation limitation of an oscillating heat pipe,” *Int. J. Heat Mass Transf.*, vol. 94, pp. 366–372, 2016.

[28] A. Faghri, “Heat Pipes: Review, Opportunities and Challenges,” *Front. Heat Pipes*, vol. 5, no. 1, p. 48, 2014.

[29] D. Bastakoti, H. Zhang, D. Li, W. Cai, and F. Li, “An overview on the developing trend of pulsating heat pipe and its performance,” *Appl. Therm. Eng.*, vol. 141, no. May, pp. 305–332, 2018.

[30] P. Cheng, “Theoretial Analysis of Oscillating Motion, Heat Transfer, Minimum Meniscus Radius and Charging Procedure in an Oscillating Heat Pipe, Thesis,” University of Missouri-Columbia, 2008.

[31] X. Wang, X. Zhang, and C. Yang, “Experimental Analysis on Non-dimensional Parameters of Closed-loop Pulsating Heat Pipes,” *Adv. Mater. Res.*, vol. 732–733, pp. 230–233, 2013.

[32] M. B. Shafii, A. Faghri, and Y. Zhang, “Thermal Modeling of Unlooped and Looped Pulsating Heat Pipes,” *J. Heat Transfer*, vol. 123, no. 6, pp. 1159–1172, 2001.

[33] S. M. Pouryoussefi and Y. Zhang, “Analysis of chaotic flow in a 2D multi-turn closed-loop pulsating heat pipe,” 2016.

[34] S. Y. Nagwase and P. R. Pachghare, “Experimetal and CFD analysis of closed loop pulsating heat pipe with DI-water,” *2013 Int. Conf. Energy Effic. Technol. Sustain. ICEETS 2013*, pp. 185–190, 2013.

[35] R. C. Givler and M. J. Martinez, “Modeling of pulsating heat pipes.,” Albuquerque, New

Mexico, 2009.

[36] A. Gupta and A. Parwani, “CFD Modeling for Thermal Performance of Closed Loop Pulsating Heat Pipe in Bottom Heated Mode,” *Adv. Civil, Struct. Mech. Eng.*, no. February, pp. 46–50, 2017.

[37] P. F. Pai, H. Peng, and H. Ma, “Thermomechanical finite-element analysis and dynamics characterization of three-plug oscillating heat pipes,” 2013.

[38] M. Manzoni, M. Mameli, C. De Falco, L. Araneo, S. Filippeschi, and M. Marengo, “Non equilibrium lumped parameter model for Pulsating Heat Pipes: Validation in normal and hyper-gravity conditions,” *Int. J. Heat Mass Transf.*, vol. 97, pp. 473–485, 2016.

[39] G. Guersel, “Analysis of the Onset of the Oscillation Motion in a Pulsating Heat Pipe,” in *3rd European Conference on Microfluidics*, 2012, pp. 1–10.

[40] T. Daimaru, S. Yoshida, and H. Nagai, “Study on thermal cycle in oscillating heat pipes by numerical analysis,” *Appl. Therm. Eng.*, vol. 113, pp. 1219–1227, 2017.

[41] H. Teng, P. Cheng, and T. S. Zhao, “Instability of condensate film and capillary blocking in small-diameter-thermosyphon condensers,” *Int. J. Heat Mass Transf.*, vol. 42, no. 16, pp. 3071–3083, 1999.

[42] N. Kammuang-Lue, P. Sakulchangsatjatai, and P. Terdtoon, “Thermal performance of a closed-loop pulsating heat pipe with multiple heat sources,” *Heat Transf. Eng.*, vol. 35, no. 13, pp. 1161–1172, 2014.

[43] B. . Tong, T. . Wong, and K. . Ooi, “Closed-loop pulsating heat pipe,” *Appl. Therm. Eng.*, vol. 21, no. 18, pp. 1845–1862, 2001.

[44] J. F. O'Hanlon, *A User's Guide to Vacuum Technology A User's Guide to Vacuum Technology Third Edition*. Wiley-Interscience, 2003.

[45] C. Schneider, W. Rasband, and K. Eliceiri, "NIH Image to ImageJ: 25 years of image analysis," *Nat. Methods*, vol. 9, no. 7, pp. 671–675, 2012.